NUMERICAL SIMULATION AND WALL SHEAR

STRESS ANALYSIS OF PULSED FLOW IN PLATE

HEAT EXCHANGER

Pichitra Uangpairoj

A Thesis Submitted in Partial Fulfillment of the Requirements for the

Degree of Master of Engineering in Mechanical Engineering

Suranaree University of Technology

Academic Year 2009

การจำลองเชิงตัวเลขและการวิเคราะห์ความเค้นเฉือนที่ผนังจากการไหลของ
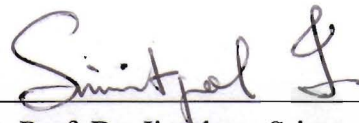ของไหลที่ไหลเป็นจังหวะในเครื่องแลกเปลี่ยนความร้อนแบบแผ่น

นางสาวพิจิตรา เอื้องไพโรจน์

NUMERICAL SIMULATION AND WALL SHEAR STRESS ANALYSIS OF PULSED FLOW IN PLATE HEAT EXCHANGER

Suranaree University of Technology has approved this thesis submitted in partial fulfillment of the requirements for a Master's Degree.
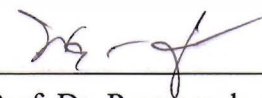
Thesis Examining Committee

_____

(Asst. Prof. Dr. Jiraphon Srisertpol)

Chairperson

_____

(Assoc. Prof. Dr. Kontorn Chamniprasart)

Member (Thesis Advisor)

_____

(Asst. Prof. Dr. Payungsak Junyusen)

Member

_____

(Dr. Keerati Suluksna)

Member

_____
(Prof. Dr. Sukit Limpijumnong)

Vice Rector for Academic Affairs

_____
(Assoc. Prof. Dr. Vorapot Khompis)

Dean of Institute of Engineering

พิจิตรา เอื้องไพโรจน์ : การจำลองเชิงตัวเลขและการวิเคราะห์ความเค้นเฉือนที่ผนังจาก
การไหลของของไหลที่ไหลเป็นจังหวะในเครื่องแลกเปลี่ยนความร้อนแบบแผ่น
(NUMERICAL SIMULATION AND WALL SHEAR STRESS ANALYSIS OF
PULSED FLOW IN PLATE HEAT EXCHANGER) อาจารย์ที่ปรึกษา :
รองศาสตราจารย์ เรืออากาศเอก ดร.กนต์ธร ชำนิประศาสน์, 169 หน้า.

การไหลแบบเป็นจังหวะมีผลต่อการเพิ่มขึ้นของความเค้นเฉือน ซึ่งเป็นพารามิเตอร์หลักตัว
หนึ่งในกระบวนการส่งเสริมการล้างสำหรับระบบการล้างภายใน (Cleaning in Place System) ใน
การศึกษาครั้งนี้ ชนิดของการไหลแบบเป็นจังหวะจึงถูกพิจารณาเพื่อใช้ในการปรับปรุง
ประสิทธิภาพของกระบวนการล้างภายใน ความเค้นเฉือนของการไหลแบบเป็นจังหวะชนิดต่าง ๆ
จึงถูกศึกษาโดยใช้วิธีปริมาตรสืบเนื่อง (Finite Volume Method) ขฮงโปรแกรมสำเร็จรูปเชิงพาณิชย์
สำหรับการจำลองการไหล (FLUENT®6.3.26) เพื่อที่จะบ่งบอกถึงประสิทธิภาพของการไหลแบบ
เป็นจังหวะชนิดต่าง ๆ นอกจากนี้ยังได้ทำการศึกษาถึงผลกระทบของพารามิเตอร์ของการสั่นแบบ
เป็นจังหวะ และรูปร่างของช่องการไหลต่อค่าความเค้นเฉือนอีกด้วย โดยการไหลแบบเป็นจังหวะ
ชนิดปั่นป่วน (Turbulent Pulsating Flow) ของสารละลายอิเล็กโทรไลต์และน้ำถูกจำลองการไหล
ผ่านท่อทรงกระบอก, ช่องลอนของเครื่องแลกเปลี่ยนความร้อนแบบแผ่น และแผ่นคู่ขนานภายใต้
สภาวะที่อุณหภูมิคงที่ (Isothermal Condition) ชนิดของการไหลแบบเป็นจังหวะจะถูกกำหนดโดย
ฟังก์ชันของความเร็วขาเข้าซึ่งเป็นฟังก์ชันที่มีคาบ ได้แก่ ฟังก์ชันที่มีลักษณะเป็นคลื่นรูปสี่เหลี่ยม
ฟันเลื่อย เส้นโค้งรูปไซน์ สี่เหลี่ยมคางหมู และสามเหลี่ยม จากผลของการศึกษา การจำลองเชิง
ตัวเลขของการไหลแบบเป็นจังหวะที่มีชนิดต่างกันแสดงให้เห็นว่า การไหลแบบเป็นจังหวะชนิด
คลื่นรูปสี่เหลี่ยมให้ค่าความเค้นเฉือนสูงที่สุด โดยการไหลแบบเป็นจังหวะชนิดที่มีการเปลี่ยนแปลง
ความเร็วกะทันหันจะให้ค่าความเค้นเฉือนสูงกว่าการไหลแบบเป็นจังหวะชนิดที่มีการเปลี่ยนแปลง
ความเร็วอย่างช้า ๆ ในขณะเดียวกันค่าความเค้นเฉือนจะเพิ่มขึ้นตามแอมพลิจูดและความเร็วเฉลี่ยขา
เข้าของการสั่น แต่ค่าความเค้นเฉือนกลับแปรผกผันกับความถี่ของการสั่น ซึ่งสังเกตเห็นได้อย่าง
ชัดเจนในช่องลอนของเครื่องแลกเปลี่ยนความร้อนแบบแผ่น นอกจากนี้ ผลของรูปร่างของช่องการ
ไหลต่อค่าความเค้นเฉือนยังแสดงให้เห็นว่าช่องการไหลที่มีความซับซ้อนเช่นในช่องลอนของ
เครื่องแลกเปลี่ยนความร้อนแบบแผ่นให้ค่าความเค้นเฉือนสูงกว่าในช่องการไหลของแผ่นคู่ขนาน

สาขาวิชา   วิศวกรรมเครื่องกล   ลายมือชื่อนักศึกษา_____
ปีการศึกษา   2552   ลายมือชื่ออาจารย์ที่ปรึกษา_____

PICHITRA UANGPAIROJ : NUMERICAL SIMULATION AND WALL SHEAR STRESS ANALYSIS OF PULSED FLOW IN PLATE HEAT EXCHANGER. THESIS ADVISOR : ASSOC. PROF. FLT.LT. KONTORN CHAMNIPRASART, Ph.D., 169 PP.

PULSED FLOW/CFD/WALL SHEAR STRESS

Pulsed flow has the effect of raising the wall shear stress which is one key parameter of the cleaning enhancement in the cleaning in place (CIP) system. In this study, the effect of type of pulsed flow was considered to improve the cleaning efficiency of the CIP system. To indicate the cleaning efficiency of pulsed flows, wall shear stresses of various types of pulsed flows were investigated by using the finite volume method of the commercial computational fluid dynamics code (FLUENT®6.3.26). In addition, the influences of pulsation parameters and the geometry of the channel flow on wall shear stress were also investigated. The turbulent pulsating flows of incompressible fluids; the electrolytic solution and water, were simulated through the cylindrical pipe, corrugated channel of plate heat exchanger and parallel plates under isothermal condition. Type of pulsed flow was characterized by functions of velocity at the inlet boundary which were periodic function such as rectangular wave, saw tooth wave, sinusoidal wave, trapezoidal wave and triangular wave. As the results of the study, the numerical simulation of different type of pulsed flows shows that pulsating flow with the rectangular waveform of pulsation gives the greatest wall shear stress. Pulsed flows whose flow velocity suddenly change can generated higher wall shear stresses than the pulsed flows whose flow velocity gradually change.

Meanwhile, wall shear stress increases with the amplitude and mean velocity inlet of pulsation. But it is inverse proportion to the frequency of pulsation. This is obviously seen only in the corrugated channel. Moreover, the effect of the geometry of the flow channel shows that the complicated channel of plate heat exchanger also gives higher wall shear stresses than the simple geometry as the parallel plates.

School of   Mechanical Engineering   Student's Signature _Pichitra Uangpairoj_

Academic Year   2009   Advisor's Signature _Keat Chint._

ACKNOWLEDGEMENT

TABLE OF CONTENTS

TABLE OF CONTENT (CONTINUED)

TABLE OF CONTENT (CONTINUED)

TABLE OF CONTENT (CONTINUED)

TABLE OF CONTENT (CONTINUED)

TABLE OF CONTENT (CONTINUED)

TABLE OF CONTENT (CONTINUED)

LIST OF TABLES

LIST OF TABLES

LIST OF TABLES

LIST OF FIGURES

LIST OF FIGURES (CONTINUED)

LIST OF FIGURES (CONTINUED)

LIST OF FIGURES (CONTINUED)

LIST OF FIGURES (CONTINUED)

Figure   **Page**

LIST OF FIGURES (CONTINUED)

LIST OF FIGURES (CONTINUED)

LIST OF FIGURES (CONTINUED)

SYMBOLS AND ABBREVIATIONS

A_i = Inner heat transfer area, [m^2]

A_o = Outer heat transfer area, [m^2]

A_0 = Model constant, [-]

A_s = Model constant, [-]

A_μ = Model constant, [-]

a = Positive constant, [#/s]

Speed of sound, [m/s]

a_1 = Constant, [-]

b = Positive constant, [#/s]

c = Positive constant, [#/s]

C_1 = Constant, [-]

$C_{1\varepsilon}$ = Constant, [-]

C_2 = Constant, [-]

$C_{2\varepsilon}$ = Constant, [-]

C_μ = Constant, [-]

C_{OH^-} = Hydroxide concentration, [M]

c_p = Specific heat capacity of fluid, [J/kg.K]

d_i = Inner diameter, [m]

f = Fanning friction factor, [-]

$F(M_t)$ = The compressibility function, [-]

g = Gravity, [m/s^2]

SYMBOLS AND ABBREVIATIONS (CONTINUED)

h_i	=	Heat transfer coefficient for inside flow, [W/m^2.K]
h_o	=	Heat transfer coefficient for outside flow, [W/m^2.K]
K	=	Constant, [-]
k	=	Thermal conductivity of heat transfer surface material, [W/m.K]
		Turbulent kinetic energy, [m^2/s^2]
k_{01}	=	Rate constant of first exciting state of soil removal reaction, [1/s]
k_1	=	Rate constant for species 1 soil removal, [1/s]
k_{12}	=	Rate constant of second exciting state of soil removal reaction, [1/s]
k_s	=	Roughness height, [m]
L	=	Length of the tube, [m]
l_ε	=	Length scale for ε field, [m]
l_μ	=	Length scale, [m]
M_{t0}	=	Constant, [-]
$\bar{p}$	=	Mean value of pressure, [N/m^2]
ΔP	=	Frictional pressure drop, [N/m^2]
Q	=	Rate of heat transfer, [W]
q_w	=	Heat at the wall, [J]
$\mathrm{Re}_{peak_{(critical)}}$	=	Critical peak Reynolds number, [-]
Re_y	=	Turbulent Reynolds number, [-]
R_{fi}	=	Fouling resistance based on inner surface, [K.m^2/W]
R_{fo}	=	Fouling resistance based on outer surface, [K.m^2/W]
R_k	=	Constant, [-]

SYMBOLS AND ABBREVIATIONS (CONTINUED)

R_t	=	Total thermal resistance, [K/W]
R_β	=	Constant, [-]
R_ω	=	Constant, [-]
r_i	=	Inside radius of tube, [m]
r_o	=	Outside radius of tube, [m]
S	=	Deformation Tensor, [1/s]
S_{ij}	=	Mean strain rate, [1/s]
St	=	Strouhal number, [-]
t	=	Thickness of the wall, [m]
		Time, [s]
T_w	=	Temperature of the wall, [K]
ΔT_m	=	Mean temperature difference, [K]
U_f	=	Overall heat transfer coefficient under fouling condition, [W/m^2.K]
U_i	=	Overall heat transfer coefficient based on the inner surface, [W/m^2.K]
U_o	=	Overall heat transfer coefficient based on the outer surface, [W/m^2.K]
u	=	Velocity of fluid flow, [m/s]
u_i	=	Instantaneous velocity component in i direction, [m/s]
$\bar{u}_i$	=	Steady mean velocity component in i direction, [m/s]
u_i'	=	Fluctuating velocity component in i direction, [m/s]
u_m	=	Mean velocity of flow, [m/s]

SYMBOLS AND ABBREVIATIONS (CONTINUED)

u^+	=	Dimensionless velocity, [-]
V	=	Average velocity of flow, [m/s]
x	=	Vector component, [-]
y	=	Height of the boundary, [m]
		Position to solid boundary, [m]
y^+	=	Dimensionless distance from the wall, [-]

Greek Symbols

α	=	Womersley number, [-]
α_0	=	Constant, [-]
α_∞	=	Constant, [-]
α_∞^*	=	Constant, [-]
$\alpha_{k,1}$	=	Constant, [-]
$\alpha_{k,2}$	=	Constant, [-]
α_s	=	Swirl constant, [-]
$\alpha_{\omega,1}$	=	Constant, [-]
$\alpha_{\omega,2}$	=	Constant, [-]
β	=	Constant, [-]
β_i	=	Constant, [-]
$\beta_{i,1}$	=	Constant, [-]
$\beta_{i,2}$	=	Constant, [-]
β_∞	=	Constant, [-]

SYMBOLS AND ABBREVIATIONS (CONTINUED)

δ_{ij}	=	Kronecker delta, [-]
ε	=	Turbulent dissipation rate, $[m^2/s^3]$
η_0	=	Constant, [-]
κ	=	Von Kármán constant, [-]
ρ	=	Density of fluid, $[kg/m^3]$
μ	=	Dynamic viscosity of fluid, $[N.s/m^2]$
μ_t	=	Turbulent viscosity, [kg/m.s]
μ_{t0}	=	Turbulent viscosity without swirl modification, [kg/m.s]
μ_{eff}	=	Effective viscosity, [kg/m.s]
Ω	=	Characteristic swirl number, [-]
$\overline{\Omega_{ij}}$	=	Mean rate of rotation tensor, [1/s]
ω	=	Specific dissipation rate, [1/s]
ω_k	=	Angular velocity, [rad]
σ_k	=	Turbulent Prandtl number for k, [-]
σ_ε	=	Turbulent Prandtl number for ε, [-]
σ_ω	=	Turbulent Prandtl number for ω, [-]
σ_t	=	Constant, [-]
τ	=	Shear stress, $[N.m^2]$
τ_w	=	Wall shear stress, $[N.m^2]$
ζ^*	=	Constan, [-]

SYMBOLS AND ABBREVIATIONS (CONTINUED)

Subscripts

f	=	Fouling
ε	=	Turbulent dissipation rate
i	=	Inner or inside
		Index of vector component
j	=	Index of vector component
k	=	Turbulent kinetic energy
m	=	Mean
μ	=	Viscosity
ω	=	Specific dissipation rate
o	=	Outer or outside
OH^-	=	Hydroxide ion
t	=	Total
		Turbulent
w	=	Wall

CHAPTER I

INTRODUCTION

1.1   Background and Significance

The inspiration of this study came from the willing to improve the cleaning in place (CIP) system. The CIP system is one of the cleaning techniques that are employed to remove the fouling from the surface of the equipment. Fouling is the undesired deposit that accumulates on the surface of the equipment, especially the heat transfer surface of heat exchanger. Fouling directly affects the performance of heat exchanger which relates to economical aspect in the industries. The effectiveness of heat exchanger is decreased by the increase of pressure and lower heat transfer (Kakaç and Liu, 2002). Consequently, an additional cost is introduced to the industrial sector (Pritchard, 1988). In addition, fouling layer that found in food processing can be the source of the microbial contamination. This contamination directly affects the quality of food product. Because of these fouling problems, there are many researches about the appearance of fouling in the equipment, the fouling reduction by modifying the geometry of the equipment (Jun and Puri, 2005) or the composition of the surface (Rosmaninho, Rizzo, Müller-Steinhagen, and Melo, 2008), etc. However, the regular cleaning is still necessary.

In CIP system, water and cleaning chemical are circulated to remove the deposits from the surfaces of the equipments. The cleaning efficiency is affected mainly by chemical concentration, temperature and fluid flow. Therefore, one way to

enhance the cleaning is fluid flow adjustment. According to other researches, pulsating flow can be one application of the fluid flow adjustment of CIP system (Gillham, Fryer, Hasting, and Wilson, 2000; Blel, Legentilhomme, Bénézech, Legrand, and Le Gentil-Lelièvre, 2009). However, the effect of type of pulsating flow on the cleaning efficiency has not found in the literature survey. Meanwhile, wall shear stress which imposed by the flow is one of the key parameter of the deposit removal. Shear stress of fluid flow helps to remove the deposits from the equipment surface by breaking down the swollen deposit layer (Gillham et al., 1999). Therefore, the effect of types of pulsed flow on wall shear stress that implicitly indicates the cleaning efficiency was considered to be the main objective of this study.

To indicate the cleaning efficiency of various types of pulsed flows, wall shear stresses of turbulent pulsating flows are investigated. Due to the complexity of turbulent pulsating flow and the complexity of the flow domain (channel of plate heat exchanger), the finite volume method of the commercial computational fluid dynamics code (FLUENT[®]6.3.26) was employed to analyze wall shear stress of turbulent pulsating flows in cylindrical pipe, parallel plates and plate heat exchanger in order to see the trend of using various type of pulsed flows in cleaning system. In addition, the effects of pulsation parameters and the geometry of flow channel on wall shear stress were also investigated in order to gain the useful results for the cleaning enhancement.

1.2   Objectives

The objectives of this thesis are discussed in the following points:

1.2.1 To study the effect of type of pulsed flow on wall shear stress in cylindrical pipe, parallel plates and channel of plate heat exchanger by using numerical simulation.

1.2.2 To study the influence of amplitude, frequency and mean velocity inlet of pulsed flow on wall shear stress by using numerical simulation.

1.2.3 To study the influence of the geometry of flow channel on wall shear stress by using numerical simulation.

1.3   Scope and Assumptions of Work

1.3.1 Wall shear stresses were obtained by three dimensional fluid flow simulations in cylindrical pipe, parallel plates and channel of plate heat exchanger.

1.3.2 A commercial computational fluid dynamics code (FLUENT$^{®}$6.3.26) was employed to simulate the flows through the element of cylindrical pipe, parallel plates and channel of plate heat exchanger.

1.3.3 Types of fluid flow which are chosen to analyze wall shear stress

(1) Steady flow

(2) Pulsed flow – Rectangular waveform

(3) Pulsed flow – Saw tooth waveform

(4) Pulsed flow – Sinusoidal waveform

(5) Pulsed flow – Trapezoidal waveform

(6) Pulsed flow – Triangular waveform

1.3.4 Flow was incompressible flow.

1.3.5 Flow was performed under isothermal condition.

1.3.6 The entrance effect was negligible.

1.3.7 The characteristics of each type of pulsed flow depended on mean velocity, amplitude and frequency of pulsation.

1.4   Outcomes of the Research

1.4.1 Better understanding of wall shear stress distribution of pulsed flows and turbulent pulsating flow phenomena in different geometry of flow channel which have been used to improve the cleaning system in different geometry of flow channel.

1.4.3 To understand the influences of amplitude, frequency and mean velocity of pulsed flow on wall shear stress. These lead to improve the cleaning efficiency.

1.4.4 To understand the effect of type of pulsating flow on wall shear stress. This leads to improve the cleaning efficiency.

1.4.5 For the cleaning efficiency evaluation, the effect of type of pulsed flow on wall shear stress has led to other analysis. To identify the effect of type of pulsed flow on the cleaning efficiency, the force accumulation that generated by different type of pulsed flow can be another way to consider.

1.4.6 This study is the basic application of CFD knowledge for the cleaning technology.

CHAPTER II

LITERATURE REVIEW

The literature review section will focus on fouling in heat exchanger, cleaning in place (CIP) system, pulsed flow and wall shear stress analysis.

2.1   Fouling in Heat Exchanger

Heat exchangers are devices that provide heat to transfer between two medium due to temperature difference. They are used in a wide variety of applications such as power production, chemical and food industries, electronics, environmental engineering, waste heat recovery, air conditioning, refrigeration and space applications. There are various types of heat exchanger which are employed in different applications. Nevertheless, there is an unavoidable problem of using heat exchanger in most of the above applications. This problem is fouling on the heat transfer surface of heat exchanger. Fouling is the undesirable substances that accumulate on the heat transfer surface. Fouling directly affects the performance of heat exchanger which relates to economical aspect in the industries.

This section focuses on type of fouling, effects of fouling on heat exchangers that help to understand the significant of fouling in heat exchangers. It also focuses on fouling in dairy process and summary of the published literature.

2.1.1 Type of Fouling

Because of the diversity of process condition, fouling can be classified into the following categories.

2.1.1.1 Particulate Fouling

This fouling occurs when the solid particles in the process stream accumulate on the surface by the effect of gravity. For example, the deposit of unburnt fuel or ashes in boiler and the deposit of dust in air-cooled condenser.

2.1.1.2 Crystallization Fouling

This fouling occurs in the crystallization of inorganic salts which are supersaturated during heating or cooling in heat exchangers, like crystal deposition of salts in cooling water system.

2.1.1.3 Corrosion Fouling

The corrosion products of the reaction between corrosive fluid and the heat transfer surface can foul on the surface of heat exchanger. For example, alkali metals and sulfur can cause corrosion in oil-fired boilers.

2.1.1.4 Chemical Reaction Fouling

Fouling deposits are formed by the chemical reaction within the process stream which does not participate with the heat transfer surface. For example, the deposits are formed by the product of hydrocarbon polymerization.

2.1.1.5 Biofouling

This is the deposition of biological materials. Fouling is known as microbial fouling when the deposits are microorganisms. Meanwhile, it is called macrobial fouling if the deposit compositions are seaweed, water weeds and

barnacles. For example, the biofouling on the surface of power plant condenser which circulate with seawater.

2.1.2 Effects of Fouling

When there is fouling in heat exchangers, their effectiveness is decreased. Lower heat transfer and the increasing of pressure drop are two major results of build-up of fouling on the heat transfer surface.

In heat exchanger, thermal analysis is governed by the conservation of energy. The rate of heat transfer, Q, is given by:

$$Q = U_i A_i \Delta T_m = U_o A_o \Delta T_m \qquad (2.1)$$

where Q is the rate of heat transfer in W, U_i and U_o are the overall heat transfer coefficient based on the inner surface and outer surface, respectively in W/m^2.K, A_i and A_o are the inner and outer heat transfer area, respectively in m^2 and ΔT_m is the mean temperature difference in K. From the equation (2.1), the overall heat transfer coefficient can be calculated from:

$$U_i A_i = U_o A_o = \frac{1}{R_t} = \frac{1}{\dfrac{1}{h_i A} + \dfrac{t}{kA} + \dfrac{1}{h_0 A}} \qquad (2.2)$$

where R_t is the total thermal resistance to heat flow across the surface between inside and outside flow in K/W, h_i and h_o are heat transfer coefficient for inside and outside flow, respectively in W/m^2.K, k is thermal conductivity of heat transfer surface material in W/m.K and t is the thickness of the wall in m.

The equation (2.1) and (2.2) are employed to analyze heat transfer in general heat exchanger. For the tubular heat exchanger as shown in Figure 2.1
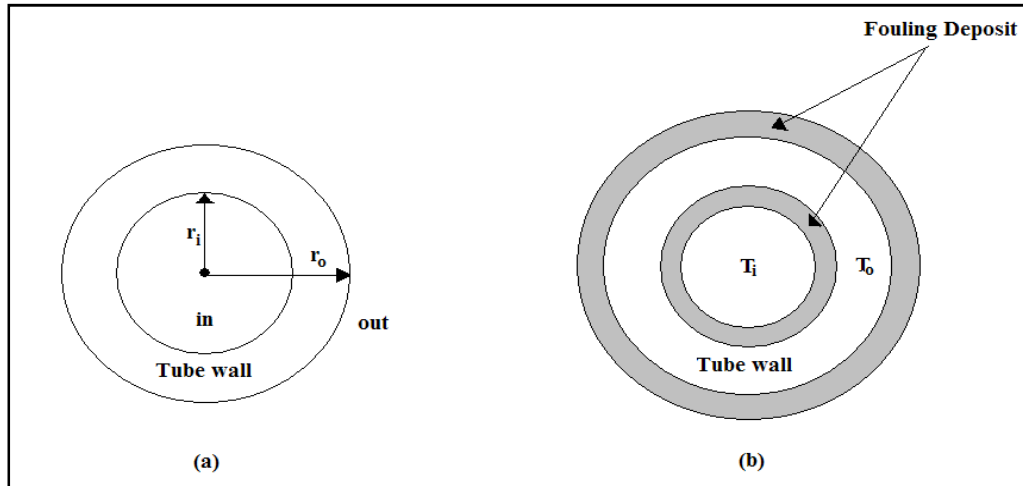
Figure 2.1 Tubular heat exchanger of clean tube (a) and fouled tube (b)

(Kakaç and Liu, 2002)

The overall heat transfer coefficient of the clean tubular heat exchanger is given by:

$$U_i A_i = U_o A_o = \frac{1}{R_t} = \frac{1}{\dfrac{1}{h_i A_i} + \dfrac{\ln(r_0 / r_i)}{2\pi k L} + \dfrac{1}{h_0 A_o}} \qquad (2.3)$$

where r_i and r_o are inside radius and outside radius in m, respectively and L is the length of the tube in m.

where R_t can be calculated from:

$$R_t = \frac{1}{h_i A_i} + \frac{\ln(r_o / r_i)}{2\pi k L} + \frac{1}{h_o A_o} \qquad (2.4)$$

If there are the deposits on heat transfer surface as in Figure 2.1 (b), fouling adds an insulating layer on the heat transfer surface. The total thermal resistance can be obtained by adding the inside and outside thermal resistances of the deposits in the equation (2.4). Thus, the total thermal resistance is given by:

$$R_t = \frac{1}{h_i A_i} + \frac{R_{fi}}{A_i} + \frac{\ln(r_o/r_i)}{2\pi kL} + \frac{R_{fo}}{A_0} \frac{1}{h_o A_o} \tag{2.5}$$

where R_{fi} and R_{fo} are the fouling resistance based on inner and outer surface, respectively. Therefore, the overall heat transfer coefficient based on inner surface area under fouled conditions, U_f, can be calculated by:

$$U_f = \frac{1}{R_t A_i} = \frac{1}{\dfrac{1}{h_i} + R_{fi} + \dfrac{A_i \ln(r_0/r_i)}{2\pi kL} + \dfrac{A_i}{A_o} R_{fo} + \dfrac{A_i}{h_0 A_o}} \tag{2.6}$$

The equation (2.3)-(2.6) show that fouling increases the heat resistance at the heat transfer surface and lower heat transfer. Thus, the increment of heat transfer surface is required, in order to make the process stream meet the heat transfer requirement.

Build-up of deposit also increases pressure drop, due to the increase of surface roughness and the decrease of cross section area of the flow channels. This effect can be described by the following equation:

$$\Delta P = 4f\left(\frac{L}{d_i}\right)\frac{\rho u_m^2}{2} \tag{2.7}$$

where ΔP is frictional pressure drop in N/m^2, f is the Fanning friction factor, L is the length of the tube in m, d_i is inner diameter of the tube in m, ρ is density of fluid in kg/m^3 and u_m is mean velocity of flow in m/s. The increment of pressure drop leads to increase the pumping power.

Consequently, an additional cost is introduced to the industrial sector. The cost is in the form of increased capital expenditure, increased maintenance cost, loss of production and energy losses (Pritchard, 1988).

2.1.3 Fouling in Dairy Process

In dairy process, the heat is introduced to the process stream in order to killing the spoilage organisms and pathogens which cause foodborne disease in humans. It can warrant the safety to the customer and increase the keeping quality. Heat exchangers are used in the continuous indirect heating systems. The selection of heat exchanger in dairy thermal process depends on the rheology of material and thermal condition. Normally, plate heat exchangers are employed in the processes, which their temperature below 100°C such as thermization, pasteurization and pre-heating in sterilization. Because plate heat exchanger consists of a series of thin plates which cannot tolerate high pressure and high temperature conditions. Meanwhile, tubular heat exchangers are used in the high pressure and high temperature process, like in heating process of sterilization and ultrahigh-temperature (UHT) process (Britz and Robinson, 2008).

In thermal processing of milk, fouling can be distinguished into type A and B (Burton, 1988), depending on reactions of fouling mechanism. Fouling type A occurs when protein in milk, which is called β-lactoglobulin denatures at temperatures 70-80°C and becomes the active form of β-lactoglobulin. This active form can

aggregate with other proteins and deposit on the surface of heat exchanger. It is soft voluminous, curd-like and its color is white or cream. Meanwhile, fouling type B is formed by the precipitation of mineral in milk such as calcium phosphates and calcium citrates which are supersaturated at temperature above 110°C (Lanlande, Tissier, and Corrieu, 1985). It is hard, brittle and grey in color.

Fouling in dairy process not only causes pressure drop and lower heat transfer but it also is the source of contamination in dairy product. In fouling, microorganisms can attach and grow better than on the unfouled surface. Fouling is used to protect microorganisms from cleaning, especially thermophile microorganism (Hinton, Trinh, Brooks, and Manderson, 2002). Because of these problems, there are many researchers who try to understand the fouling formation. Grijspeerdt, Hazarika, and Vucinic (2003) used 2D and 3D computational fluid dynamics (CFD) to investigate flow pattern of milk between two corrugated plates. The calculations identified the influence of corrugation shape on fouling. Because of the angle of corrugation shape, the reverse flow regions were created. The longer heating time of fluid particle causes more fouling in the reverse flow regions. As same as Bonis and Ruocco (2006), they used CFD simulation (COMSOL Multiphysics v.3.2a) to study the deposit of β-lactoglobulin on the plate heat exchanger surface. They found that the temperature and velocity distribution could be used to explain the fouling distribution. The stagnation regions and the regions where the fluid was slowed down were the weak spots with respect to fouling, because the contact time between fluid and heating wall was longer than other regions. At the same time, the outlet channel where the fluid temperature increases from 60°C to 97°C, the most of the fouling is created due to β-lactoglobulin denaturation. These outcomes led to the new plate heat exchanger

system, designed for the uniformity of flow distribution. The new system could reduce the deposited mass to 1/10, compare to the current system (Jun and Puri, 2005). Moreover, Rosmaninho et al. (2008) studied the relationship between surface properties and fouling. They found that the difference of surface composition (TiN modified surface) affected surface energy properties which related to fouling. The deposition rate was higher for the surface having higher surface energy. TiN modified surfaces also reduced the remains of deposit after cleaning. This useful results led to reduce fouling by using surface modifying as part of an anti-fouling strategy.

2.2 Cleaning in Place System

Cleaning in Place (CIP) System is a closed cleaning technique which is daily used to remove the deposits from the process plant, especially in the dairy industry. In CIP system, water and chemicals from the storage tanks are circulated through the target food equipment and pipework by the management of the automation system.

2.2.1 Cleaning in Place Cycles

The cleaning procedure consists of a series of cleaning cycles which employ the different medium for the different purpose of cleaning. The cleaning regimes generally involve the following cycles (Fryer et al., 2006; Heldman and Lund, 2007).

2.2.1.1 Prerinse Cycle

The circulation of water is used to remove product residues and loosely bound substances from the surface. Water is rinsed for 3-10 min.

2.2.1.2 Detergent Cycle

The action of the cleaning chemical (acid or alkaline) to release the deposit from the surface and the majority of cleaning take place during this cycle. For alkaline solution, the equipment is cleaned by circulation of the solution at 75°C about 10 min. If the detergents are alkaline and acid solutions, after the circulation of alkaline is introduced to the equipment, rinsing with warm water is employed. Then, the acid solution is circulated for about 5 min. at 65°C. But the hot equipment, like pasteurizer, requires longer circulation times and stronger solutions.

2.2.1.3 Postrinse Cycle

The circulation of water is used to remove the deposit and cleaning chemical from the surface of equipment.

2.2.1.4 Disinfection Cycle

The aim of disinfection is to kill the microorganisms that present on the surfaces of the equipments. This step can be finished by the circulation of disinfectants (hydrogen peroxide, peracetic acid and sodium hypochlorite) or hot water.

2.2.1.5 Final Rinse Cycle

The circulation of cold water is used to remove the disinfectants from the system before starting the new process.

Some of these cycles could be repeated or omitted during the procedure, depending on the cleaning strategy.

2.2.2 General Reaction Scheme

In the detergent cycle, when the detergent solutions are circulated to remove the deposits from the surface of the equipment, there is a heterogeneous reaction between the detergent solutions and deposits layer. The general sequence of the mechanisms that occur in this cycle can be categorized into the following steps (Heldman and Lund, 2007):

2.2.2.1 Bulk Reaction

The detergents in the bulk fluid react with the dissolved soil or water hardness (calcium and magnesium salts) in the bulk fluid. If there is a large amount of soil or salts in the bulk fluid, the detergents that are available for the deposit removal will be consumed by the reaction between detergents and soil or salts. Thus, the amount of soil and water hardness relates to the remaining detergents.

2.2.2.2 Transport to Surface

The mass of detergents is transported to the surface of fouled layer by the turbulence of flow and the molecular diffusion.

2.2.2.3 Transport into Fouled Layer

The detergents are transferred through the layer of fouling by capillary or molecular diffusion. These cause the reaction zone in the whole area of fouled layer.

2.2.2.4 Cleaning Reaction

When the detergents contact with the fouled layer, there are the physicochemical transformations (soaking, swelling, emulsification, etc.) and the chemical reactions (hydrolization, saponification, solubilization and so on) in the fouled layer. These reactions help to overcome the cohesion forces of deposit bond

and adhesion forces of bond between deposits and surface of the equipment. Consequently, fouling is easier to remove from the surface.

2.2.2.5 Transport Back to Interface

The products of the reactions diffuse through the fouled layer by concentration gradients.

2.2.2.6 Transport to Bulk

When the deposit bond and bond between deposits and surface are weaken by the cleaning reaction, the reaction products are transported to the bulk fluid by concentration gradients and the turbulence of fluid flow.

The example of the reaction scheme in the detergent cycle is the stages of dairy deposit cleaning. The reaction starts with the swelling stage. When alkaline solution contacts and reacts the deposit and causes swelling of protein matrix (Christian and Fryer, 2006). In this stage, the cleaning rate increase with the temperature, exposure time and the chemical concentration. After that the swollen deposits were removed by shear forces of fluid flow and molecular diffusion. The rate of cleaning is relatively constant. This stage is called uniform stage. Finally, when the swollen deposit is thin, the rate of cleaning decays. This stage is known as decay stage. The removal of the residues occurs by shear stress and mass transport. This stage requires more time than first two stages.

2.2.3 The Influencing Factors of the Cleaning Rate

To remove the deposits from the surface of equipment, there are many different parameters on the cleaning rate. These parameters are both of system parameters and operational parameters. The main factors that affect on the cleaning rate can be listed as the following parameters:

2.2.3.1 Nature of the Deposits

The nature of the deposit will determine the strength of the deposits bond and bond between the deposits and surface. In the cleaning procedure, this factor is used to choose the type of cleaning agents which must achieve the desired cleaning reaction.

2.2.3.2 The Amount of Soil and Salts in the Cleaning Solution

When there is a large amount of soil or salts (calcium and magnesium salts) which disperses in the solution, the large amount of detergents will be consumed by the reaction between detergents and dispersed soil or salts. The remaining detergents may not be enough to react with the deposits. This causes the lower effectiveness of the cleaning solution.

2.2.3.3 Type of Cleaning Agents or Detergents

To achieve the desired reaction of the deposit removal, type of detergents must correspond to the nature of the deposit: alkaline solutions are normally used to react with organic deposits, meanwhile, acid solutions are used for mineral deposits.

2.2.3.4 Detergent Concentration

To overcome the strength of the deposits bond and bond between the deposits and surface, the necessary energy would be supplied to the fouled layer. Detergents also provide the chemical energy to deposit layer. This chemical energy can be raised by the increasing of detergent concentration. The effect of the detergent concentration on the cleaning rate was studied by many researchers as summarized in Table 2.1.

Table 2.1 Influence of detergent (C_{OH^-}) concentration on cleaning rates

Model*	References
$k_1 = a\ C_{OH^-}$	Jennings, 1959, 1963, 1965
$\ln k_{01} = a + bC_{OH^-}$	Gallot-Lavallee, 1982
$\ln k_{12} = a + bC_{OH^-} - cC_{OH^-}^{-2}$	Gallot-Lavallee et al., 1984

Remark: *a, b, c are positive constants

2.2.3.5 Temperature

Heat is one form of energy that is supplied to the fouled layer to overcome the strength of the deposits bond and bond between the deposits and surface. Therefore, as temperature increases, the cleaning rate increases (Fryer and Bird, 1994). The effect of temperature on the cleaning rate can be expressed in the form of an Arrhenius-type equation (Gallot-Lavallee, 1982; Jennings, 1959; Hoffmann and Reuter, 1984; Schlüssler, 1970). Moreover, in dairy deposit cleaning, Gillham et al. (1999) found that temperature strongly affected the cleaning rate in the swelling stage and uniform stage. Meanwhile, when the deposit-liquid interface temperature exceeded $50^{o}C$, the length of decay stage decreased significantly.

2.2.3.6 Fluid Flow

Shear force and turbulence, imposed by fluid flow, provides the mechanical energy to the deposit layer. This energy also helps to overcome the strength of the deposits bond in the cleaning procedure. The increment of flow rate and the fluctuation of flow induce greater shear force on the deposit layer. This reduces the cleaning time. As in dairy deposit cleaning, Gillham et al. (1999) also studied the effect of fluid flow on the cleaning rate under fixed temperature conditions. The study range of Reynolds number is 500 to 5000. They found that the

total cleaning time, could be reduced by the increase of Reynolds number which mainly affected the length of decay stage.

The mechanical effects of fluid flow on the cleaning rates can be expressed in the form of mathematical models which are the relationship between the cleaning rate and a variety of flow parameters as summarized in Table 2.2

Table 2.2 The mechanical effect on cleaning rates

Relation*	Parameter range
$\ln k_{01} = a + bV$ [1]	0.3<V<1.9 m/s
$\ln k_{12} = a + bV + cV^2$ [1]	0.3<V<1.9 m/s
$\ln k_1 = a + bV$ [1]	0.3<V<1.9 m/s
$k_1 = a + b\tau_w$ [2]	1<τ_w<14 Pa
$\ln k_{01} = a + b\ \tau_w$ [3]	0.19<τ_w<7.5 Pa

Remark: *a, b, c are positive constants.

Sources: [1] Gallot-Lavallee (1982); [2] Timperley (1981); [3] Graßhoff (1983)

These are main factors which must be considered very carefully for planning and building the cleaning system.

2.3   Pulsed Flow

Pulsed flow or pulsating flow is one kind of the unsteady flows whose velocity and pressure varies with time periodically. This flow can be found in biological system as well as engineering field. In mammalian cardiovascular system, pulsating flow is in the form of the rhythmic change in blood-flow velocity with time. This rhythm is caused by cardiac action and respiration which are controlled by a portion

of the autonomic nervous system. In Engineering, such as turbomachinery, rotor blade aerodynamics, etc., pulsating flow is normally generated by motive forces of reciprocating or peristaltic positive displacement pumps. These forces are most commonly caused by the acceleration and deceleration of the pumped fluid. The uncontrolled energy is appeared as pressure spikes. Vibration is the example of pulsation that usually leads the way to component failure. Thus, there are many researches that attempted to describe the characteristics of the flow in order to be the benefit of the development of those fields.

2.3.1 Previous Studies Relating to Pulsed Flow

Ishii (1990) investigated the velocity distribution of pulsatile flow in circular pipe with sudden expansion. The Poisson equation for the stream function and the vorticity transport equation of the Navier-Stokes equations were solved using finite different method (ADI difference method and upwind scheme). The flow was considered as incompressible viscous flow. The characteristics of pulsatile flow were controlled by cosine waveform for the various Reynolds and Womersley number. As the results of the study, he found that the velocity distribution of pulsatile flow in circular pipe without back step became plug flow when the Reynolds and Womersley number increased. Additionally, the reverse flow also appeared near the wall and increased when the Womersley number increased. For the velocity distribution of pulsatile in the circular pipe with back step flow, the reattachment length extended downstream and the vortex behind the back step stretched backward when the Reynolds number increased.

Peacock, Jones, Tock, and Lutz (1998) studied the onset of turbulence of pulsatile flow in a straight tube by the experiment. Pulsatile flows with the sinusoidal component, which generated by a Scotch yoke mechanism, were detected the onset of the flow instabilities by using hot film wall shear stress probes. At the same time, centerline velocities and instantaneous volumetric flow were measured by using a Laser Doppler Anemometer and an ultrasound flow probe, respectively. The onset of turbulence was in the form of the critical peak Reynolds number. From the experimental data, the critical peak Reynolds number correlated with the Womersley and the Strouhal number as a power law function as in equation (2.8):

$$\mathrm{Re}_{peak_{(critical)}} = 169\alpha^{0.83}St^{-0.27} \qquad (2.8)$$

where $\mathrm{Re}_{peak_{(critical)}}$ is the critical peak Reynolds number. This peak Reynolds number is defined from the maximum velocity of flow. α is the Womersley number and St is the Strouhal number. Moreover, there was a good agreement of velocity profile between the laminar experimental data and the theoretical predictions from Poiseuille's law and Womersley's solution. On the other hand, there was no adequate theoretical prediction for transitional and turbulent profiles.

Yakhot, Arad, and Ben-Dor (1999) studied laminar pulsating flow in a rectangular duct and parallel plates by using finite difference method. The characteristics of pulsatile flow were induced by sinusoidal waveform of pressure gradient. High-order-accurate scheme was chosen as discretization scheme. The induced oscillating velocity and wall shear stress of different flow conditions that varied with frequency and aspect ratio of the duct were analyzed. As the results of the

study, the frequency of pulsating flow affected phase lag or shift of the induced velocity and wall shear stress with respect to the imposed pressure gradient. In parallel plates, at high frequency, the oscillating mean velocity and the wall shear stress had phase lags of 90° and 45°, respectively. Meanwhile, there was no phase lag between the mean velocity and pressure gradient at the low frequency of pulsation. These phenomena could be found when flows were in square and rectangular duct. The influence of aspect ratio on velocity profile, oscillating velocity and wall shear stress showed that flow in the square duct was affected by two dimensional effects. Meanwhile, flow in rectangular duct with higher aspect ratio had velocity profiles at center plate similar to velocity profile of one dimensional flow between parallel plates. The difference was found only near the side wall of rectangular duct where disappeared in parallel plates, the amplitude of the induced velocity and the wall shear stress decreased when approaching the side wall. These caused by the friction effects in the duct especially at the corner of the duct.

Misra, A. Pal, B. Pal, and Gupta (1999) studied oscillating entry flow in a plane channel with pulsating walls by using numerical method. The study flow was unsteady laminar flow of an incompressible viscous flow whose flux varied with time in the form of cosine wave. This flow behavior was studied in the entrance region of plane channel whose walls oscillated along their normal direction. The vorticity transport equation of the Navier-Stokes equations was solved using finite different method (ADI difference method and central difference scheme). From the numerical computation, they found that the velocity profile of oscillating flow was flat in the entrance region and tend to be parabolic shape in downstream region. The maximum axial velocity increased with the length of channel. When the channel stayed still,

wall shear stress never vanished and there was no back flow in the channels. On the other hand, when the channel walls moved with high frequency, there were reverse flows near the wall at different time intervals within the time period. These can be concluded that oscillation of channel walls affects the behavior of the entry oscillating flow.

Karagöz (2002) investigated the behavior of the laminar oscillating flow in a two dimensional channel by using both of analytical and numerical methods. The flows were considered to be incompressible flow. The pressure gradient of the oscillating flow varied sinusoidally with time. The characteristics of the oscillating flow were controlled by frequency parameter in the form of Womersley number. In the case of analytical method, mass and momentum equations were solved by using similarity transformation. Meanwhile, the finite volume technique was used to solve mass and momentum equations for numerical method. The central difference and hybrid scheme were employed to discretize the diffusive and convective terms, respectively. As the results of the study, there was a good agreement between analytical and numerical solutions. The velocity profile seemed to be quasi steady solution when the frequency of oscillation was low. At the same time, when the frequency parameter increased, the velocity profile resembled the plug flow and the effects of oscillation became dominant in the near wall region. The high values of the frequency parameter also gave rise in the amount of amplitude of skin friction coefficient. Moreover, there was phase lag between the induced velocity and pressure oscillation, whereas, the skin friction coefficient had phase lead of 45° with respect to the imposed pressure gradient.

The similar flow characteristics were found in the laminar pulsating pipe flow which was studied by Ünsal, Ray, Durst, and Ertunç (2005). They studied the behavior of laminar pulsating flows in a pipe using analytical and experimental method. The flow was considered as incompressible viscous flow. The characteristics of pulsating flow were controlled by sinusoidal waveform of mass flow rate. The analytical solutions were obtained by solving mass and momentum equations using Bessel function, whereas, the velocity distributions were measured by using a hot-wire anemometer for the experiment. The results of the study showed that there was a good agreement between the analytical solutions and the experimental data. The velocity distributions changed with the variation of frequency of pulsation. At very low frequency, the velocity profile resembled the parabolic profile of the steady laminar flow. The corresponding phase lags were almost zero. The velocity amplitudes in the center region of the pipe decreased and the accelerating profiles tended to be flatter with the increase of frequency. On the other hand, the velocity amplitudes at near wall region increased and the decelerating profiles appeared to be more inflections near the pipe wall with the increase of frequency. In addition, the increase of mass flow rate amplitude also induced more inflections in the velocity profiles at near wall region.

Moreover, the frequency of pulsation also affects the velocity distribution of the turbulent pulsating flow in a pipe. He and Jackson (2009) investigated the behavior of turbulent pulsating flow in a pipe by the experiment. The periodic pulsating flow was incompressible flow. The instantaneous velocities were measured by using a two-component Laser Doppler Anemometer system. The results of the study showed that the amplitude of velocity modulation was affected by the

frequency of pulsation. In the lowest frequency case, the velocity profile was similar to quasi-steady shape which the amplitude of velocity was highest at the center of the pipe. When the frequency of pulsation increased, the maximum amplitude of velocity was reduced and tended to locate near the wall of pipe. In the high frequency cases, the amplitude of velocity was constant in the center part of the pipe. This behavior was called a frozen slug-like behavior. This behavior of flow was also found when the axial and radial components of root mean square turbulence fluctuation were considered. In addition, they found that the response of turbulence to the imposed pulsating flow initially occurred in the wall region and then propagated into and cross the core of pipe.

2.3.2 The Effect of Pulsed Flow on the Cleaning Enhancement

From section 2.2.3, one of the factors which affect the cleaning rate in the cleaning in place procedure is fluid flow. This factor leads many researchers to enhance the cleaning efficiency by using fluid flow adjustment.

Gillham et al. (2000) investigated the whey protein cleaning enhancement using pulsed flows. This investigation based on the experiment. Pulsating flows of sodium hydroxide solution were generated by a bellow unit and a piston unit in pulsed cleaning devices. The condition of pulsing was studied at a steady flow Reynolds numbers of 580, the characteristics of pulsed flow were controlled by amplitude and frequency of pulsation (frequency was less than 2 Hz and the amplitude was greater than the steady flow velocity). These pulsed flows were employed to clean the deposit of whey protein in a tubular heat exchanger. The performance of pulsed flow was indicated by observing the progress of cleaning and thermal resistance of the deposit during cleaning test. As the results of the study, the

alkaline pulsating flow could enhance the cleaning rate of whey protein removal by breaking down the swollen deposit. The cleaning rates in the uniform stage and decay stage were raised, and then the overall cleaning time was reduced. The enhancement was controlled by the combination effect of amplitude and frequency of pulsation. Meanwhile, the thermal resistance monitoring also corresponded to the cleaning progress. There was a rapid decrease in the thermal resistance of the deposit when the cleaning system was operated by pulsating flow.

There is another study that corresponds to the study of Gillham et al. (2000). Blel et al. (2009) studied the effect of turbulent pulsating flow on the bacterial removal during a cleaning in place procedure. The turbulent pulsating flows of sodium hydroxide were characterized by the pulsations parameter (mean velocity, amplitude and frequency). Pulsating flows were generated by solenoid valve in pulsation generator system. The range of amplitude and frequency of pulsed flow were 0-0.81 m/s and 0-2.86 Hz, respectively. These flows were flushed through the cylindrical pipes with the deposit of *Bacillus cereus* spores. To evaluate the cleaning efficiency of pulsating flow, the cleaning efficiency of pulsating flow was compared to the cleaning efficiency of steady flow. The residual contamination of *B. cereus* spores after cleaning procedure and the removal kinetic were analyzed. The results of the study showed that the pulsating flow was more effective than the steady flow in the cleaning procedure. With the same of mean velocity of flow, the residual contamination was less important in pulsed flow. The effective removal rate constant of pulsating was greater than the steady flow as well. Using pulsating flow generated higher shear stress at the wall which made it easier to break down the deposit. Pulsed flows with high pulsation parameters (amplitude and frequency) also remained the

effectiveness even at moderate mean velocity. As same as pulsating flow with the recirculation at low mean velocity, the recirculation at the core of the pipe induced high fluctuation shear rate at the wall which made it easier to remove the soil from the surface. Moreover, the statistical analysis showed that the bacteria removal enhancement was controlled by the combination of amplitude and frequency effects. For *Bacillus cereus* spores removal, the optimal amplitude and frequency are 0.73 m/s and 2.5 Hz, respectively. Thus, the cleaning efficiency can be enhanced significantly by using pulsating flow in the cleaning procedure.

2.4   Wall Shear Stress Analysis

A shear stress is the tangential component of force acting on a surface per unit area. For all laminar Newtonian fluid, the relationship between shear stress and strain rate can be defined by Newton's law of viscosity. For laminar flow between parallel plates, Newton's law of viscosity can be written as in equation (2.9):

$$\tau = \mu \frac{du}{dy} \tag{2.9}$$

where τ is a shear stress in N/m^2, μ is the dynamics viscosity in N.s/m^2, u the velocity of fluid along the plate boundary in m/s and y is the height of the boundary in m.

In a turbulent flow, the flow variables vary with time. The instantaneous velocity component can be decomposed into a steady mean value and a fluctuating component as in equation (2.10):

$$u_i = \overline{u}_i + u_i' \tag{2.10}$$

where, u_i is the instantaneous velocity component in m/s, $\bar{u}_i$ is the steady mean velocity component in m/s and u_i' is the fluctuating velocity component in m/s. The effects of turbulent fluctuation on fluid motion can be described by Reynolds-averaged Navier-Stokes (RANS) equations. For incompressible flow of Newtonian fluid and the effect of gravity is ignored, RANS equations can be written as:

$$\frac{\partial \bar{u}_i}{\partial t} + \bar{u}_j \frac{\partial \bar{u}_i}{\partial x_j} = -\frac{1}{\rho}\frac{\partial \bar{p}}{\partial x_i} + \frac{1}{\rho}\frac{\partial}{\partial x_j}\left(\mu \frac{\partial \bar{u}_i}{\partial x_j} - \rho \overline{u_i' u_j'} \right) \qquad (2.11)$$

where x is vector component, $\bar{p}$ is the mean value of pressure in N/m^2, ρ is density in kg/m^3 and t is time in s. From the viscous term in equation (2.11), the turbulent shear stress becomes:

$$\tau_{ij} = \mu \frac{\partial \bar{u}_i}{\partial x_j} - \rho \overline{u_i' u_j'} \quad ; i \neq j \qquad (2.12)$$

The difference between shear stress of laminar flow and turbulent flow is the extra stress terms $(-\rho \overline{u_i' u_j'})$ which are called the Reynolds stresses. These stresses involve the fluctuating velocity of the flow. The Reynolds stress is dominant except the near wall region. Therefore, in the turbulent flow, the Reynolds stress is a good approximation for the shear stress except in the vicinity of a solid boundary. Consequently, the wall shear stress is given by:

$$\tau_w = \mu \left(\frac{du}{dy} \right)_{y=0} \qquad (2.13)$$

There are many researches in various fields which study about wall shear stress, for example in biomedical engineering, food engineering, etc. In biomedical engineering, wall shear stress is one parameter that relates to flow characteristics in blood vessel or in the airways of body. Thus, the behavior of wall shear stress of flow in arteries and in the airways of the lung were studied (Green, 2004; Ooi, Blackburn, Zhu, Lui, and Tae; 2007). In cleaning in place system of food processing, shear stress of fluid flow is one important factor that helps to remove the deposits from the equipment surface by breaking down the swollen deposit layer, especially in uniform and decay cleaning stage. Shear stress increases with the flow velocity, turbulent flow can generate greater shear stress at the wall or deposit layer than laminar flow. Reverse flow that causes by oscillatory flow and pulsating flow also increase wall shear stress. Qi, Scott, and Willson (2008) modeled the laminar pulsating flow of an incompressible Newtonian fluid through rectangular duct using Green functions. The characteristics of pulsed flow were controlled by the periodic pressure gradient. The analytical solutions were obtained in the form of Green function for volumetric flow rate, velocity distribution and wall shear stress distribution. From the calculation, the various flow effects over one period of pulsation were investigated. In one period, there was the appearance of bulk flow reversal at sometime over a cycle. The flow reversal started in some regions, especially near wall region, then, followed by the flow reversal in the whole cross-section. From the comparison of wall shear stress between the steady flow and pulsed flow, the maximum wall shear stress of pulsed flow was greater than the steady flow. For low period, there was a phase lag between the flow rate and pressure gradient approached 90°, whereas, the phase of wall shear stress shifted 45° respect to the periodic pressure gradient. However, when the period

became larger, all phase lag and shift disappeared. Moreover, from the solutions, it could be concluded that the flow reversal in pulsating flow and phase lag or shift were determined by the properties of the fluid, the dimensions of duct and the parameters of pressure gradient. The study of Qi et al. can be confirmed by the experiment of Blel et al. (2009). They studied the effect of turbulent pulsating flow on mean wall shear stress and the fluctuation energy of the shear rate. This studied investigated the flow in a straight pipe using electrochemical measurement and spectral analysis to measure wall shear stress and the fluctuation energy of the shear rate, respectively. The turbulent pulsating flows were characterized by the pulsations parameter (mean velocity, amplitude and frequency). Pulsating flows were generated by solenoid valve in pulsation generator system. The range of amplitude and frequency of pulsed flow were 0-0.81 m/s and 0-2.86 Hz, respectively. The effects of pulsating flow were compared to the steady flow. As the results of the study, with the same mean velocity of flow, pulsating flow generated greater mean wall shear stress and the fluctuation energy of the shear rate than steady flow. Wall shear stress increased with mean velocity of the flow. At the same time, both of amplitude and frequency induced higher wall shear stress and fluctuation energy of the shear rate respect to the steady flow. But frequency of pulsation was more effective on the shear stress than amplitude of pulsation. The amplitude had the significant effect on wall shear stress when the mean velocity is low. In addition, the recirculation flow at the center core of pipe also induced high fluctuation energy of the shear rate. In addition, there are some previous studies relating to wall shear stress analysis:

Mao and Hanratty (1986) measured the time variation of wall shear stress imposed by sinusoidal turbulent pulsating flows in a pipe. The pulsating flows were characterized by the oscillation of pressure gradient with high frequency and low amplitude. The wall shear stress variation was measured by using electrochemical technique which gave the relationship between mass transfer of species in the flow and the velocity gradient at the wall or wall shear stress. The results of the study showed that the imposed oscillation of pressure gradient had no effect on the time-mean velocity gradient at the wall. The time-average intensities of turbulent fluctuations of velocity gradient at the wall were independent of Reynolds number and the oscillation of pressure gradient. Both of phase averaged velocity gradient and the intensity of velocity gradient at the wall were shifted from the phase averaged pressure gradient. Moreover, the amplitude and phase of the velocity gradient at the wall also shifted to the imposed oscillation.

Nishimura and Matsune (1998) used finite element method to study the behavior of vortices generated by pulsed flow in asymmetric and symmetric channel. The study showed that there was rotating vortex in furrow of channel. The channel geometry affected on the behavior of vortices. The vortex expanded in each furrow during deceleration phase and shrank during the acceleration phase. The frequency of pulsed flow affected on the vortex strength. An increment of frequency led to promote vortex strength which caused higher wall shear stress.

Metwally and Manglik (2004) studied the effect of corrugated-plate channel geometry and Reynolds number on the flow field and local wall shear stress. The steady laminar flows of viscous Newtonian fluids were studied by using finite difference methods. To study the effect of channel geometry, the channel geometry

was described by the corrugation aspect ratio from 0 to 1. Meanwhile, the Reynolds number was varied from 10 to 1000 when the effect of Reynolds number was considered. Their results showed that with increasing corrugation aspect ratio, the furrow of the channel was deeper, swirl flows were generated in the corrugation troughs. The peak wall shear stress increased with the corrugation aspect ratio as well. At the same time, the increase of Reynolds produced similar effect as the increasing of corrugation aspect ratio.

Jensen, Friis, Bénézech, Legentilhomme, and Lelièvre (2005) predicted local wall shear stress variations by using computational fluid dynamics (CFD). The steady turbulent flow was flowed through the pipe with various diameter changes (gradual and sudden expansions and contractions). Predicted wall shear stress by CFD code (STAR-CD) was compared with the actual wall shear stress which measured by electrochemical technique. For wall shear stress prediction, the Reynolds average Navier-Stokes (RANS) RNG k-ε model was chosen for turbulence modeling. The performance of near wall modeling between two-layer model and wall function was also studied. As the results of the study, There was a good agreement of the trend of the variation of mean wall shear stress and wall shear stress fluctuation along the pipe between the prediction and the measured data. The variation of mean wall shear stress and wall shear stress fluctuation could be seen explicitly at the expansion and contraction part of the pipe. The two-layer model provided better qualitative comparison to the measured data than wall function model.

The previous studies that relate to pulsating flow and wall shear stress analysis are summarized in appendix A (Table A.1).

2.5   Conclusion

The literature review of fouling shows the type of fouling, the significant effects of fouling on the heat exchanger efficiency and the study of fouling in dairy process. These are the initiation of the cleaning process. From the cleaning procedure, it showed that fluid flow is one factor that affects the cleaning rate. To enhance the cleaning efficiency, pulsating flow can be one application of the fluid flow adjustment of CIP system. But the effect of type of pulsed flow on the cleaning efficiency has not found in the literature survey. Meanwhile, wall shear stress is one parameter that helps to remove the deposits from the equipment surface by breaking down the swollen deposit layer. It is also enhanced by oscillatory and pulsating flow. Thus, the effect of types of pulsed flow on wall shear stress that implicitly indicates the cleaning efficiency was considered to be the main objective of this study.

CHAPTER III

MATHEMATICAL MODELS

This section focuses on the mathematical models that describe the physical phenomena of fluid flows in the study system. The physical phenomena of fluid flow are described by mathematical models that base on the conservation of mass and momentum. In this section, the mass and momentum conservation equations are presented first. Because this study focuses on the turbulent flow, the mean flow and the effect of turbulence on mean flow properties are also considered. Thus, the mass and momentum conservation equations of turbulent flow which can be written in the Cartesian form of Reynolds-averaged Navier-Stokes (RANS) equations and the turbulence models with near wall treatment will be presented later.

3.1   Mass Conservation Equation

The general form of the mass conservation equation for the case that there is no mass source in the system is given by:

$$\frac{\partial \rho}{\partial t} + \frac{\partial}{\partial x_i}\left(\rho u_i\right)$$
(3.1)

where ρ is density in kg/m^3, u_i is the instantaneous velocity component in m/s, x is vector component and t is time in s.

3.2   Momentum Conservation Equation

The general form of the momentum conservation equation for the case that there is no momentum source in the system is described by:

$$\frac{\partial(\rho u_i)}{\partial t} + u_j \frac{\partial(\rho u_i)}{\partial x_j} = \rho g_i - \frac{\partial p}{\partial x_i} + \frac{\partial}{\partial x_j}\left(\mu \frac{\partial u_i}{\partial x_j}\right)$$

(3.2)

where ρg is the gravitational body force in N/m^2, p is the mean value of pressure in N/m^2 and μ is the dynamics viscosity in N.s/m^2.

3.3   Reynolds-averaged Navier-Stokes (RANS) Equations

When there is the appearance of turbulent fluctuations in the system, the velocity and all other flow properties vary randomly with time. The easy way to describe the phenomena of turbulent flow is to define the velocity and other flow properties in the composition of mean component and a time varying fluctuating component. Therefore, the instantaneous velocity can be decomposed into a steady mean value and a fluctuating component as in equation (3.3):

$$u_i = \overline{u}_i + u_i^{'}$$

(3.3)

where, u_i is the instantaneous velocity component in m/s, $\bar{u}_i$ is the steady mean velocity component in m/s and $u_i^{'}$ is the fluctuating velocity component in m/s.

Because of the effect of turbulent fluctuations, the mass and momentum conservation equation can be written in the time-averaged form:

$$\frac{\partial \rho}{\partial t} + \frac{\partial}{\partial x_i}\left(\rho \overline{u_i}\right)$$
(3.4)

$$\frac{\partial(\rho \overline{u_i})}{\partial t} + u_j \frac{\partial(\rho \overline{u_i})}{\partial x_j} = \rho g_i - \frac{\partial \overline{p}}{\partial x_i} + \frac{\partial}{\partial x_j}\left(\mu \frac{\partial \overline{u_i}}{\partial x_j} - \rho \overline{u_i' u_j'}\right)$$
(3.5)

Equation (3.4) and (3.5) are called Reynolds-averaged Navier-Stokes (RANS) equations. The additional terms that represent the effect of turbulent fluctuations, $-\rho \overline{u_i' u_j'}$, which are called the Reynolds stresses. The Reynolds stress can be related to the mean velocity gradients by using Boussinesq hypothesis as in equation (3.6):

$$-\rho \overline{u_i' u_j'} = \mu_t \left(\frac{\partial u_i}{\partial x_j} + \frac{\partial u_j}{\partial x_i}\right) - \frac{2}{3}\left(\rho k + \mu_t \frac{\partial u_k}{\partial x_k}\right)\delta_{ij}$$
(3.6)

where μ_t is the turbulent viscosity in kg/m.s, k is the turbulent kinetic energy in m^2/s^2 and δ_{ij} is the kronecker delta. The turbulent viscosity, μ_t, in equation (3.6) can be determined from turbulent kinetic energy, k, turbulent dissipation rate, ε and the specific dissipation rate, ω. These are obtained from k-ε and k-ω turbulence models.

3.4   Turbulence Models

3.4.1 Standard k-ε Model

The standard k-ε model is a semi-empirical model based on model transport equations for the turbulent kinetic energy (k) and its dissipation rates (ε) which are presented in equation (3.7) and (3.8), respectively:

$$\rho \frac{Dk}{Dt} = \frac{\partial}{\partial x_j}\left[\left(\mu + \frac{\mu_t}{\sigma_k}\right)\frac{\partial k}{\partial x_j}\right] + \mu_t S^2 - \rho\varepsilon \tag{3.7}$$

$$\rho \frac{D\varepsilon}{Dt} = \frac{\partial}{\partial x_j}\left[\left(\mu + \frac{\mu_t}{\sigma_\varepsilon}\right)\frac{\partial \varepsilon}{\partial x_j}\right] + \frac{\varepsilon}{k}\left(C_{1\varepsilon}\mu_t S^2 - \rho C_{2\varepsilon}\varepsilon\right) \tag{3.8}$$

where

$$S = \sqrt{2S_{ij}S_{ij}} \tag{3.9}$$

$$S_{ij} = \frac{\partial u_j}{\partial x_i} + \frac{\partial u_i}{\partial x_j} \tag{3.10}$$

where ε is the turbulent dissipation rate in m^2/s^3. S is the deformation tensor in 1/s, S_{ij} is the mean strain rate in 1/s, σ_k and σ_ε are the turbulent Prandtl numbers for k and ε, respectively. $C_{1\varepsilon}$ and $C_{2\varepsilon}$ are constants.

The turbulent viscosity, μ_t, is computed by combining k and ε as follows:

$$\mu_t = \rho C_\mu \frac{k^2}{\varepsilon} \tag{3.11}$$

where C_μ is a constant.

The model constants have the default values that determined from benchmark experiments of simple flows using air and water as follows:

$\sigma_k = 1.0$, $\sigma_\varepsilon = 1.3$, $C_{1\varepsilon} = 1.44$, $C_{2\varepsilon} = 1.92$ and $C_\mu = 0.09$.

3.4.2 RNG k-ε Model

The RNG k-ε model was derived using renormalization group theory. The transport equation of the turbulent kinetic energy, k is similar to the standard k-ε model as in equation (3.12). But the significant difference between standard and RNG k-ε models is the additional strain rate term in the transport equation of the turbulent dissipation rate, ε, as in equation (3.13), (3.15) and (3.16):

$$\rho \frac{Dk}{Dt} = \frac{\partial}{\partial x_j}\left(\alpha_k \mu_{eff} \frac{\partial k}{\partial x_j}\right) + \mu_t S^2 - \rho\varepsilon \tag{3.12}$$

$$\rho \frac{D\varepsilon}{Dt} = \frac{\partial}{\partial x_j}\left(\alpha_\varepsilon \mu_{eff} \frac{\partial \varepsilon}{\partial x_j}\right) + \frac{\varepsilon}{k}\left(C_{1\varepsilon}\mu_t S^2 - \rho C_{2\varepsilon}^* \varepsilon\right) \tag{3.13}$$

where

$$\mu_{eff} = \mu + \mu_t \tag{3.14}$$

$$C_{2\varepsilon}^* = C_{2\varepsilon} + \frac{C_\mu \rho \eta^3\left(1 - \dfrac{\eta}{\eta_0}\right)}{1 + \beta\eta^3} \tag{3.15}$$

$$\eta = S\frac{k}{\varepsilon} \tag{3.16}$$

where μ_{eff} is the effective viscosity in kg/m.s. η_0 and β are constants.

For the RNG k-ε model, the model constants have the default values as follows: $\sigma_k = 1.393$, $\sigma_\varepsilon = 1.393$, $C_{1\varepsilon} = 1.42$, $C_{2\varepsilon} = 1.68$, $C_\mu = 0.0845$, $\eta_0 = 4.38$ and $\beta = 0.012$.

The RNG k-ε model also includes the effects of swirl or rotation by modifying the turbulent viscosity as the following functional form:

$$\mu_t = \mu_{t0}\, f\left(\alpha_s, \Omega, \frac{k}{\varepsilon}\right) \tag{3.17}$$

where μ_{t0} is the turbulent viscosity without swirl modification in kg/m.s, α_s is a swirl constant which its default value is set to 0.07 and Ω is a characteristic swirl number.

3.4.3 Realizable k-ε model

The transport equation of the turbulent kinetic energy, k, is same as the standard k-ε model as in equation (3.18). Meanwhile, the transport equation of the turbulent dissipation rate, ε, is based on a transport equation for the mean-square vorticity fluctuation as in equation (3.19):

$$\rho \frac{Dk}{Dt} = \frac{\partial}{\partial x_j}\left[\left(\mu + \frac{\mu_t}{\sigma_k}\right)\frac{\partial k}{\partial x_j}\right] + \mu_t S^2 - \rho\varepsilon \tag{3.18}$$

$$\rho \frac{D\varepsilon}{Dt} = \frac{\partial}{\partial x_j}\left[\left(\mu + \frac{\mu_t}{\sigma_\varepsilon}\right)\frac{\partial \varepsilon}{\partial x_j}\right] + C_1 S \rho\varepsilon - C_2 \frac{\rho\varepsilon^2}{k + \sqrt{v\varepsilon}} \tag{3.19}$$

where

$$C_1 = \max\left[0.43, \frac{\eta}{\eta + 5}\right] \qquad (3.20)$$

The model constants have the default values as follows: $\sigma_k = 1.0$, $\sigma_\varepsilon = 1.2$ and $C_2 = 1.9$.

Another difference between the realizable k-ε model and the standard and RNG k-ε model is that the realizable k-ε model contains a new formulation for the turbulent viscosity. This model can satisfy the mathematical constraints on the Reynolds stresses. The turbulent viscosity, μ_t, is obtained from the same formula as in the standard k-ε model, but C_μ is no longer constant. It is computed from:

$$C_\mu = \frac{1}{A_0 + A_s \dfrac{kU^*}{\varepsilon}} \qquad (3.21)$$

where

$$U^* \equiv \sqrt{S_{ij}S_{ij} + \tilde{\Omega}_{ij}\tilde{\Omega}_{ij}} \qquad (3.22)$$

$$\tilde{\Omega}_{ij} = \Omega_{ij} - 2\varepsilon_{ijk}\omega_k \qquad (3.23)$$

$$\Omega_{ij} = \overline{\Omega_{ij}} - \varepsilon_{ijk}\omega_k \qquad (3.24)$$

where $\overline{\Omega_{ij}}$ is the mean rate of rotation tensor, ω_k is the angular velocity in rad. The model constant A_0 equals to 4.04 and A_s is given by:

$$A_s = \sqrt{6}\cos\phi \qquad (3.25)$$

where

$$\phi = \frac{1}{3}\cos^{-1}\left(\sqrt{6}W\right) \qquad (3.26)$$

$$W = \frac{S_{ij}S_{jk}S_{ki}}{\tilde{S}^3} \qquad (3.27)$$

$$\tilde{S} = \sqrt{S_{ij}S_{ij}} \qquad (3.28)$$

3.4.4 Standard k-ω model

The standard k-ω model is an empirical model based on model transport equation of the turbulent kinetic energy, k, and the specific dissipation rate, ω which are computed from the following transport equations:

$$\rho\frac{Dk}{Dt} = \frac{\partial}{\partial x_j}\left[\left(\mu + \frac{\mu_t}{\sigma_k}\right)\frac{\partial k}{\partial x_j}\right] + \mu_t S^2 - \rho\beta^* f_{\beta^*} k\omega \qquad (3.29)$$

$$\rho\frac{D\omega}{Dt} = \frac{\partial}{\partial x_j}\left[\left(\mu + \frac{\mu_t}{\sigma_\omega}\right)\frac{\partial\omega}{\partial x_j}\right] + \alpha\frac{\omega}{k}\mu_t S^2 - \rho\beta f_\beta\omega^2 \qquad (3.30)$$

where

$$f_{\beta^*} = \begin{cases} 1 & \chi_k \le 0 \\ \dfrac{1 + 680\chi_k^2}{1 + 400\chi_k^2} & \chi_k > 0 \end{cases} \qquad (3.31)$$

$$\chi_k = \frac{1}{\omega^3}\frac{\partial k}{\partial x_j}\frac{\partial \omega}{\partial x_j} \tag{3.32}$$

$$\beta^* = \beta_i^*[1 + \xi^* F(M_t)] \tag{3.33}$$

$$\beta_i^* = \beta_\infty^*\left(\frac{4/15 + (\mathrm{Re}_t/R_\beta)^4}{1 + (\mathrm{Re}_t/R_\beta)^4}\right) \tag{3.34}$$

$$\mathrm{Re}_t = \frac{\rho k}{\mu\omega} \tag{3.35}$$

and

$$\alpha = \frac{\alpha_\infty}{\alpha^*}\left(\frac{\alpha_0 + \mathrm{Re}_t/R_\omega}{1 + \mathrm{Re}_t/R_\omega}\right) \tag{3.36}$$

$$\alpha^* = \alpha_\infty^*\left(\frac{(\beta_i/3) + \mathrm{Re}_t/R_k}{1 + \mathrm{Re}_t/R_k}\right) \tag{3.37}$$

$$f_\beta = \frac{1 + 70\chi_\omega}{1 + 80\chi_\omega} \tag{3.38}$$

$$\chi_\omega = \left|\frac{\Omega_{ij}\Omega_{ij}S_{ki}}{(\beta_\infty^*\omega)^3}\right| \tag{3.39}$$

$$\Omega_{ij} = \frac{1}{2}\left(\frac{\partial u_i}{\partial x_j} - \frac{\partial u_j}{\partial x_i}\right) \tag{3.40}$$

$$\beta = \beta_i \left[1 - \frac{\beta_i^*}{\beta_i} \zeta^* F(M_i) \right] \tag{3.41}$$

where $F(M_t)$ is the compressibility function which is given by:

$$F(M_t) = \begin{cases} 0 & M_t \le M_{t0} \\ M_t^2 - M_{t0}^2 & M_t > M_{t0} \end{cases} \tag{3.42}$$

$$M_t^2 \equiv \frac{2k}{a^2} \tag{3.43}$$

where a is a speed of sound in m/s.

The turbulent viscosity, μ_t, is obtained from the combination of k and ω as follows:

$$\mu_t = \alpha^* \frac{\rho k}{\omega} \tag{3.42}$$

The model constants have the default values as follows: $\alpha_\infty^* = 1$, $\alpha_\infty = 0.52$, $\alpha_0 = 1/9$, $\beta_\infty^* = 0.09$, $\beta_i = 0.072$, $R_\beta = 8$, $R_k = 6$, $R_\omega = 2.95$, $\zeta^* = 1.5$, $M_{t0} = 0.25$, $\sigma_k = 2.0$ and $\sigma_\omega = 2.0$.

3.4.5 Shear-Stress Treansport (SST) k-ω model

The SST k-ω model derived from the blending of the accurate formulation of the k-ω model and the free-stream independence of the k-ε model in the far field. The transport equations of the turbulent kinetic energy, k, and the specific dissipation rate, ω, are presented in the following equations:

$$\rho \frac{Dk}{Dt} = \frac{\partial}{\partial x_j}\left[\left(\mu + \frac{\mu_t}{\sigma_k}\right)\frac{\partial k}{\partial x_j}\right] + \min(\mu_t S^2, 10\rho\beta^* k\omega) - \rho\beta^* k\omega \qquad (3.43)$$

$$\rho \frac{D\omega}{Dt} = \frac{\partial}{\partial x_j}\left[\left(\mu + \frac{\mu_t}{\sigma_\omega}\right)\frac{\partial \omega}{\partial x_j}\right] + \alpha\rho S^2 - \rho\beta\omega^2 + 2(1-F_1)\rho\sigma_{\omega,2}\frac{1}{\omega}\frac{\partial k}{\partial x_j}\frac{\partial \omega}{\partial x_j} \quad (3.44)$$

where

$$\alpha_k = \frac{1}{F/_1 \sigma_{k,1} + (1-F_1)/\sigma_{k,2}} \qquad (3.45)$$

$$\alpha_\omega = \frac{1}{F/_1 \sigma_{\omega,1} + (1-F_1)/\sigma_{\omega,2}} \qquad (3.46)$$

$$F_1 = \tanh(\Phi_1^4) \qquad (3.47)$$

$$\Phi_1 = \min\left[\max\left(\frac{\sqrt{k}}{0.09\omega y}, \frac{500\mu}{\rho y^2 \omega}\right), \frac{4\rho k}{\sigma_{\omega,2} D_\omega^+ y^2}\right] \qquad (3.48)$$

$$D_\omega^+ = \max\left[2\rho\frac{1}{\sigma_{\omega,2}}\frac{1}{\omega}\frac{\partial k}{\partial x_j}\frac{\partial \omega}{\partial x_j}, 10^{-10}\right] \qquad (3.49)$$

where y is the distance next to the surface in m.

Meanwhile, β^*, α and β are computed as same as the standard k-ω model in equation (3.33), (3.36) and (3.41), respectively. But for the SST k-ω model, α_∞ in the equation (3.36) is defined as the following equation:

$$\alpha_\infty = F_1\alpha_{\infty,1} + (1 - F_1)\alpha_{\infty,2} \tag{3.50}$$

and

$$\alpha_{\infty,1} = \frac{\beta_{i,1}}{\beta_\infty^*} - \frac{\kappa^2}{\sigma_{\omega,1}\sqrt{\beta_\infty^*}} \tag{3.51}$$

$$\alpha_{\infty,2} = \frac{\beta_{i,2}}{\beta_\infty^*} - \frac{\kappa^2}{\sigma_{\omega,2}\sqrt{\beta_\infty^*}} \tag{3.52}$$

where κ is the von Kármán constant (0.4187).

As same as α_∞, for the SST k-ω model, β_i in the equation (3.41) is given by:

$$\beta_i = F_1\beta_{i,1} + (1 - F_1)\beta_{i,2} \tag{3.53}$$

Another difference between the standard k-ω model and the SST k-ω model is that the turbulent viscosity, μ_t, in the SST k-ω model is computed as follows:

$$\mu_t = \frac{\rho k}{\omega} \frac{1}{\max\left[\dfrac{1}{\alpha^*}, \dfrac{SF_2}{a_1\omega}\right]} \tag{3.54}$$

where α^* can be obtained from equation (3.37) and F_2 is given by:

$$F_2 = \tanh(\Phi_2^2) \tag{3.55}$$

$$\Phi_2 = \max\left[2\frac{\sqrt{k}}{0.09\omega y}, \frac{500\mu}{\rho y^2 \omega}\right] \qquad (3.56)$$

The default values of model constants are defined as follows: $\alpha_{k,1} = 1.176$, $\alpha_{\omega,1} = 2.0$, $\alpha_{k,2} = 1.0$, $\alpha_{\omega,2} = 1.168$, $a_1 = 0.31$, $\beta_{i,1} = 0.075$ and $\beta_{i,2} = 0.0828$.

3.5   Near Wall Treatment and Wall Boundary Conditions

The appearance of the wall directly affects the mean velocity and other flow properties that describe the transport phenomena of fluid flow. In the near wall region, viscous damping reduces the tangential velocity fluctuations, while kinematic blocking reduces the normal fluctuations. Therefore, the accurate predictions of wall-bounded turbulent flows are essential.

3.5.1 Enhance Wall Treatment

The k-ε models are only valid for turbulent core flows; they need the additional near wall treatment to describe wall-bounded turbulent flows. Based on the viscous sub-layer region that needs to be resolved in this work, the flow is almost laminar and the viscosity has a major effect on the momentum, heat and mass transfer. The enhance wall treatment was chosen to predict wall-bounded turbulent flows.

Enhance wall treatment predicts turbulent flows in the near wall region by the combination of a two-layer model and enhance wall functions. The two-layer model is used to determine the near-wall ε field and μ_t .

In the two-layer models, the turbulent viscosity, μ_t, is evaluated by the length scale, l_μ, as in the following equations:

$$\mu_t = \rho C_\mu l_\mu \sqrt{k} \tag{3.57}$$

where

$$l_\mu = y C_l^* (1 - e^{-\mathrm{Re}_y/A_\mu}) \tag{3.58}$$

$$C_l^* = \kappa C_\mu^{-3/4} \tag{3.59}$$

$$\mathrm{Re}_y \equiv \frac{\rho y \sqrt{k}}{\mu} \tag{3.60}$$

and $\quad A_\mu = 70$

where y is the normal distance from the wall at the cell centers in m and Re_y is the turbulent Reynolds number based on the wall distance.

The near-wall ε field is also computed by the length scales, l_ε, as follows:

$$\varepsilon = \frac{k^{3/2}}{l_\varepsilon} \tag{3.61}$$

where

$$l_\varepsilon = y C_l^* (1 - e^{-\mathrm{Re}_y/A_\varepsilon}) \tag{3.62}$$

$$A_\varepsilon = 2 C_l^* \tag{3.63}$$

Meanwhile, momentum boundary condition bases on blended law-of-the-wall by Kader (1981) in the enhance wall functions which were developed by smoothly blending an enhanced turbulent wall with laminar wall law as follows:

$$u^+ = e^\Gamma u^+_{lam} + e^{\frac{1}{\Gamma}} u^+_{turb} \tag{3.64}$$

where u^+ is the dimensionless velocity which is defined as follows:

$$u^+ = \frac{u}{U_\tau}; \quad U_\tau = \sqrt{\frac{\tau_w}{\rho}} \tag{3.65}$$

where U_τ is the friction velocity in m/s, τ_w is wall shear stress in N/m2. And the blending function in equation (3.64) is given by:

$$\Gamma = -\frac{a(y^+)^4}{1 + by^+} \tag{3.66}$$

where a=0.01, b=5 and y^+ is the dimensionless distance from the wall which is defined as follows:

$$y^+ = \frac{\rho y U_\tau}{\mu} \tag{3.67}$$

When the effect of pressure gradients and thermal are counted, the enhance wall functions can be modified using the approaches of White and Christoph (1997) as shown in the form of the derivative $\frac{du^+}{dy^+}$:

$$\frac{du^+}{dy^+} = e^{\Gamma} \frac{du^+_{lam}}{dy^+} + e^{\frac{1}{\Gamma}} \frac{du^+_{turb}}{dy^+} \qquad (3.68)$$

where

$$\frac{du^+_{turb}}{dy^+} = \frac{1}{\kappa y^+} \left[\left(1 + \alpha y^+\right)\left(1 - \beta u^+ - \gamma (u^+)^2\right) \right]^{1/2} \qquad (3.69)$$

$$\alpha \equiv \frac{\mu}{\rho^2 U_\tau^3} \frac{dp}{dx} \qquad (3.70)$$

$$\beta \equiv \frac{\sigma_t q_w}{\rho c_p U_\tau T_w} \qquad (3.71)$$

$$\gamma \equiv \frac{\sigma_t U_\tau^2}{2 c_p T_w} \qquad (3.72)$$

where q_w is heat at the wall in J, c_p is the specific heat capacity of fluid in J/kg.K, T_w is the temperature of the wall, K and σ_t is the model constant.

3.5.2 Wall boundary conditions

For the k-ω models, they provide the sufficient resolution to predict the flow in near wall region. The wall boundary conditions for the k equation correspond to the wall function approach as same as the k-ε models, while the value of ω at the wall is defined as follows:

$$\omega_w = \frac{\rho U_\tau^2}{\mu} \omega^+ \qquad (3.73)$$

where ω^+ in the laminar sublayer is given by:

$$\omega^+ = \min\left(\omega_w^+, \frac{6}{\beta_i(y^+)^2}\right) \tag{3.74}$$

$$\omega_w^+ = \begin{cases} \left(\dfrac{50}{k_s^+}\right)^2 & k_s^+ < 25 \\[2ex] \dfrac{100}{k_s^{100}} & k_s^+ \geq 25 \end{cases} \tag{3.75}$$

$$k_s^+ = \max\left(1.0, \frac{\rho k_s U_\tau}{\mu}\right) \tag{3.76}$$

where k_s is the roughness height in m.

and the value of ω^+ in the laminar sublayer is given by:

$$\omega^+ = \frac{1}{\sqrt{\beta_\infty^*}} \frac{du_{turb}^+}{dy^+} \tag{3.77}$$

3.6   Conclusion

In this section, the conservation equations of mass and momentum, including the Reynolds-averaged Navier-Stokes (RANS) equations, the turbulence models (k-ε and k-ω models), near wall treatment and wall boundary conditions that describe the transport phenomena of turbulent flow in this work were presented. In this study, these equations were solved through the mesh elements by the space and time discretization of the finite volume method in the commercial software (FLUENT®6.3.26).

CHAPTER IV

RESEARCH METHODS

This thesis aims to study the influence of type of pulsed flow, pulsation parameters and the geometry of channel flow on wall shear stress. To approach the objectives of this thesis, the apparatus that used in this work and the study methods will be described in the following section. Then, the statistical methods and the simulation methods of the FLUENT 6.3.26 will be focused later.

4.1 Apparatus

In this study, the following apparatus were used:

(1) The HP Pavilion a63851 Home PC: Intel$^{®}$ Core^{TM} 2 Duo Processor E6550 2.33 GHz with 2.00 GB of RAM.

(2) SUT-High Performance Computing Cluster (SUT-HPCC): Parallel Processing 100 Intel$^{®}$ Xeon$^{®}$ CPUs 45408 MHz with 111262 MB of RAM.

(3) An operating system of Microsoft Windows XP Professional version 2007-2008 Service Pack 2 for the personal computer and the operating system of Linux for the SUT-HPCC.

(4) The commercial software: GAMBIT^{TM}, FLUENT$^{®}$6.3.26, Microsoft Office Professional Edition 2003 and 2007.

4.2   Study Methods

The following methods are used to achieve the objectives of this thesis:

4.2.1 Wall Shear Stress Prediction

This section aims to test the response of the commercial software FLUENT®6.3.26 on wall shear stress generated by pulsating flows. This section consists of the turbulence model testing and wall shear stress prediction. The turbulence model testing was investigated to find the suitable turbulent model for wall shear stress analysis. Meanwhile, wall shear stress prediction was studied in order to find the pulsating conditions that are suitable for the program to analyze the wall shear stress.

4.2.1.1   The Turbulent Model Testing

In this section, Standard k-ε, RNG k-ε, Realizable k-ε model, Standard k-ω and SST k-ω model were employed to predict wall shear stress of sinusoidal pulsating flow with mean velocity 1.47 m/s, amplitude 0.4 m/s and frequency 2.5 Hz. The cylindrical pipe was used to be the flow domain. The numerical data of mean wall shear stress of pulsed flows was compared to the experimental data of Blel et al. (2009). The turbulent model that predicted the closest mean wall shear stress was used in wall shear stress prediction and wall shear stress analysis of pulsed flows.

4.2.1.2   Wall Shear Stress Prediction

The most suitable turbulent model from the turbulent model testing was employed to predict mean wall shear stress generated by sinusoidal pulsating flows in the cylindrical pipe. The pulsating conditions were shown in Table 4.1. Fluid properties and flow condition based on the experiment of Blel et al. (2009).

The numerical data of mean wall shear stress of pulsed flows was compared to the experimental data. The pulsating conditions that program gave the closest results compared to the experimental data were chosen to control the characteristics of pulsating flow for wall shear stress analysis.

Table 4.1 Hydrodynamic parameters for each pulsating condition

Sample	Mean velocity (m/s)	Amplitude of pulsations (m/s)	Frequency of pulsation (Hz)
A	1.47	0.40	2.50
B	1.21	0.73	2.50
C	1.03	0.60	2.86
D	1.02	0.81	1.66
E	0.78	0.73	2.50
F	1.47	0.00	0.00

4.2.2 The Effect of Type of Pulsed Flow on Wall Shear Stress

The following types of flows were studied:

(1) Steady flow

(2) Pulsed flow – Rectangular waveform

(3) Pulsed flow – Saw tooth waveform

(4) Pulsed flow – Sinusoidal waveform

(5) Pulsed flow – Trapezoidal waveform

(6) Pulsed flow – Triangular waveform

From wall shear stress prediction, the characteristics of pulsed flows were controlled by pulsation parameters which are suitable to simulate by FLUENT® 6.3.26 as shown in Table 4.2. Pulsed flows were simulated in the cylindrical pipe,

parallel plates and corrugated channel of plate heat exchanger. To investigate the effect of type of pulsating flow on wall shear stress, wall shear stresses of different pulsating flows were compared under the same pulsating condition, flow domain, flow condition and length of time by using statistical procedure.

Table 4.2 Hydrodynamic parameters for the study of the effect of type of pulsation on wall shear stress

Sample	Mean velocity (m/s)	Amplitude of pulsations (m/s)	Frequency of pulsation (Hz)
B*	1.21	0.73	2.50
C	1.03	0.60	2.86
D*	1.02	0.81	1.66

Remark: *are cases that are studied in parallel plates and channel of plate heat exchanger.

4.2.3 The Effect of Amplitude of Pulsation on Wall Shear Stress

Sinusoidal pulsating flows with pulsating condition as shown in Table 4.3 were simulated in cylindrical pipe, parallel plates and corrugated channel of plate heat exchanger. Mean wall shear stresses generated by pulsed flow with different amplitude of pulsation were compared under the same mean velocity inlet, frequency of pulsation, flow domain, flow condition and length of time. The results of the study were in the form of the relationship between wall shear stress and the amplitude of pulsation.

4.2.4 The Effect of Frequency of Pulsation on Wall Shear Stress

Sinusoidal pulsating flows with pulsating condition as shown in Table 4.4 were simulated in cylindrical pipe, parallel plates and corrugated channel of plate heat exchanger. Mean wall shear stresses generated by pulsed flow with different frequency of pulsation were compared under the same mean velocity inlet, amplitude of pulsation, flow domain, flow condition and length of time. The results of the study were in the form of the relationship between wall shear stress and the frequency of pulsation.

Table 4.3 Hydrodynamic parameters for each pulsating condition that studied the effect of amplitude of pulsation on wall shear stress

Sample	Mean velocity (m/s)	Amplitude of pulsations (m/s)	Frequency of pulsation (Hz)
G*	1.02	0.20	1.66
H*	1.02	0.40	1.66
I	1.02	0.50	1.66
J*	1.02	0.60	1.66
K	1.02	0.70	1.66
D*	1.02	0.81	1.66

Remark: *are cases that are studied in parallel plates and channel of plate heat exchanger.

Table 4.4 Hydrodynamic parameters for each pulsating condition that studied the

effect of frequency of pulsation on wall shear stress

Sample	Mean velocity (m/s)	Amplitude of pulsations (m/s)	Frequency of pulsation (Hz)
L	1.02	0.81	1.00
D	1.02	0.81	1.66
M	1.02	0.81	2.50
N	1.02	0.81	2.86

4.2.5 The Effect of Mean Velocity of Pulsation on Wall Shear Stress

Sinusoidal pulsating flows with pulsating condition as shown in Table 4.5 were simulated in cylindrical pipe, parallel plates and corrugated channel of plate heat exchanger. Mean wall shear stresses generated by pulsed flow with different mean velocity inlet of pulsation were compared under the same amplitude, frequency of pulsation, flow domain, flow condition and length of time. The results of the study were in the form of the relationship between wall shear stress and mean velocity inlet of pulsation.

Table 4.5 Hydrodynamic parameters for each pulsating condition that studied the

effect of mean velocity inlet of pulsation on wall shear stress

Sample	Mean velocity (m/s)	Amplitude of pulsations (m/s)	Frequency of pulsation (Hz)
O	0.78	0.73	2.50
P	1.02	0.73	2.50
B	1.21	0.73	2.50
Q	1.54	0.73	2.50

4.2.6 The Effect of Geometry of Flow Channel on Wall Shear Stress

With the same type of pulsed flow, pulsating conditions, flow condition and length of time, wall shear stresses of flows in parallel plates and corrugated channel of plate heat exchanger were compared to study the effect of geometry of flow channel on wall shear stress.

4.3   Statistical Methods

In this study, the Analysis of Variance (ANOVA) was employed to indicate mean wall shear stress differences that generated by different type of pulsed flow. The comparison tests (t-test and Duncan's multiple range test) were used to determine which of the mean differences are significant. The detail about the ANOVA and the comparison tests are presented in the following section.

4.3.1 t-Test of Two Independent Samples

The t-test of two independent samples is used to assess the significance of the difference between the means of two independent samples which are randomly drawn from normally distributed populations. But the standard deviations of the populations are not known. The test hypothesis is shown as follows:

$$H_0 : \mu_1 - \mu_2 = 0$$

$$H_A : \mu_1 - \mu_2 \neq 0$$

where μ_1 and μ_2 are the mean of the population 1 and 2, respectively. H_0 is the null hypothesis. This hypothesis assumes that there is no difference between the mean of two samples. H_A is the alternate hypothesis which assumes that there is the significant difference between the mean of two samples. To test the hypothesis, the following equation is used:

$$t = \frac{(\bar{x}_1 - \bar{x}_2) - (\mu_1 - \mu_2)}{\sqrt{\dfrac{s_1^2}{n_1} + \dfrac{s_2^2}{n_2}}}$$
(4.1)

where t is the value which belongs to t-distribution defined by degree of freedom (df) = $(n_1\text{-}1) + (n_2\text{-}1)$, $\bar{x}_1$ and $\bar{x}_2$ are the mean of the sample 1 and 2, respectively. S_1 and S_2 are the standard derivative of the sample 1 and 2, respectively. n_1 and n_2 are the number of sample 1 and 2, respectively. To satisfy null hypothesis, μ_1- μ_2 must equal to zero. The new equation for t-value is:

$$t = \frac{(\bar{x}_1 - \bar{x}_2)}{\sqrt{\dfrac{s_1^2}{n_1} + \dfrac{s_2^2}{n_2}}}$$
(4.2)

To accept or reject the null hypothesis, the calculated t-value is compare to t-value from the t-distribution table (Table B.1). When the calculated t-value is higher than t-value from table, the null hypothesis is rejected. This means there is the significant difference between the mean of two samples.

In this study, the t-test of two independent samples was employed to test the mean differences between mean wall shear stress of two different pulsating conditions.

4.3.2 Analysis of Variance (ANOVA)

Generally, the Analysis of Variance (ANOVA) is used to assess the mean differences between three groups of samples or more. The test hypothesis is shown as follows:

$$H_0 : \mu_1 = \mu_2 = \mu_3$$

$$H_A : \mu_i \neq \mu_j; \quad i \neq j; \quad i, j = 1, 2, 3 \text{ at least one couple}$$

To test the hypothesis, the total variation is separated into two components; the variation between groups of samples and the variation within group of sample. If the variation between groups of samples is greater than the variation within group of sample, it means that the mean difference between groups is greater than the mean differences within group. Thus, the null hypothesis is rejected, there is the significant difference between the means at least a couple of samples.

In the following, the general data layout for a single-factor design is presented in Table 4.6. To assess the significant difference for the single-factor design, the One-Way ANOVA is employed to test the hypothesis as follows:

Table 4.6 The general data layout for a completely randomized single-factor design

Factor (Treatment)					
1	**2**	**...**	**j**	**...**	**k**
x_{11}	x_{12}	...	x_{1j}	...	x_{1k}
x_{21}	x_{22}	...	x_{2j}	...	x_{2k}
$\vdots$	$\vdots$	...	$\vdots$	...	$\vdots$
x_{i1}	x_{i2}	...	x_{ij}	...	x_{ik}
$\vdots$	$\vdots$	...	$\vdots$	...	$\vdots$
x_{n1}	x_{n2}	...	x_{nj}	...	x_{nk}

To estimate the variance between the groups of sample, the estimated variance is in the following form:

$$S_T^2 = n \frac{\sum_{j=1}^{k} (\bar{x}_j - \bar{x}_\bullet)^2}{k-1} \tag{4.3}$$

where S_T^2 is the estimated variance between the groups or the between groups mean square, $\bar{x}_j$ is the sample mean of data from population j and $\bar{x}_\bullet$ is the grand mean of all observations in the data set.

To estimate the variance within the group of sample, the estimated variance is in equation (4.4):

$$S_e^2 = \frac{\sum_{j=1}^{k} \sum_{i=1}^{n} (x_{ij} - \bar{x}_j)^2}{k(n-1)} \tag{4.4}$$

where S_e^2 is the estimated variance within the group or the within group mean square.

To compare the variance between the groups and the within the group, the comparison can be stated in the form of the F-ratio which belongs to F-distribution defined by degree of freedom (df) = $(k\text{-}1)$, $k\,(n\text{-}1)$ as follows:

$$F = \frac{S_T^2}{S_e^2} \tag{4.5}$$

When the calculated F-ratio is higher than the F-ratio from the F-distribution table (Table B), the null hypothesis is rejected. This means that there is the significant mean difference between groups at least one couple. The summary of the One-Way ANOVA is presented in Table 4.7.

Table 4.7 ANOVA table for the completely randomized single-factor design

Source of Variation	Degrees of Freedom	Sum of Squares	Mean Square	F-ratio
Between Groups (regression)	$k-1$	$n\sum_{j=1}^{k}(\bar{x}_j - \bar{x}_\bullet)^2$	S_T^2	$\dfrac{S_T^2}{S_e^2}$
Within Group (error)	$k(n-1)$	$\sum_{j=1}^{k}\sum_{i=1}^{n}(x_{ij} - \bar{x}_j)^2$	S_e^2	
Totals	$kn-1$	$\sum_{j=1}^{k}\sum_{i=1}^{n}(x_{ij} - \bar{x}_\bullet)^2$		

When there are more than one factors are considered, the Factorial Analysis of Variance (Factorial ANOVA) is used to assess the significant mean difference between groups. From the two-factor Factorial ANOVA, the main effects of each factor and the interaction of factors are assessed by the estimation of variance as in Table 4.8 and 4.9.

In this study, the two-factor factorial ANOVA was used to assess the mean differences between mean wall shear stress of different types of pulsed flow and different pulsating conditions.

Table 4.8 ANOVA table for a two-factorial design

Source of Variation	Degrees of Freedom	Sum of Squares	Mean Square	F-ratio
Factor A	$n-1$	$rk \sum_{i=1}^{n} (\bar{x}_i - \bar{x}_\bullet)^2$	S_A^2	$\dfrac{S_A^2}{S_e^2}$
Factor B	$k-1$	$rn \sum_{j=1}^{k} (\bar{x}_j - \bar{x}_\bullet)^2$	S_B^2	$\dfrac{S_B^2}{S_e^2}$
Factor AB	$(k-1)(n-1)$	$r \sum_{j=1}^{k} \sum_{i=1}^{n} (\bar{x}_{ij} - \bar{x}_i - \bar{x}_j + \bar{x}_\bullet)^2$	S_{AB}^2	$\dfrac{S_{AB}^2}{S_e^2}$
Between Replications	$r-1$	$kn \sum_{m=1}^{r} (\bar{x}_m - \bar{x}_\bullet)^2$	S_R^2	$\dfrac{S_R^2}{S_e^2}$
Error	$(nk-1)(r-1)$	By subtraction	S_e^2	
Totals	$rkn-1$	$\sum_{j=1}^{k} \sum_{i=1}^{n} \sum_{m=1}^{r} (y_{ijm} - \bar{y}_\bullet)^2$		

Table 4.9 The general data layout for a two factorial design

Factor B	Replication																				
	1						...	m						...	r					
	Factor A																				
	1	2	...	i	...	n	...	1	2	...	i	...	n	...	1	2	...	i	...	n
1	x_{111}	x_{211}	...	x_{i11}	...	x_{n11}	...	x_{11m}	x_{21m}	...	x_{i1m}	...	x_{n1m}	...	x_{11r}	x_{21r}	...	x_{i1r}	...	x_{n1r}
2	x_{121}	x_{221}	...	x_{i21}	...	x_{n21}	...	x_{12m}	x_{22m}	...	x_{i2m}	...	x_{n2m}	...	x_{12r}	x_{22r}	...	x_{i2r}	...	x_{n2r}
⋮	⋮	⋮	...	⋮	...	⋮	...	⋮	⋮	...	⋮	...	⋮	...	⋮	⋮	...	⋮	...	⋮
j	x_{1j1}	x_{2j1}	...	x_{ij1}	...	x_{nj1}	...	x_{1jm}	x_{2jm}	...	x_{ijm}	...	x_{njm}	...	x_{1jr}	x_{2jr}	...	x_{ijr}	...	x_{njr}
⋮	⋮	⋮	...	⋮	...	⋮	...	⋮	⋮	...	⋮	...	⋮	...	⋮	⋮	...	⋮	...	⋮
k	x_{1k1}	x_{2k1}	...	x_{ik1}	...	x_{nk1}	...	x_{1km}	x_{2km}	...	x_{ikm}	...	x_{nkm}	...	x_{1kr}	x_{2kr}	...	x_{ikr}	...	x_{nkr}

4.3.3 Duncan's New Multiple Range Test (DMRT)

The ANOVA indicates at least one couple mean contrasts is significant, but does not indicate which of the mean differences are significant. To determine which of the mean differences are significant, the comparison tests are employed. Duncan's new multiple range test (DMRT) is a multiple comparison tests that the F-test does not need to show the significant differences. The procedure of DMRT is described as follows:

(1) Calculate $S_{\bar{x}}$ from the following equation:

$$S_{\bar{x}} = \sqrt{\frac{MSE}{n}} \tag{4.6}$$

where $S_{\bar{x}}$ is the standard error of the treatment mean, MSE is the mean square of error and n is the number of treatments.

(2) Calculate the Least Significant Range (LSR) from:

$$LSR = (SSR)(S_{\bar{x}}) \tag{4.7}$$

where SSR is the significant studentized ranges, this value can be obtained from the SSR table (Table B.3) for new multiple range tests.

(3) Rearrange the means in order.

(4) Compare the mean difference of every couple of treatment with the LSR-value at the same range. If the mean difference is greater than the LSR-value, the means of these couple are significant different.

In this study, the DMRT was employed to indicate which of the differences of mean wall shear stress of different types of pulsed or different pulsating conditions are significant.

4.4   Simulation Methods

To achieve the objectives of this study, numerical simulation using the commercial software FLUENT®6.3.26 was employed to analyze wall shear stress in the study system. In this section, the simulation methods which consist of the geometry of the flow domain, mesh generation, physical definition and solver are described as follows:

4.4.1 Geometry

In this study, pulsed flows were simulated through the cylindrical pipe, parallel plates and corrugated channel of plate heat exchanger in order to predict wall shear stress and study the effect of flow channel on wall shear stress generated by pulsed flows. All of flow channels were created in three dimensional geometries using the commercial software GAMBIT^{TM}.

4.4.1.1   Cylindrical Pipe

To analyze wall shear stress of pulsed flows through the cylindrical pipe, the dimension of pipe based on the experiment of Blel (2009). Pipe made of stainless steel with the average absolute roughness 0.3±0.05μm. The inner diameter is 23 mm and the total length is 1630 mm. It was separated into three zones; zone 1 with 690 mm length, zone 2 with 250 mm length and zone 3 with 690 mm length as shown in Figure 4.1. Wall shear stresses were investigated in zone2 in order to eliminate the entrance and exit effects as same as the experiment.
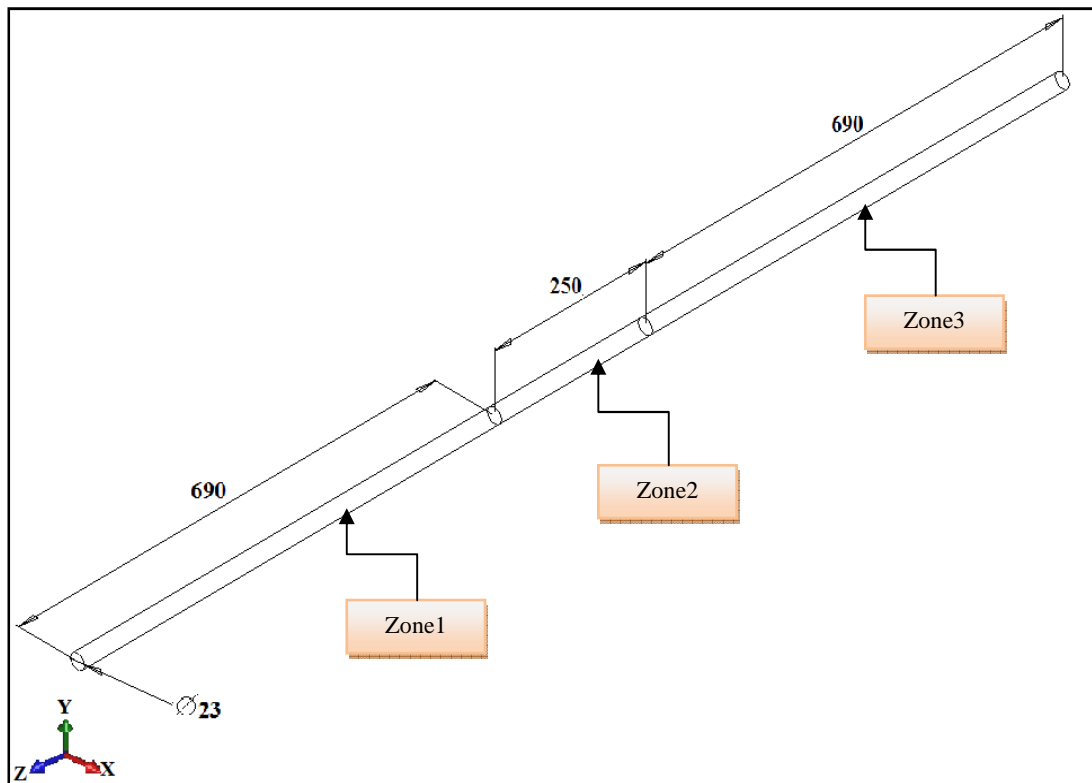
Figure 4.1 The geometry and dimensions of the cylindrical pipe.

4.4.1.2 Channel of Plate Heat Exchanger

The channel of plate heat exchanger that used to be the flow domain is the corrugated channel of chevron plates model RS22. The schematic diagram of the chevron plate and the characteristics of plates are shown in Figure 4.2 and Table 4.10, respectively.
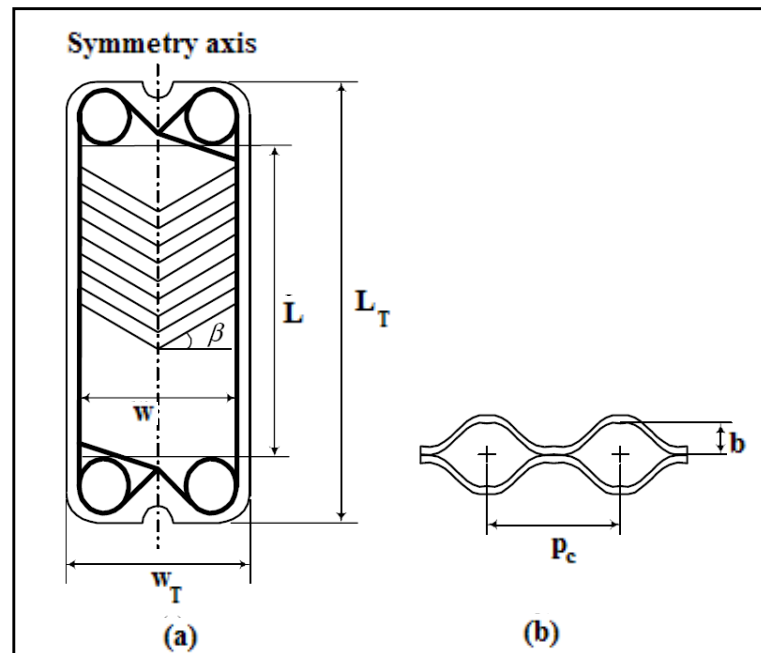
Figure 4.2 (a) Schematic representation of a chevron plate;

(b) Corrugations dimensions.

Source: Fernandes et al. (2005)

Table 4.10 The geometrical characteristics of the chevron plates

Material	Stainless steel AISI 316
Plate Model	RS 22
Area, A (m^2)	0.015
Length, L_T (m)	0.265
Width, w_T (m)	0.102
Effective length, L (m)	0.190
Effective width, w (m)	0.072
Area enlargement factor, Φ	1.096
Corrugation angle, β	30°
Wavelength of corrugation, $p_c \times 10^{-3}$ (m)	10.000
Distance between plates, $b \times 10^{-3}$ (m)	2.600
Thickness, $x_p \times 10^{-3}$ (m)	0.500
Thermal conductivity, k (Wm^{-1}k^{-1})	16.300

In this work, wall shear stresses were considered only in the corrugated part of the chevron plate heat exchanger. The length of the flow domain is equal to the effective length, L, 190 mm length. Because the corrugated plates are symmetry as in Figure 4.2, therefore, flows were simulated through the half of corrugated channel plates as shown in Figure 4.3. The corrugated channel is characterized by the following sinusoidal function:

$$x(y) = \frac{b}{2}\sin\left[\frac{2\pi}{p_c}\left(y - \frac{p_c}{4}\right)\right] + \frac{b}{2}$$
(4.8)

where x and y are the position in Cartesian coordinate system.
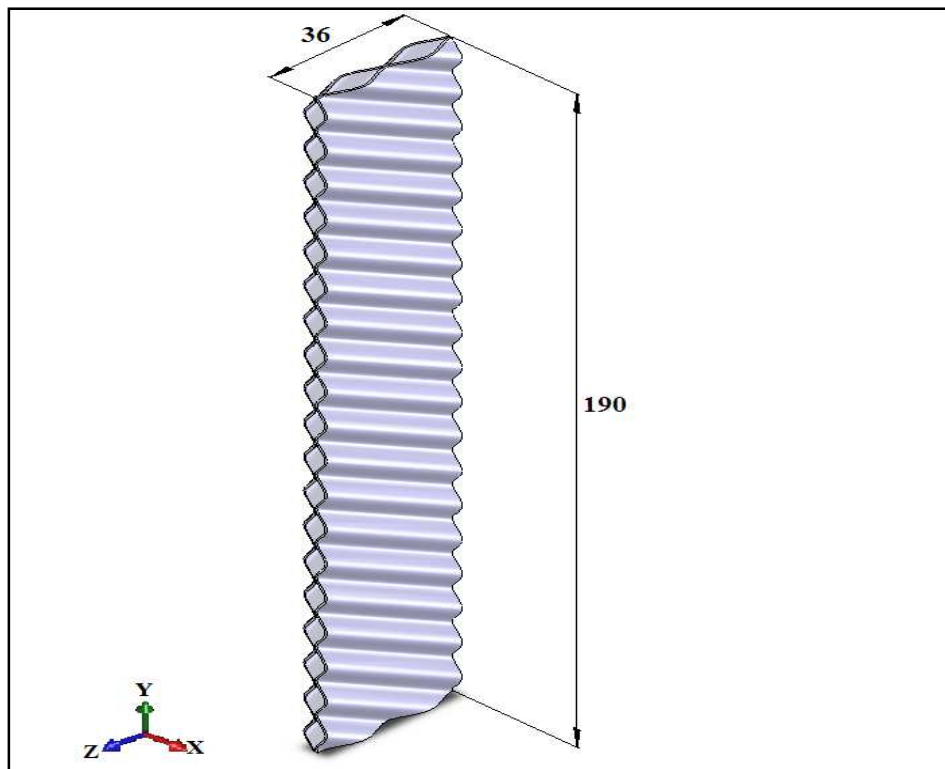
Figure 4.3 The 3D corrugated channel of the chevron plates

The characteristics of the flow domain that created in GAMBIT^{TM} are shown in Figure 4.4.
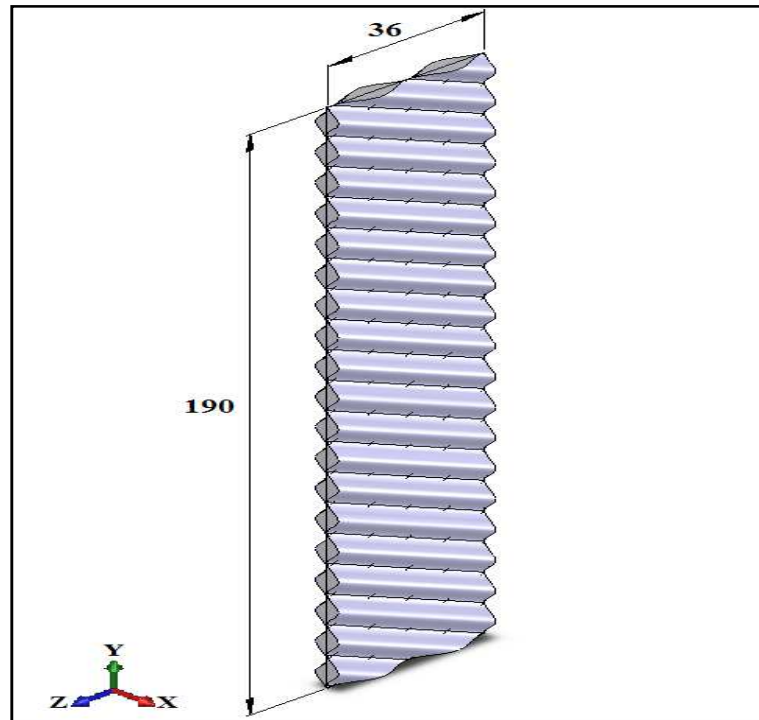
Figure 4.4 The flow domain of the corrugated channel

From Figure 4.4, the hydraulic diameter, D_h, of the corrugated channel is 0.00517 m or 5.17mm which is computed from the following equation:

$$D_h = \frac{4V}{A} \tag{4.9}$$

where V is the volume of the corrugated channel in m^3 and A is the surface area of the chevron plates in m^2.

4.4.1.3   Parallel Plates

To study the effect of geometry of flow channel on wall shear stress, the dimensions of parallel plates are controlled by the dimensions of the corrugated channel. The length of parallel plates is 190 mm. The hydraulic diameter, D_h, of parallel plates is 5.17 mm which based on the hydraulic diameter of the corrugated channel. The characteristics of the flow domain that created in GAMBIT^{TM} are shown in Figure 4.5.
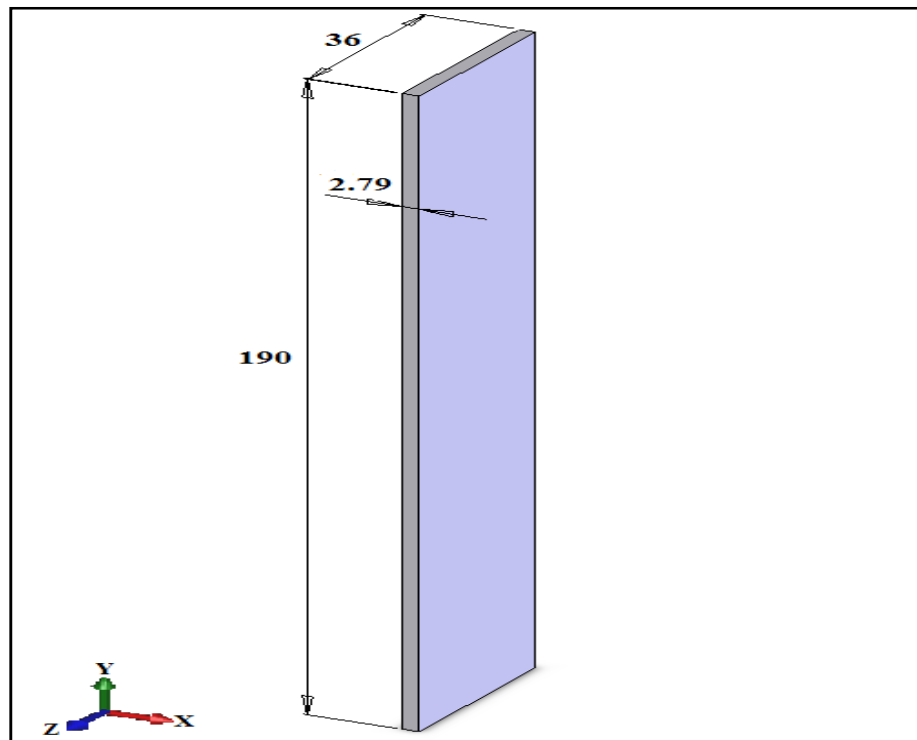
Figure 4.5 The 3D geometry of the parallel plates

4.4.2 Mesh

To analyze wall shear stress of pulsating flows using finite volume method of FLUENT®6.3.26, the governing equations of fluid flow are integrated over a control volume to yield a discretized equation in the form of algebraic equation. This control volume is called grid, element or mesh which created by dividing the computational domain into discrete control volumes. In this study, mesh was created by GAMBIT^TM with the following steps. First, all edges in the model were divided into small pieces by mesh edges command. Then, the 2D mesh on the boundary of the flow domain was created using mesh faces command. Finally, this 2D mesh was extrapolated into the body of the domain using mesh volume command. It made flow domain volume was broken into the discrete volumes. The shape of the 3D elements depends on the geometry of the computational domain. The basic shape of the volume elements that generated by GAMBIT^TM are hexahedron, wedge, tetrahedron and pyramid. The point that is used to store the computational data at any position of the domain is defined as the nodal point or node. The number of nodes and the node pattern associated with the volume element shape. In this section, the optimum mesh size procedure and the mesh characteristic of each flow domain are presented as follows:

4.4.2.1 The Optimum Mesh Size Procedure

For numerical method, mesh size is indispensible to the accuracy and the convergence of the numerical results. To find the optimum mesh size, first, rough mesh was created. Mesh size was set to 5-8% of the entire domain size. Then, this mesh was employed to be the flow domain of the computation with the specific conditions (pulsating conditions, fluid properties and flow condition).

Second, the density of mesh in the first step was increased by mesh refining. Again, the fine mesh was simulated with the same conditions as in the first step. Then, the numerical results of rough mesh were compared to fine mesh. If the difference of the numerical results was higher than the criteria (1%), the fine mesh would be refined again until the difference of numerical results between rough mesh and fine mesh was less than the criteria. The summary of the optimum mesh size of flow domains that used in this study is shown in the Table 4.11.

Table 4.11 The summary of the optimum mesh size of flow domains

Flow Domain	Cylindrical Pipe	Corrugated Channel	Parallel Plates
Number of Mesh Elements	457,704	2,372,258	194,504
Number of Faces	1,384,296	5,301,581	633,100
Number of Nodes	469,245	752,274	244,263

4.4.2.2 Mesh Characteristic of Cylindrical Pipe

The entire flow domain was created from blocks of hexahedron mesh element. In axial direction, the interval size of mesh is 5 mm as in Figure 4.6. Non-uniform mesh in the radial direction was performed to satisfy y^+ value limits ($y^+<5$) valid for the enhance-wall treatment which was used for wall shear stress analysis. The height of first row elements from the wall of pipe is 0.02875 mm. The height of row increased with growth factor 1.2. The non-uniform mesh in radial direction is shown in Figure 4.7.
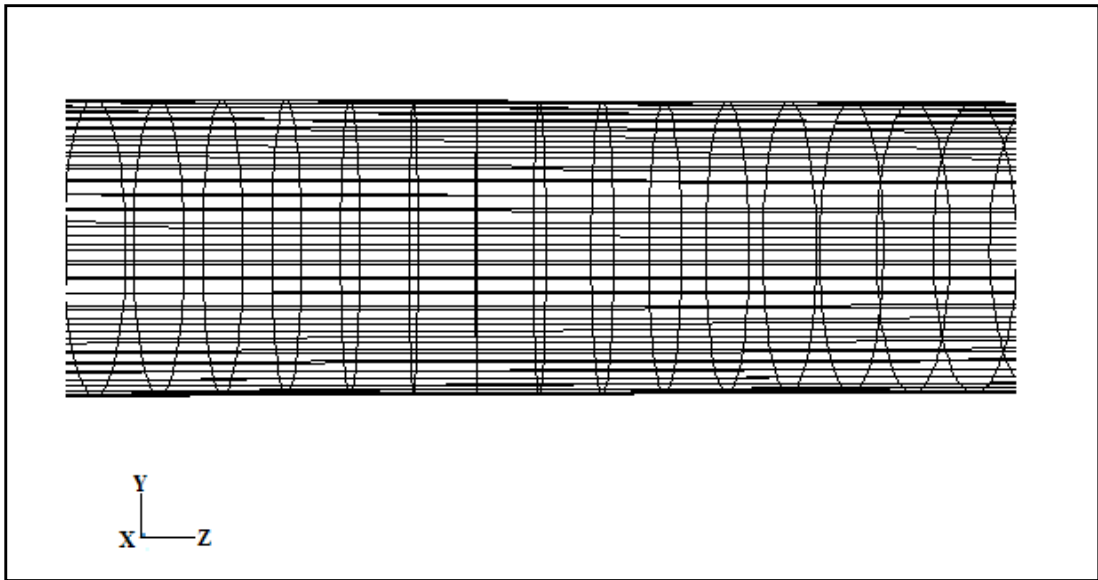
Figure 4.6 Part of hexahedron mesh elements in axial direction of the flow domain.
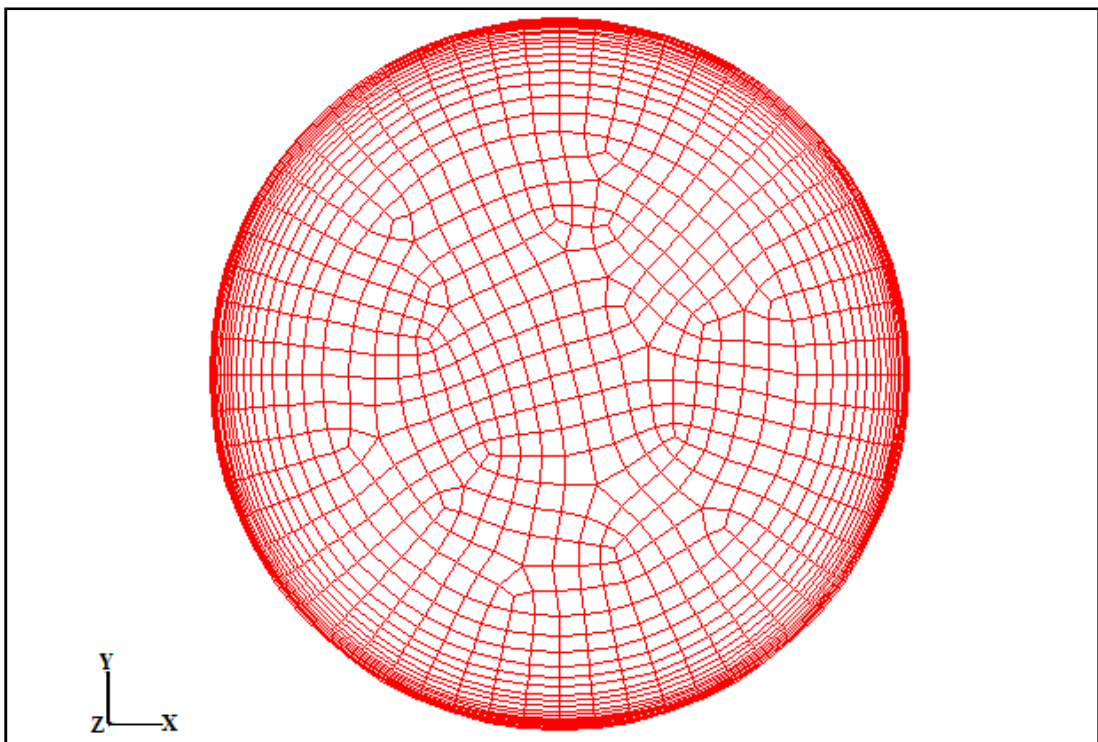
Figure 4.7 The hexahedron mesh elements in the radial direction of the flow domain.

4.4.2.3   Mesh Characteristic of Corrugated Channel

The entire flow domain was created from blocks of tetrahedron mesh element. Generally, the interval size of the elements of the entire flow domain started from 0.001 mm to 0.6 mm. The small elements were generated in the narrow region of the plate, whereas, the larger mesh elements were created in the wide region of the flow domain.

Because of the complexity of flow domain and the condition that the first row elements must satisfy y^+ value limits ($y^+<5$) valid for the enhance-wall treatment, at the contact point of plates was cut as circular with 2 mm diameter. In this case, it was assumed that flow will never flow through those cutting zones. The height of the first row elements from the wall is 0.001 mm. The height of row increased with growth factor 1.15. The 3D mesh elements of the corrugated channel are shown in Figure 4.8 and 4.9.
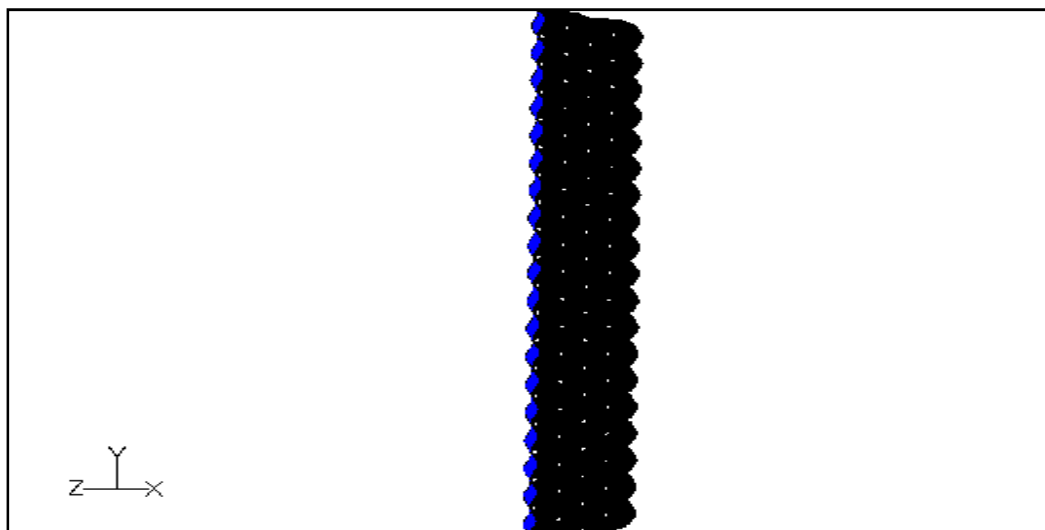
Figure 4.8 3D mesh elements of the modify corrugated channel
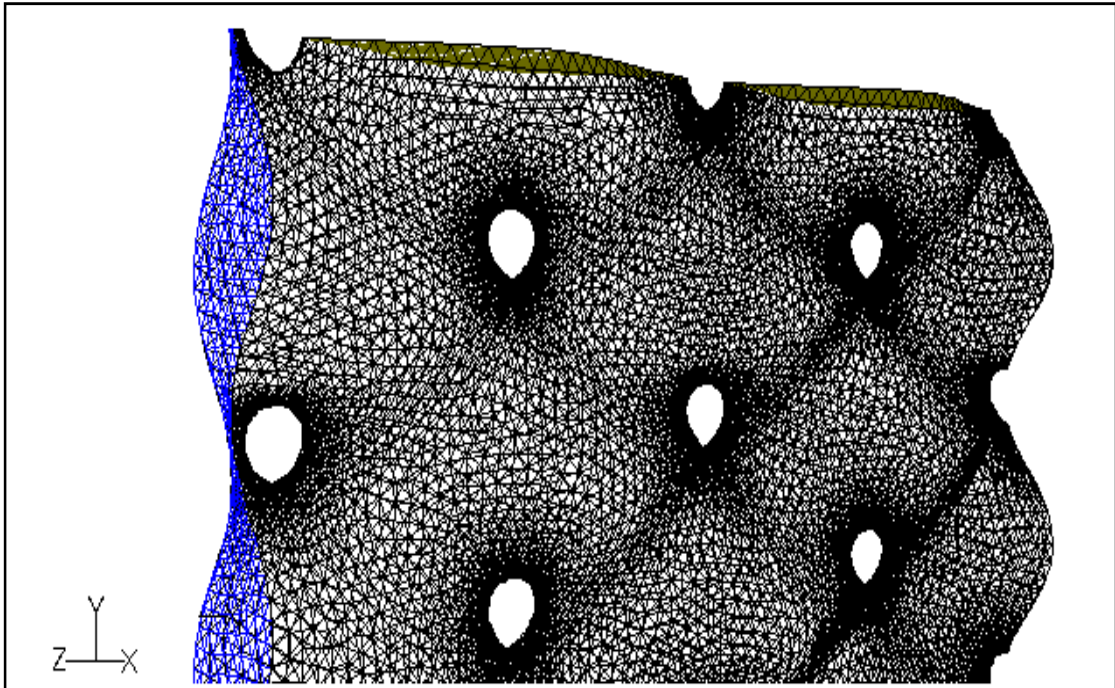
Figure 4.9 Part of 3D mesh elements of the modify corrugated channel

4.4.2.4 Mesh Characteristic of Parallel Plates

The entire flow domain was created from blocks of hexahedron mesh element. The interval size of the elements of the entire flow domain started from 0.05 mm to 1.9 mm. To satisfy y^+ value limits, the height of the first row elements from the wall is 0.05 mm. The height of row increased with growth factor 1.15. The 3D mesh elements of the parallel plates are shown in Figure 4.10 and 4.11.
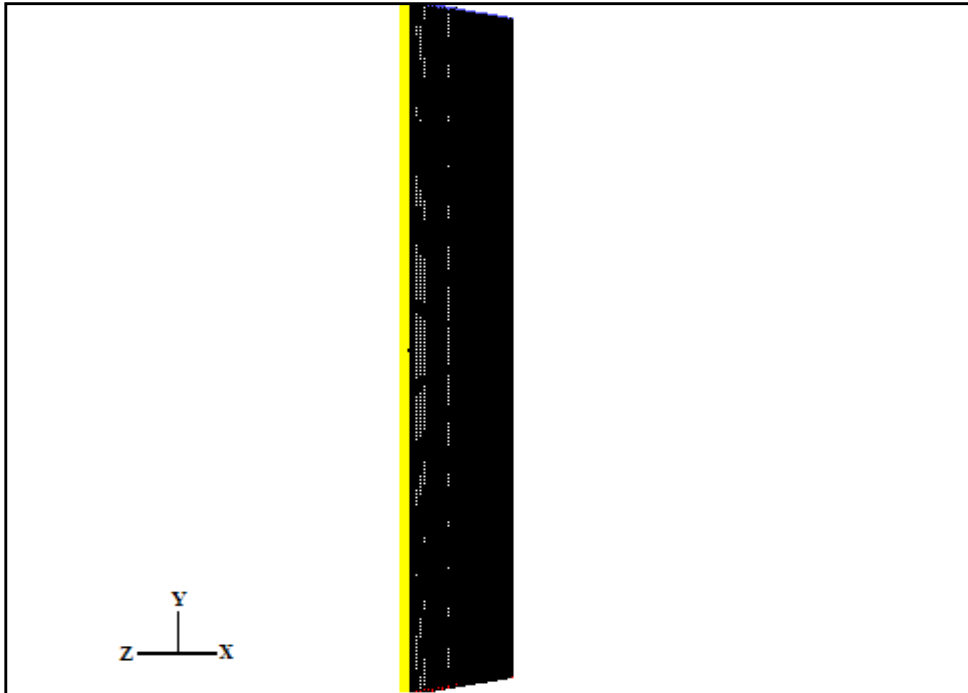
Figure 4.10 3D mesh elements of the parallel plates
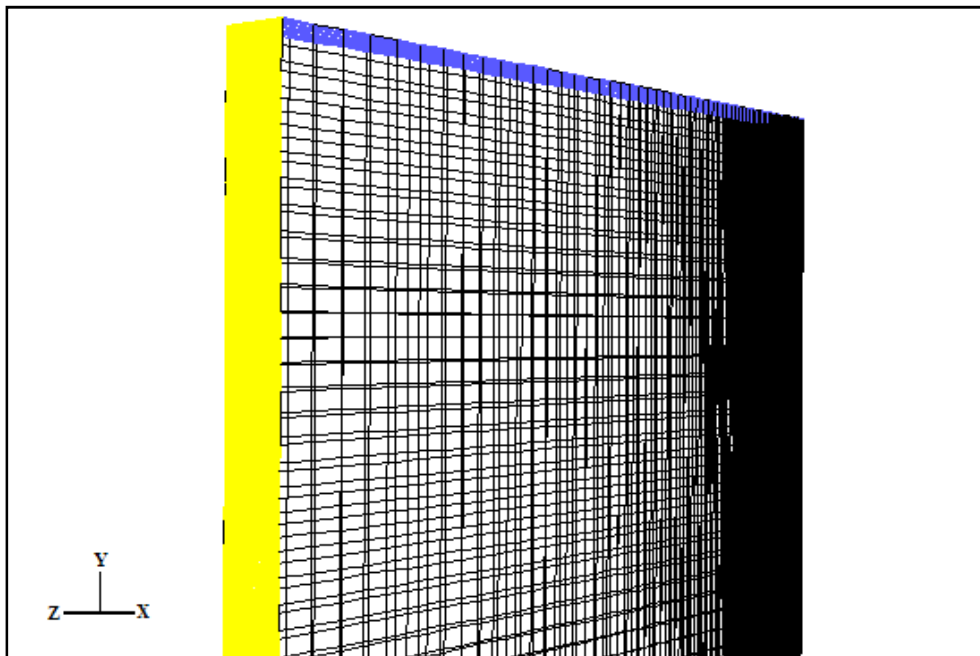
Figure 4.11 Part of 3D mesh elements of the parallel plates

4.4.3 Physical Definition

After mesh was generated, the physical models that include fluid properties, flow conditions, boundary and initial conditions were defined as follows:

4.4.3.1 Fluid Properties

In wall shear stress prediction, the numerical data was compared to the experimental data of Blel (2009). Thus, the working fluid based on the fluid in the experiment of Blel (2009) which was the electrolytic solution of a mixture of potassium ferricyanide, potassium ferrocyanide and sodium hydroxide. The density of this solution is 1028 kg/m^3 and its dynamic viscosity is 0.985×10^{-3} kg/m.s at 22°C. For the rest of the study, water at 50°C was used to be the working fluid. The density of water at 50°C is 988.1 kg/m^3 and its dynamic viscosity is 0.547×10^{-3} kg/m.s.

4.4.3.2 Flow conditions

In this study, flows were considered to be turbulence. The steady and unsteady state flows were assumed for turbulent steady flow and turbulent pulsating flow, respectively. Two working fluid were assumed to be constant object property and incompressible. The characteristics of pulsating flow were controlled by the pulsating condition in Table 4.1-4.5. For flow in the cylindrical pipe, pipe was laid on horizon level; the effect of gravitation could be ignored. On the other hand, when fluid was flowed in the corrugated channel and parallel plates, both of flow domains were on vertical level; the effect of gravitation could be considered. Flows were performed under isothermal condition. And the operating pressure was equal to 101325 Pa.

4.4.3.3 Boundary Conditions

Boundary conditions on the surfaces of flow domains were defined for the flow simulation by FLUENT®6.3.26. The following boundary conditions are available in FLUENT®6.3.26. and were chosen to be the boundary condition on the surfaces of flow domains:

(1) At the Inlet Surface

The velocity inlet was defined as the boundary condition at the inlet surface of the flow domain. The flow direction is perpendicular to the inlet surface. The velocity inlet could be set as a constant and periodic function for steady flow and pulsating flow, respectively. The periodic functions are presented in the following equation.

Rectangular waveform pulsation:

$$u(t) = \bar{u} + \frac{2u_p}{\pi} \sum_{n=1}^{\infty} \left(\frac{1 - \cos n\pi}{n} \right) \sin(2n\pi f) \qquad (4.10)$$

Saw tooth waveform pulsation:

$$u(t) = \bar{u} + \frac{2u_p}{\pi} \sum_{n=1}^{\infty} \left(\frac{\cos n\pi}{n} \right) \sin(2n\pi f) \qquad (4.11)$$

Sinusoidal waveform pulsation:

$$u(t) = \bar{u} + u_p \sin(2\pi f t) \qquad (4.12)$$

Trapezoidal waveform pulsation:

$$u(t) = \bar{u} + \frac{8u_p}{\pi^2} \sum_{n=1}^{\infty} \left[\frac{1}{n^2} \left(\sin\left(\frac{n\pi}{4}\right) + \sin\left(\frac{3n\pi}{4}\right) \right) \right] \sin(2n\pi f) \qquad (4.13)$$

Triangular waveform pulsation:

$$u(t) = \bar{u} + \frac{8u_p}{\pi^2} \sum_{n=1}^{\infty} \left(\frac{1}{n^2} \sin\left(\frac{n\pi}{2}\right) \right) \sin(2n\pi f) \qquad (4.14)$$

where u is the instantaneous velocity inlet in m/s, $\bar{u}$ is the mean velocity inlet in m/s, u_p is the amplitude of pulsation in m/s and f is the frequency of pulsation. The periodic velocity inlet boundary conditions were applied to the inlet surface using User-defined functions (UDF) in FLUENT[®]6.3.26. The source code of the periodic velocity inlet boundary conditions are shown in appendix C.

(2) At the Outlet Surface

In the cylindrical pipe, the outflow boundary condition was employed to be the boundary condition at outlet of pipe. The zero diffusion flux condition was applied at the outflow plane. The conditions of the outflow plane are extrapolated from the upstream flow within the domain. By extrapolation, the outflow velocity and pressure were updated in a manner of fully develop flow assumption.

In the corrugated channel and parallel plates, the pressure outlet boundary condition was applied at the outlet surface. The outlet pressure was extrapolated from the upstream condition. The gauge pressure was set to be zero Pascal by the assumption that fluid was sent out to the atmosphere.

(3) At the Wall

Wall boundary condition was applied at the wall of domains. These walls were the stationary wall. The no-slip boundary condition was enforced at walls means that fluid sticks at the wall. Thus, the velocity of fluid is zero at the stationary wall.

(4) At the Symmetry Plane

Symmetry boundary condition was applied at the symmetry plane of the corrugated channel and the parallel plates. At the symmetry plane, the flow patterns have mirror symmetry. There is zero flux of all quantities a symmetry boundary. The normal velocity component at the symmetry plane is also zero.

The positions of the boundary conditions of each computational domain are presented in Figure 4.12, 4.13, 4.14 and 4.15.
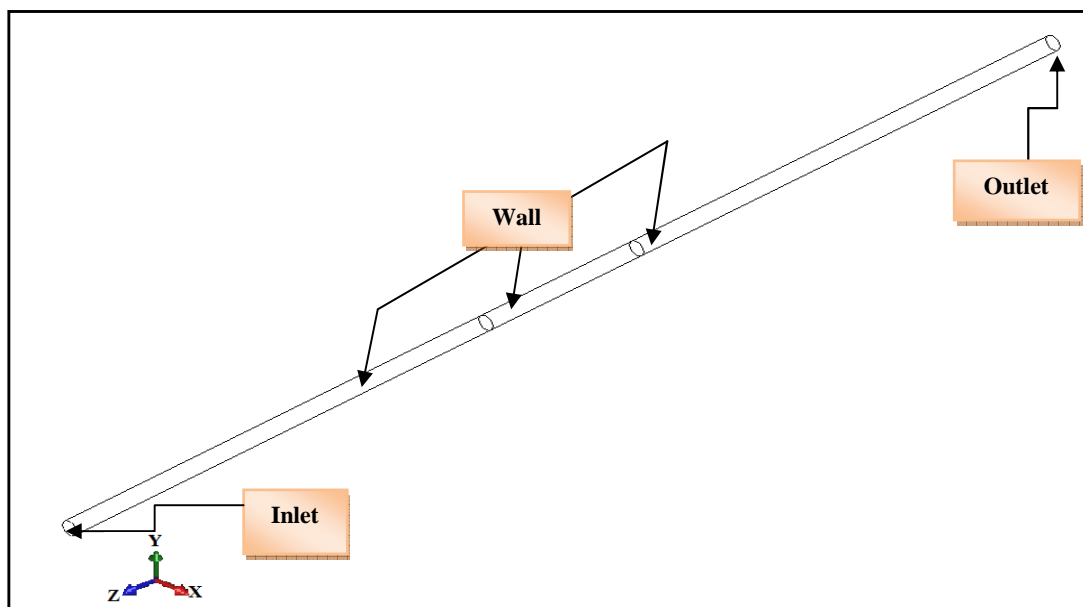
Figure 4.12 The positions of boundary conditions of the cylindrical pipe
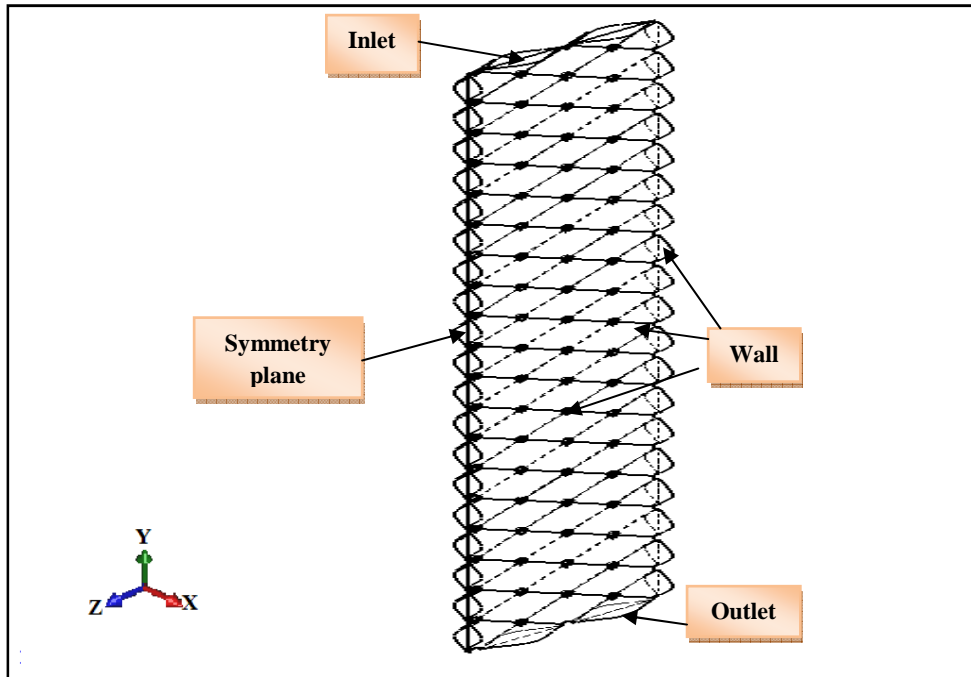
Figure 4.13 The positions of boundary conditions of the corrugated channel
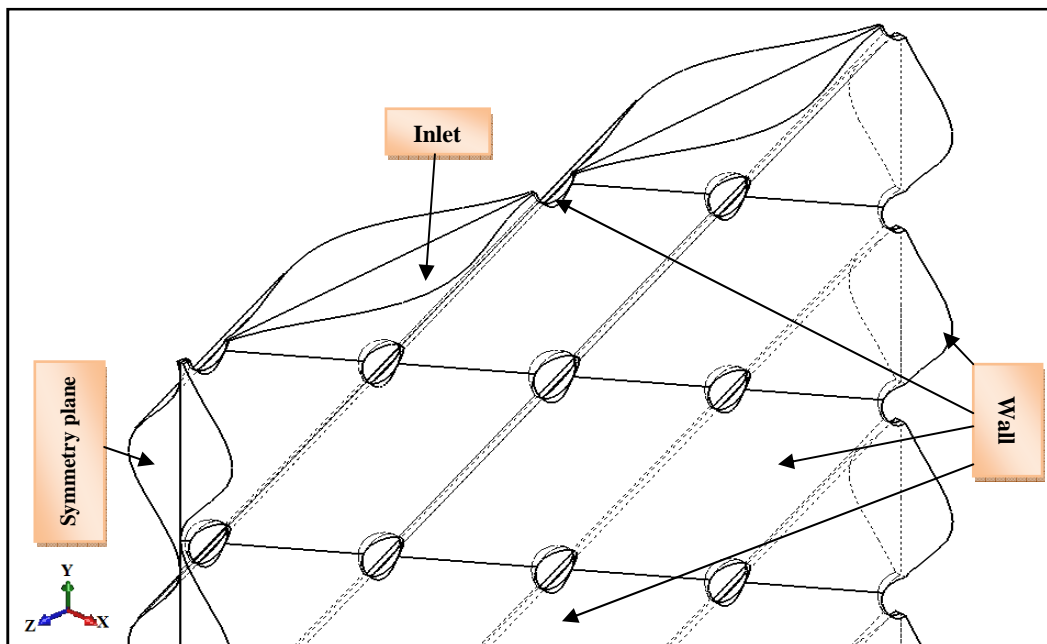
Figure 4.14 The positions of boundary conditions of the

corrugated channel (large view)
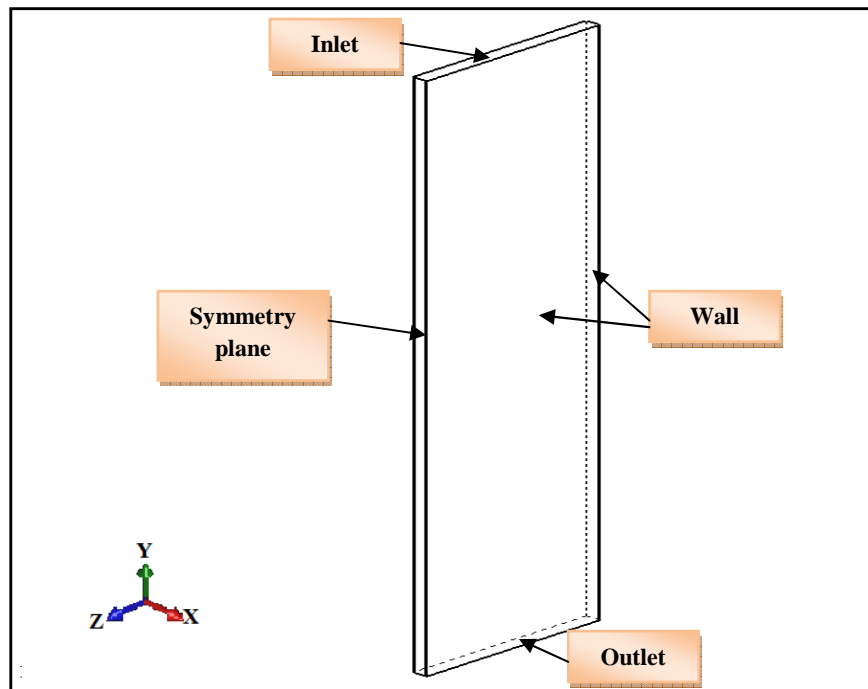
Figure 4.15 The positions of boundary conditions of the parallel plates

4.4.3.4 Initial Condition

The initial velocity in each component based on the velocity inlet at t=0 of each pulsating condition. While, the initial gauge pressure was set to be zero Pascal.

4.4.4 Solver

Based on the finite volume method of FLUENT®6.3.26, the pressure based solver was chosen to solve all variables for incompressible flow simulation. Using this solver, each iteration consists of the following solving steps:

(1) Fluid properties are updated based on the current solution.

(2) The momentum equations are solved by using the updated pressure and face mass fluxes.

(3) The pressure correction equation is solved by using the recently obtained velocity field and the mass-flux.

(4) The face mass fluxes, pressure, and the velocity field are corrected by using the pressure correction obtained from Step (3).

(5) The turbulent quantities are solved.

(6) Check for the convergence of the equations.

From the turbulent testing model the RNG k-ε model was used to predict wall shear stress of pulsed flows with the enhanced wall treatment. The second order upwind difference scheme was chosen to predict momentum in each control volume. Turbulent kinetic energy and turbulent dissipation rate in each control volume were predicted by the second order upwind difference scheme and the first order upwind difference scheme for flows in cylindrical pipe and the channel of plate heat exchanger and parallel plates, respectively. The SIMPLE algorithm was applied for the iteration procedure. For the simulation time, size of time step and the number of iteration per time step are presented in appendix D (Table D.1 and D.2).

4.5   Conclusion

This section described the apparatus that were used in this study, followed by the study methods used to achieve the objective of this thesis. The wall shear stress prediction, the studies of the effects of type of pulsed flow, amplitude, frequency, mean velocity inlet and the geometry of the flow channel on wall shear stress were described. After that, the analysis of variance and the mean comparison tests of the statistical methods were presented. This showed tools that used to compare the mean wall shear stress of various types of pulsed flow. To analyze wall shear stress of

pulsed flow, the finite volume method was employed to solve the problems. Thus, the simulation methods were focused as the later subject. The simulation methods consisted of the description of the geometry of flow domains which are the cylindrical pipe, the corrugated channel and the parallel plates. Then, the mesh creation of each domain was presented with the optimum mesh size procedure and the mesh characteristic of each computational domain. The physical model of the problem such as fluid properties, flow conditions, boundary and initial condition were described as well. Finally, the solving step of pressure-based solver in FLUENT®6.3.26, discretization scheme and the solution algorithm for pressure-velocity coupling were presented in the last part of this section.

CHAPTER V

RESULTS AND DISCUSSION

By working on the study methods and simulation methods that are shown in section 4.2 and 4.4, the results of wall shear stress prediction are presented in the first part of this section. Then, the effect of type of pulsed flow on wall shear stress is shown in the form of instantaneous wall shear stress, mean wall shear stress, wall shear stress distribution and velocity vector of flows in the channel flows. Next, the influences of amplitude, frequency and mean velocity inlet of pulsation on wall shear stress are presented in the form of the relationship between those factors and wall shear stress. Finally, the effect of the geometry of flow channel on wall shear stress is presented in the form of mean wall shear stress as the last of this section.

5.1   Wall Shear Stress Prediction

5.1.1 Turbulence Model Testing

To find the most suitable turbulence model that will be used to predict wall shear stress of pulsating flows for the study in section 4.2.1-4.2.6, Standard k-ε, RNG k-ε, Realizable k-ε model, Standard k-ω and SST k-ω model were employed to predict wall shear stress of sinusoidal pulsating flow with mean velocity 1.47 m/s, amplitude 0.4 m/s and frequency 2.5 Hz. The flows were simulated in the cylindrical pipe domain. The numerical data of mean wall shear stress of pulsed flows was compared to the experimental data of Blel et al. (2009) as shown in Figure 5.1.
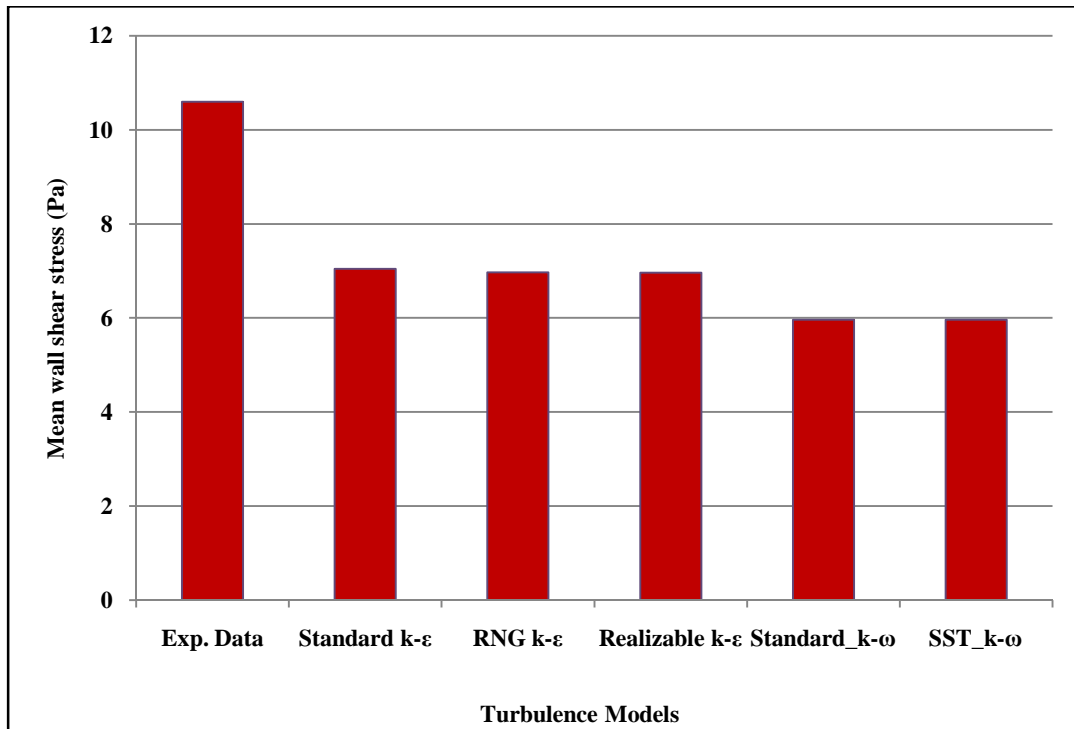
Figure 5.1 The comparison of mean wall shear stress between the experimental data

and the numerical data predicted by various types of the turbulence model

Figure 5.1 shows that there is much difference between the
experimental data and the numerical data. However, the k-ε models are greater than
the k-ω models in the wall shear stress prediction. The differences between the
experimental data and the numerical data that predicted by the k-ε models are about
33.5-34.3%. Meanwhile, The differences between the experimental data and the
numerical data that predicted by the k-ε models are about 43.7%. Within the group of
the k-ε models, there is no significant difference between mean wall shear stress
predicted by the standard k-ε, RNG k-ε and realizable k-ε models as same as the
comparison within the group of the k-ω models. However, to find the most suitable
turbulence model for wall shear stress analysis of pulsed flow, researcher also

considered the flow characteristic in the domain. When the domain is complicated such as the corrugated channel, the recirculation can possibly occur. The k-ε model that includes the effect of swirl on turbulence and has the term that improves the accuracy for rapidly strained flows is the RNG k-ε model. The RNG k-ε model has also proven superior to the standard k-ε model in general (Boysan, 1993). Thus, the RNG k-ε model was chosen to be the represent turbulent model in this study.

5.1.2 Wall Shear Stress Prediction

Wall shear stresses generated by pulsed flows with pulsating conditions that were shown in Table 4.1 were predicted using FLUENT[®]6.3.26 in order to find the suitable pulsating conditions for wall shear stress analysis. The fluid properties, flow domain and flow condition based on the experiment of Blel et al. (2009). The comparison between the numerical data of mean wall shear stress of pulsating flows and the experimental data is shown in Figure 5.2.
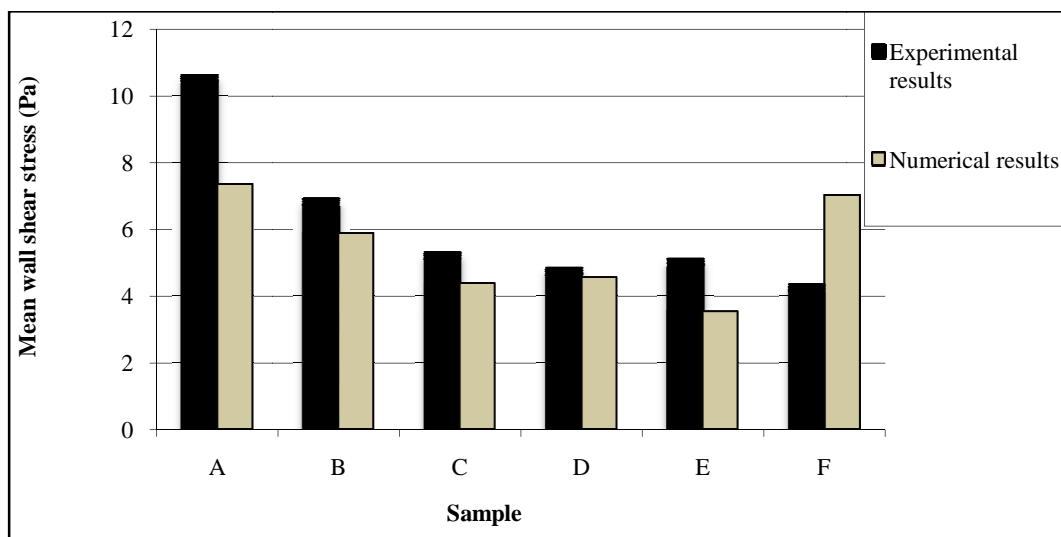
Figure 5.2 The comparison of mean wall shear stress between numerical data and experimental data of each pulsating condition.

Figure 5.2 shows that there are some differences between the numerical data and the experimental data. With the same mean velocity inlet, the comparison of mean wall shear stress between pulsed flow (sample A) and the steady flow (sample F) is seen that there is a little difference between them when they are analyzed by the numerical simulation, whereas, mean wall shear stress of pulsed flow is much higher the mean wall shear stress of steady flow in the experiment. This contrast is caused by the difference of the methodology of wall shear stress measurement between the experiment and the simulation. The electrochemical technique was used to measure wall shear stress in the experiment of Blel et al. (2009). This technique considers mass transfer of chemical species by measuring the diffusional currents given by a redox reaction of the electrolytic solution. These currents are transformed into the dimensionless form of Sherwood number which relates to the wall shear rate and wall shear stress. Therefore, the increase of the fluctuation generated by pulsating flow could be counted by this technique. By the method of this technique, the increase of the fluctuation can cause the increase of wall shear stress. Meanwhile, wall shear stresses were obtained by solving the Reynolds-averaged Navier-stokes (RANS) equations in the numerical simulation. For RANS equations, wall shear stress is affected by the viscous force of the flow that acts on the wall only. The effect of mass transfer of chemical species in the flow is neglected. The increase of the fluctuation generated by pulsating flow could not be captured by the numerical simulation. Although, pulsed flow can generate higher wall shear stress than the steady flow, the difference between mean wall shear stress of pulsed flow and steady flow cannot be explicitly seen by numerical simulation. However, there are some samples that the difference of mean wall shear stress between numerical result

and the experimental results were accepted such as sample B, C and D. The differences between the experimental data and the numerical data are about 5.8-17.6%. With the pulsating conditions of sample B, C and D, FLUENT®6.3.26 can predict the closest mean wall shear stress compare to the experimental data. Therefore, these pulsating conditions were used to control the characteristics of pulsating flow for wall shear stress analysis.

5.2 The Effect of Type of Pulsed Flow on Wall Shear Stress

With the same pulsating condition in Table 4.2, wall shear stresses generated by different type of pulsating flow were analyzed under the same flow condition by using finite volume method of FLUENT®6.3.26. Wall shear stress analysis was done in the cylindrical pipe, corrugated channel and parallel plates. In these flow domains, the instantaneous wall shear stresses correspond to the velocity inlet function. For example, the pulsed flow with sinusoidal waveform whose velocity inlet varies with time as sinusoidal function generates the instantaneous wall shear stress that also varies with time as sinusoidal function as in Figure 5.3. As same as pulsed flow with the trapezoidal waveform pulsation that also creates the trapezoidal waveform pulsation of wall shear stress as in Figure 5.4. The instantaneous wall shear stress varies periodically in the same phase as the velocity inlet. This can be seen in both of Figure 5.3 and 5.4.
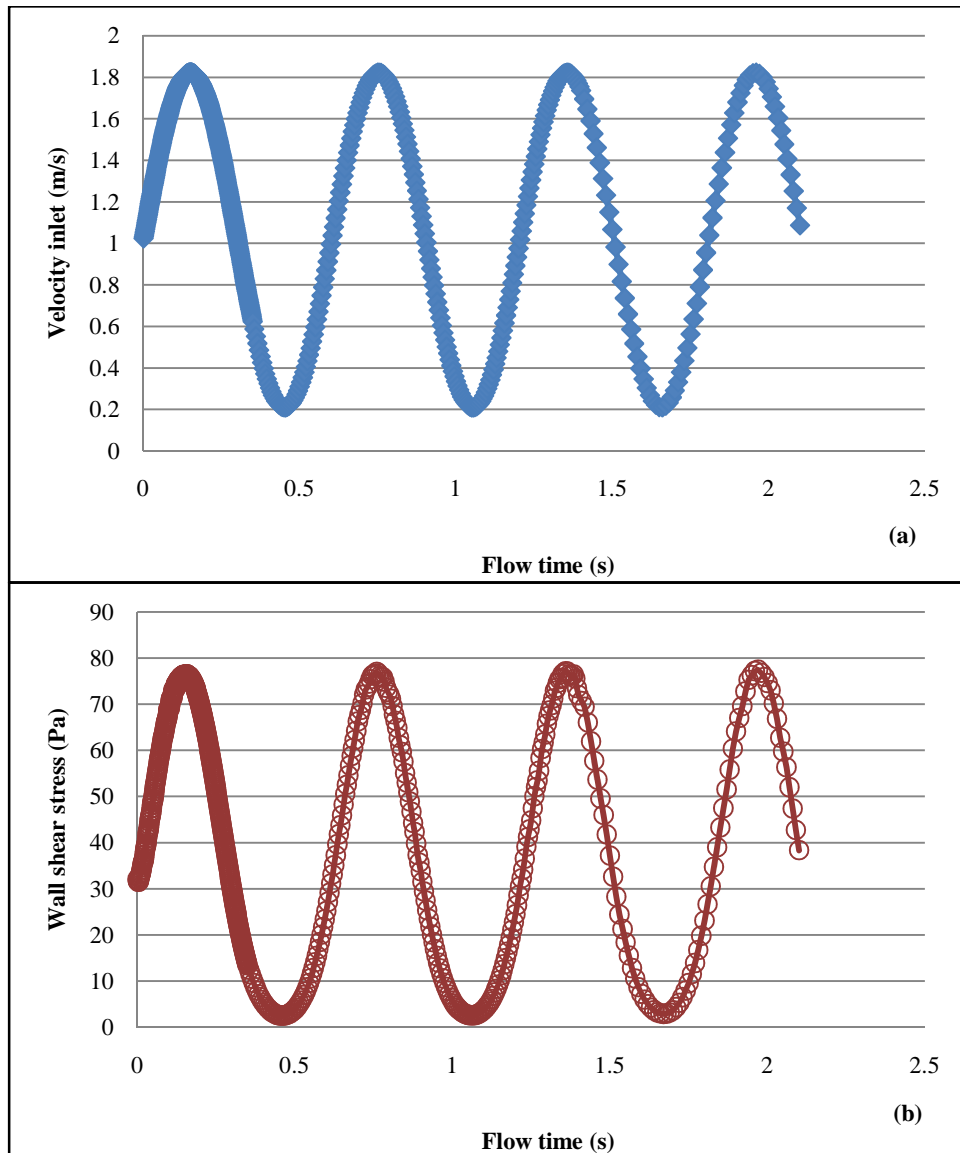
Figure 5.3 The variation of velocity inlet (a) and the instantaneous wall shear stress

(b) with time for the sinusoidal waveform pulsation (mean velocity 1.02 m/s,

amplitude 0.81 and frequency 1.66 Hz) in corrugated channel.
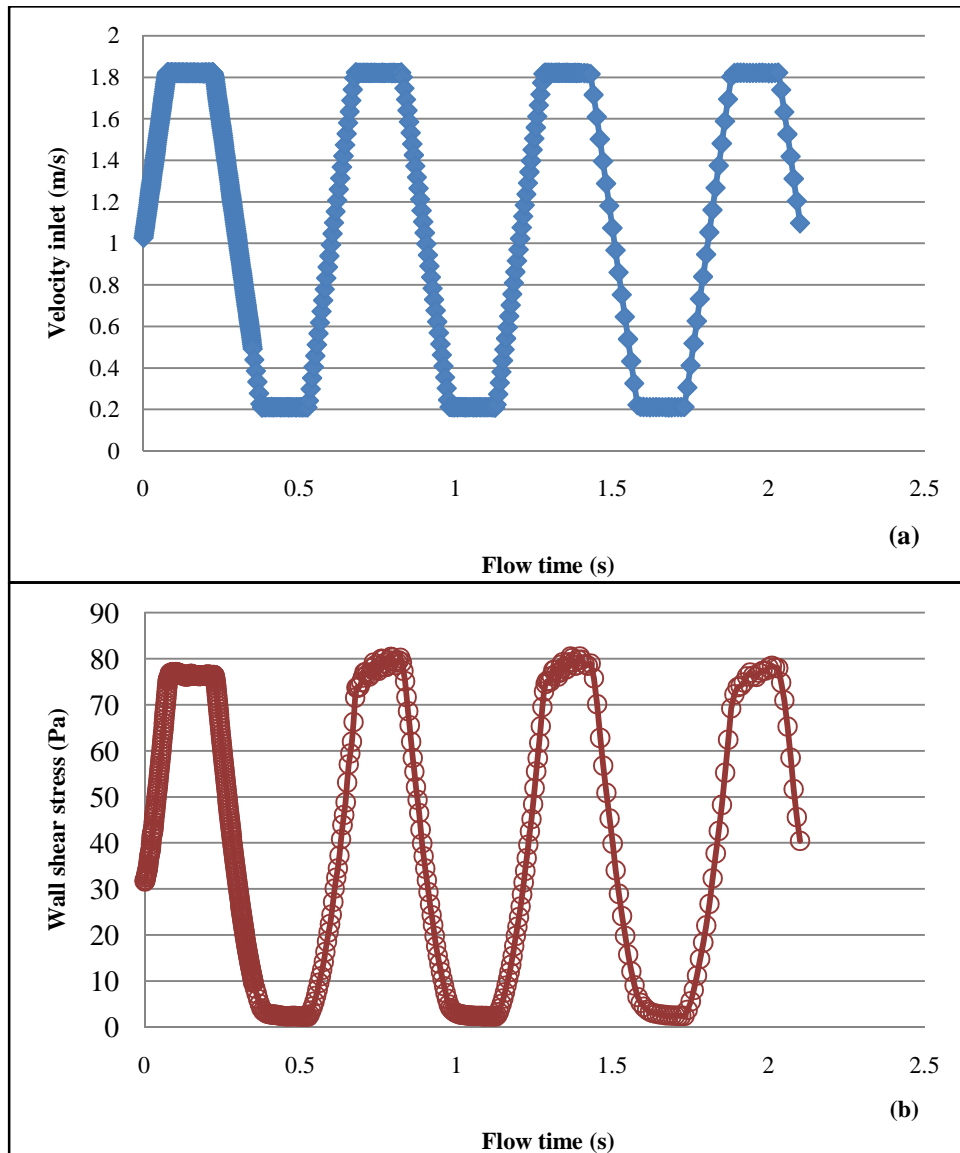
Figure 5.4 The variation of velocity inlet (a) and the instantaneous wall shear stress

(b) with time for the trapezoidal waveform pulsation (mean velocity 1.02 m/s,

amplitude 0.81 and frequency 1.66 Hz) in corrugated channel.

When the time-averaged wall shear stresses or mean wall shear stresses of various types of pulsating flows were considered, there are some significant differences between mean wall shear stress generated by different type of pulsed

flows. These differences can be seen in all flow domains. In cylindrical pipe, the results show that pulsed flow generates higher mean wall shear stress than the steady flow. At the same time, within group of pulsed flows, pulsed flow with the rectangular waveform pulsation generates the highest mean wall shear stress. Pulsed flow, which behaves like trapezoidal wave, also generates significantly higher wall shear stress than the triangular waveform pulsation. Meanwhile, mean wall shear stresses generated by saw tooth and sinusoidal waveform pulsation are not statistically different from both of mean wall shear stressed of trapezoidal waveform pulsation and triangular waveform pulsation. These results can be seen in the Figure 5.5.
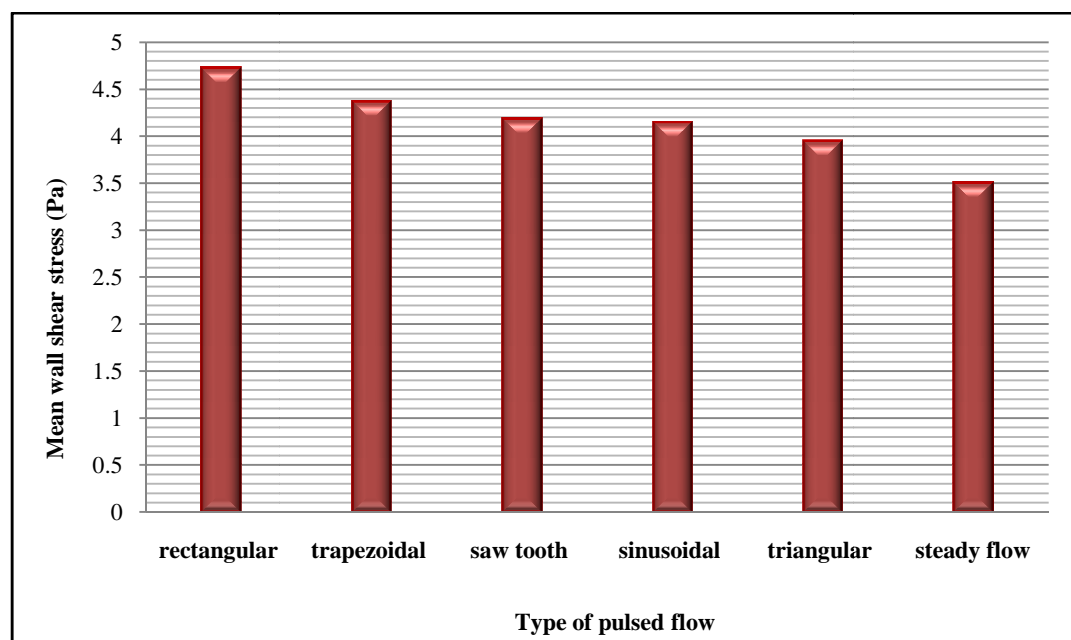
Figure 5.5 The effect of type of pulsed flow on mean wall

shear stress in the cylindrical pipe

In corrugated channel of plate heat exchanger and parallel plates, the response of mean wall shear stresses to pulsating flow and steady flow similar to the response in the cylindrical pipe. However, there are some differences between the response of mean wall shear stress on different type of pulsed flow in the cylindrical pipe and the other ones. In corrugated channel and parallel plates, pulsed flow, which behaves like rectangular wave, generates the highest mean wall shear stress. Pulsating flow with the trapezoidal waveform generates greater mean wall shear stress than the sawtooth and triangular waveform pulsation. Meanwhile, mean wall shear stresses generated by sinusoidal waveform pulsation are not significantly different from mean wall shear stressed of trapezoidal, sawtooth and triangular waveform pulsation. The influences of type of pulsed flow on mean wall shear stress in corrugated channel and parallel plates are shown in Figure 5.6 and 5.7, respectively.
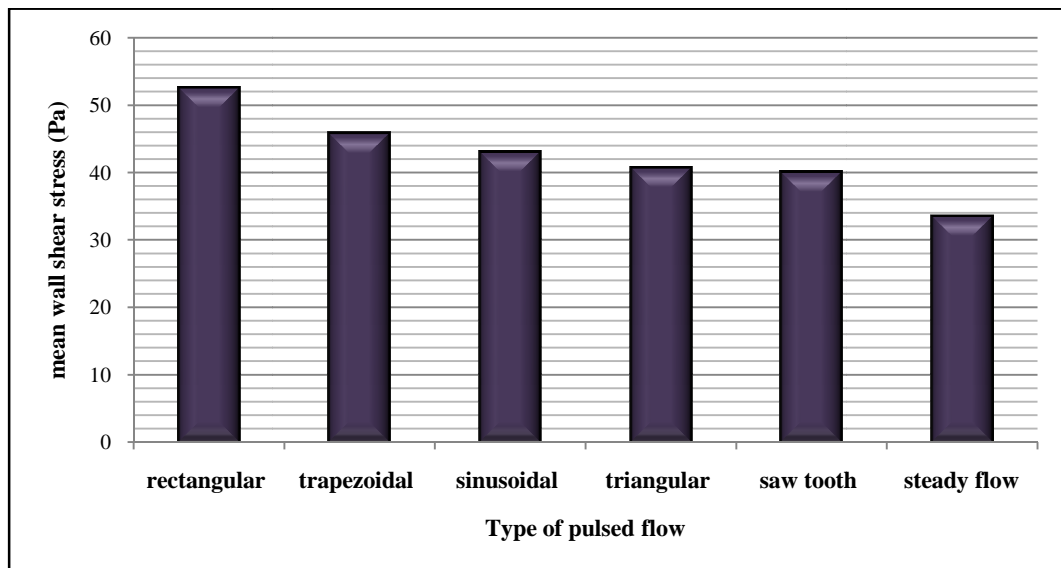
Figure 5.6 The effect of type of pulsed flow on mean wall shear stress

in the corrugated channel of plate heat exchanger
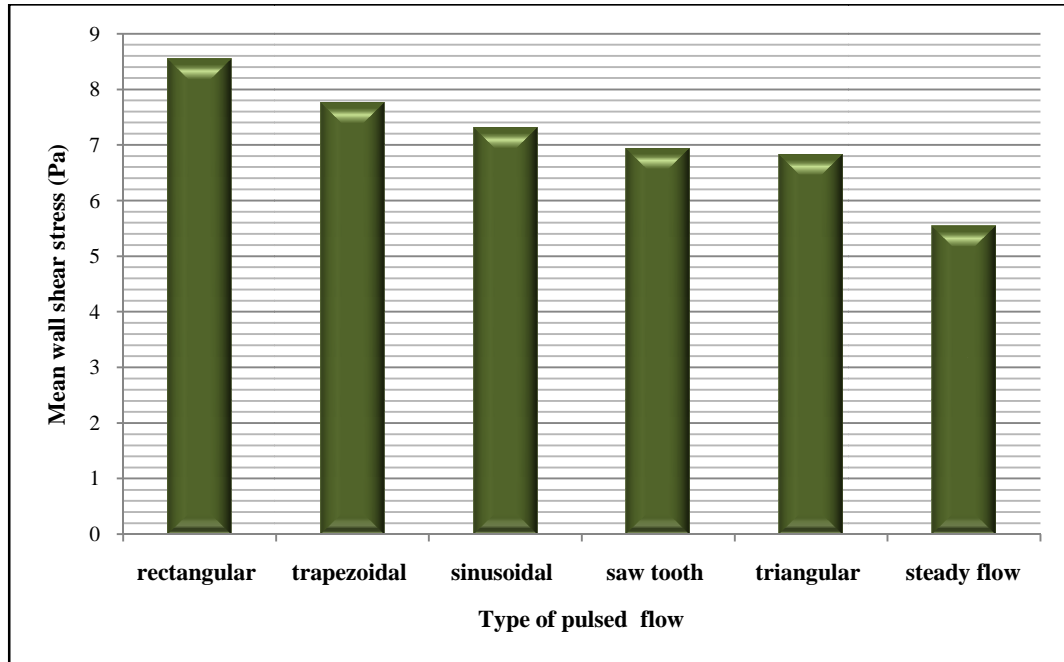
Figure 5.7 The effect of type of pulsed flow on mean wall

shear stress in the parallel plates

The response of mean wall shear stress on different type of pulsed flow corresponds to wall shear stress distribution and velocity profile of pulsed flows in each flow domain.

Generally, wall shear stress distribution of pulsating flows in the cylindrical pipe has a pattern of the distribution as in Figure 5.8 and 5.10. Wall shear stress is constant around the circumference of pipe. In axial direction, wall shear stress is greatest at inlet of pipe, then, it gradually decreases in downstream region. This phenomenon occurs because of the entrance effect. Wall shear stress will reduce until flow velocity profile is fully developed. The flow pattern is in the form of plug flow at high velocity as in Figure 5.9, whereas, the flow seems to be the Poiseuille's type flow at low velocity as shows in Figure 5.11. However, there is a different pattern of

wall shear stress distribution. This pattern can be found in the pulsating flow with the rectangular and trapezoidal waveform pulsation. When the flow velocity suddenly changes, the reverse flow occurs at near wall region of pipe. It makes wall shear stress in downstream region is higher than the upstream position. The second wall shear stress distribution and the flow velocity profile are shown in Figure 5.12, 5.13 and 5.14, respectively.
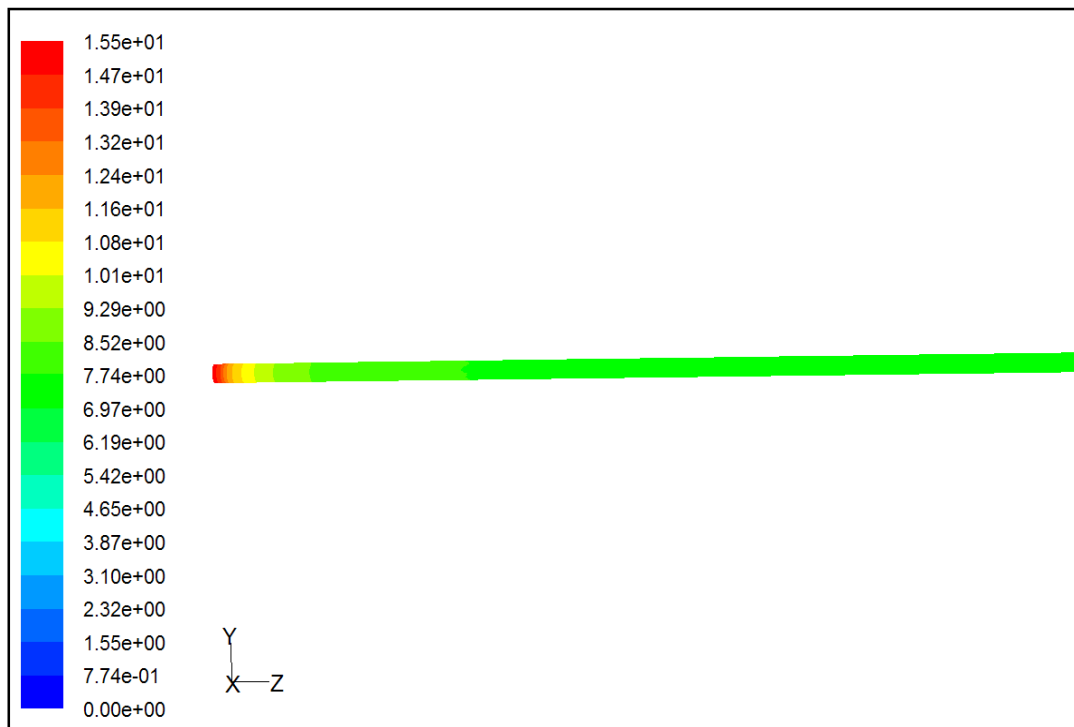
Figure 5.8 The wall shear stress distribution of pulsed flow with sinusoidal wave

form (mean velocity inlet 1.02 m/s, amplitude 0.81 m/s,

frequency 1.66 Hz) in the cylindrical pipe at 1.4 s
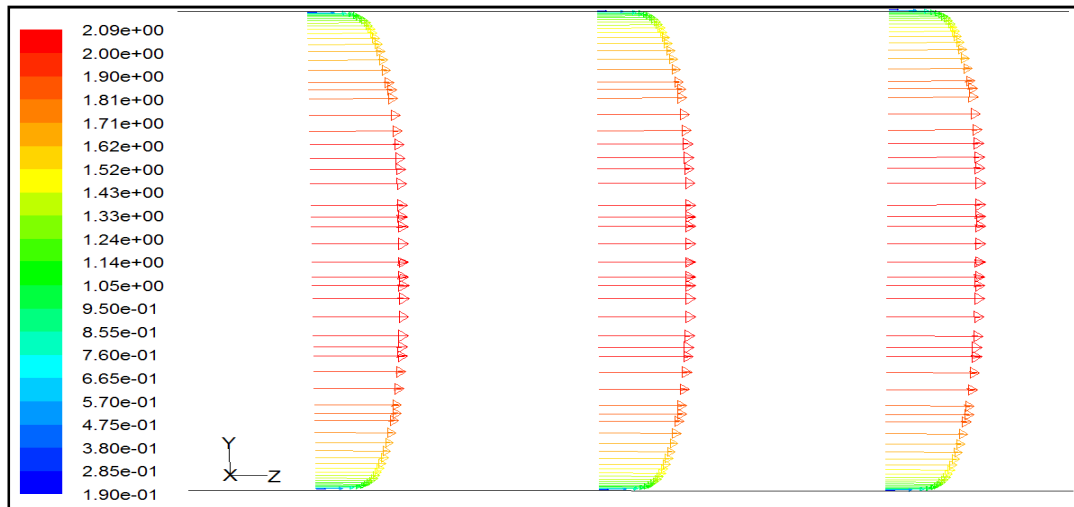
Figure 5.9 The velocity profile of pulsed flow with sinusoidal wave form (mean

velocity inlet 1.02 m/s, amplitude 0.81 m/s, frequency

1.66 Hz) in the cylindrical pipe at 1.4 s
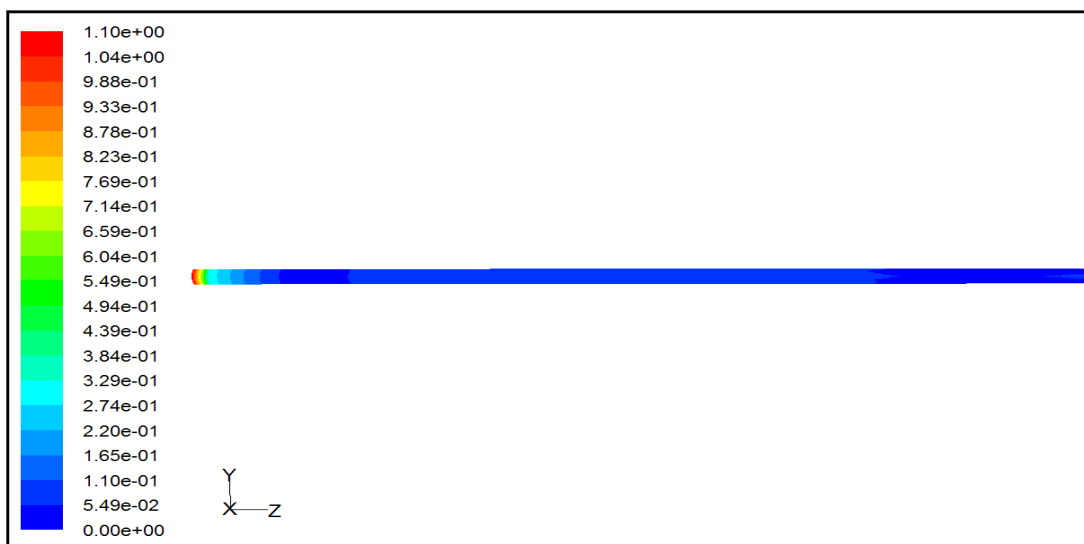
Figure 5.10 The wall shear stress distribution of pulsed flow with sinusoidal wave

form (mean velocity inlet 1.02 m/s, amplitude 0.81 m/s,

frequency 1.66 Hz) in the cylindrical pipe at 1.6 s
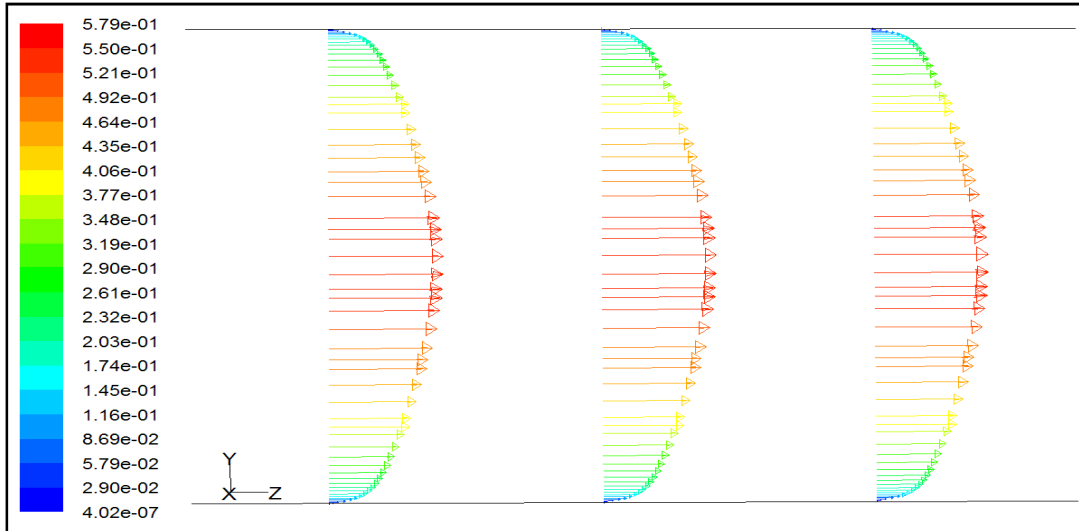
Figure 5.11 The velocity profile of pulsed flow with sinusoidal wave form (mean

velocity inlet 1.02 m/s, amplitude 0.81 m/s, frequency

1.66 Hz) in the cylindrical pipe at 1.6 s
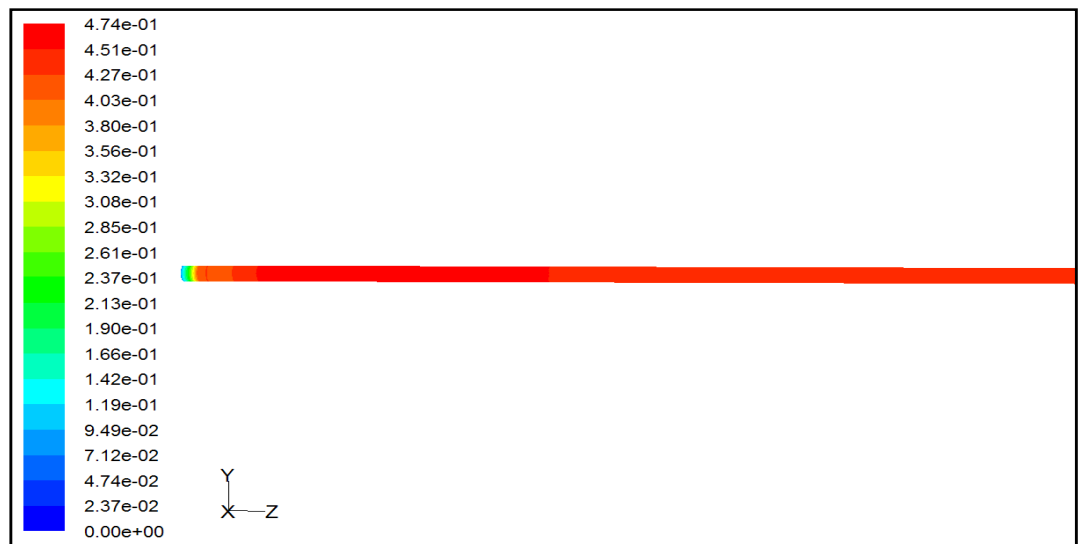
Figure 5.12 The wall shear stress distribution of pulsed flow with rectangular wave

form (mean velocity inlet 1.02 m/s, amplitude 0.81 m/s,

frequency 1.66 Hz) in the cylindrical pipe at 1.2 s
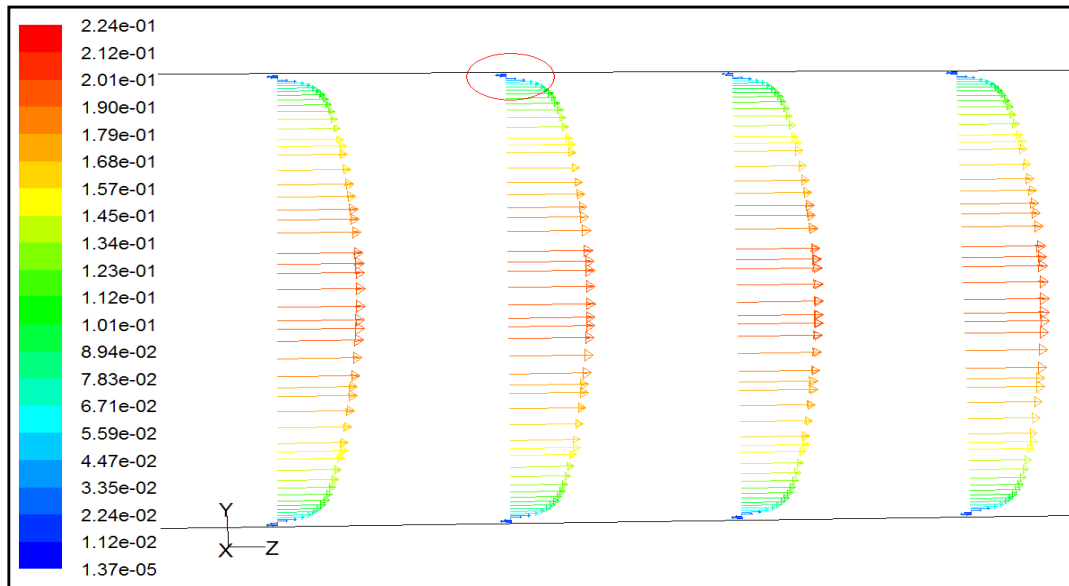
Figure 5.13 The velocity profile of pulsed flow with rectangular wave form (mean

velocity inlet 1.02 m/s, amplitude 0.81 m/s, frequency

1.66 Hz) in the cylindrical pipe at 1.2 s
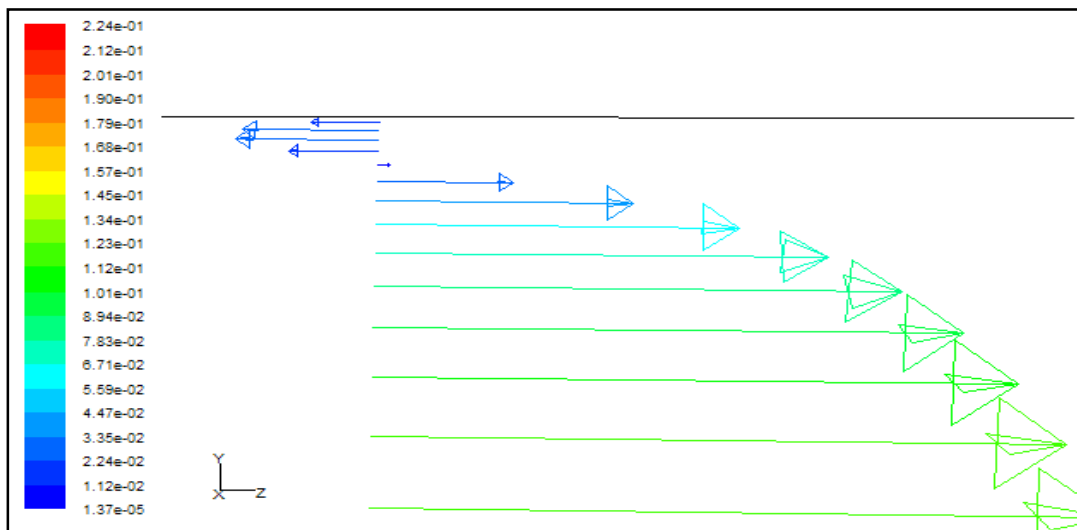
Figure 5.14 The reverse flow of pulsed flow with rectangular wave form (mean

velocity inlet 1.02 m/s, amplitude 0.81 m/s, frequency

1.66 Hz) in the cylindrical pipe at 1.2 s

In parallel plates, wall shear stress distribution has the similar pattern as in the cylindrical pipe. When the flow velocity is high, wall shear stress is highest at the inlet of parallel plates. Then, it gradually decreases in downstream region because of the entrance effect as in Figure 5.15 and 5.16. The velocity profile is in the form of plug flow as in Figure 5.17. This pattern is also seen when the flow velocity is high as in Figure 5.18. But at low velocity, not only the inlet region of plates but also the near symmetry plane region can be seen the high wall shear stress. This is because the flow is similar to the Poiseuille's type (Figure 5.19) which the maximum velocity is in the center region of the flow channel. Thus, high wall shear stress can be found near the symmetry plane of the parallel plates.
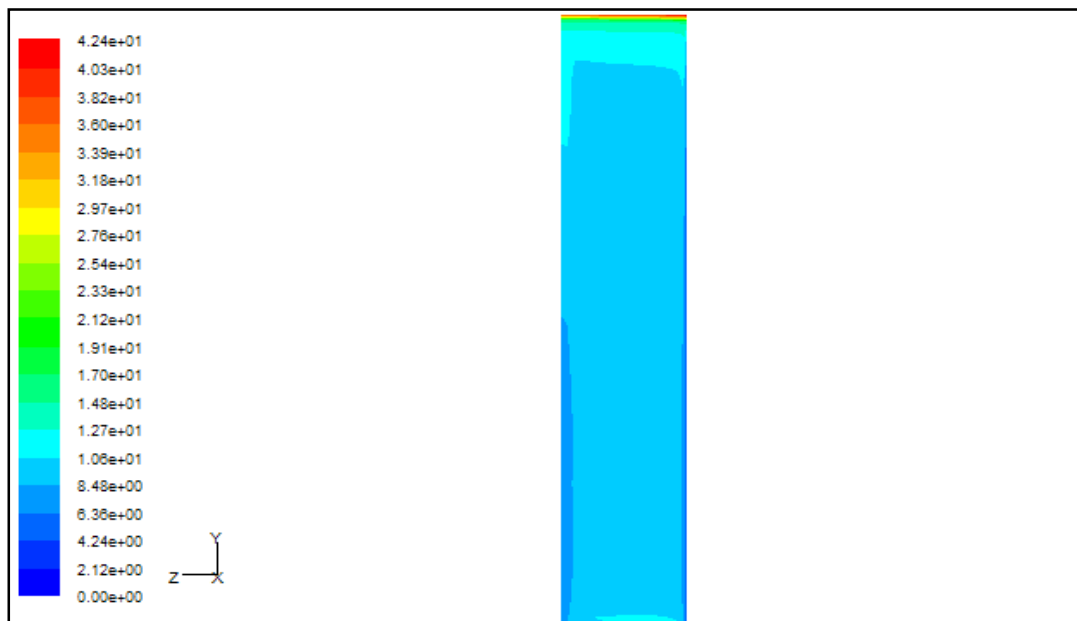
Figure 5.15 The wall shear stress distribution of pulsed flow with triangular wave

form (mean velocity inlet 1.02 m/s, amplitude 0.81 m/s,

frequency 1.66 Hz) in the parallel plates at 2.0 s
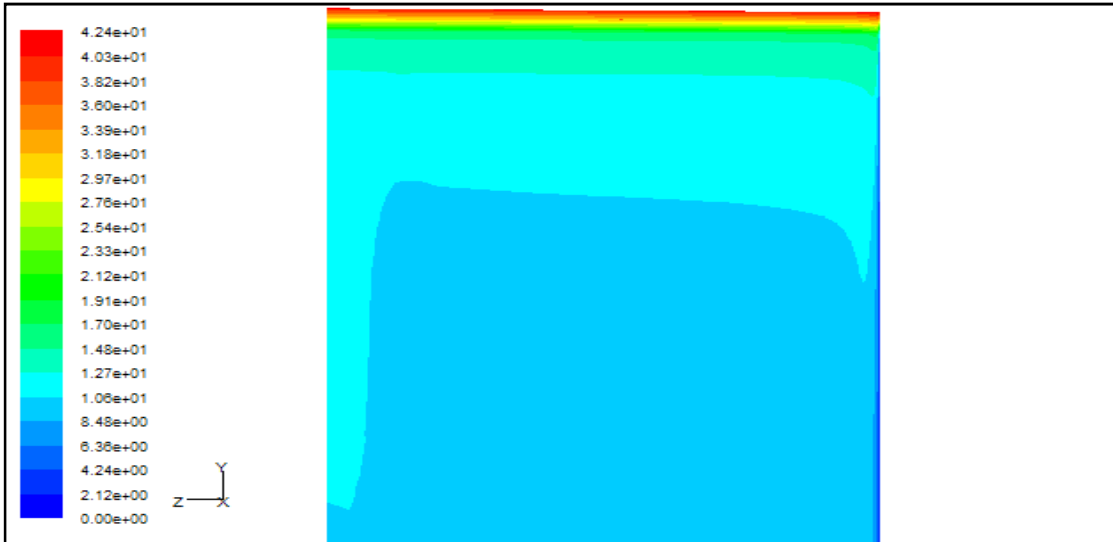
Figure 5.16 The wall shear stress distribution of pulsed flow with triangular wave

form (mean velocity inlet 1.02 m/s, amplitude 0.81 m/s, frequency

1.66 Hz) in the parallel plates at 2.0 s (large view)
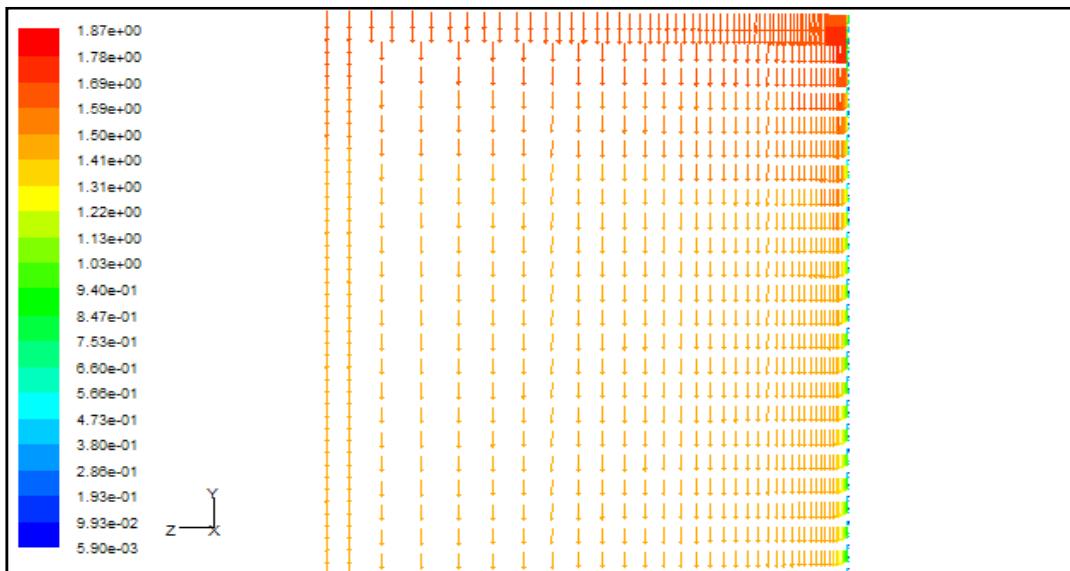
Figure 5.17 The velocity profile of pulsed flow with triangular wave form (mean

velocity inlet 1.02 m/s, amplitude 0.81 m/s, frequency 1.66 Hz) at

the plane x = 0.0012 m in the parallel plates, Time 2.0 s
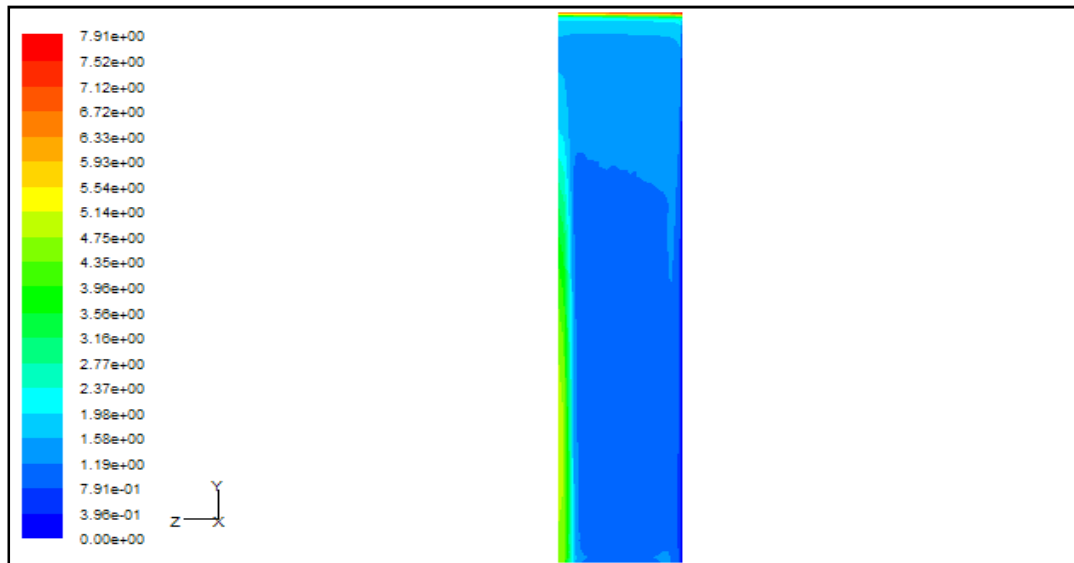
Figure 5.18 The wall shear stress distribution of pulsed flow with triangular wave

form (mean velocity inlet 1.02 m/s, amplitude 0.81 m/s,

frequency 1.66 Hz) in the parallel plates at 1.6 s
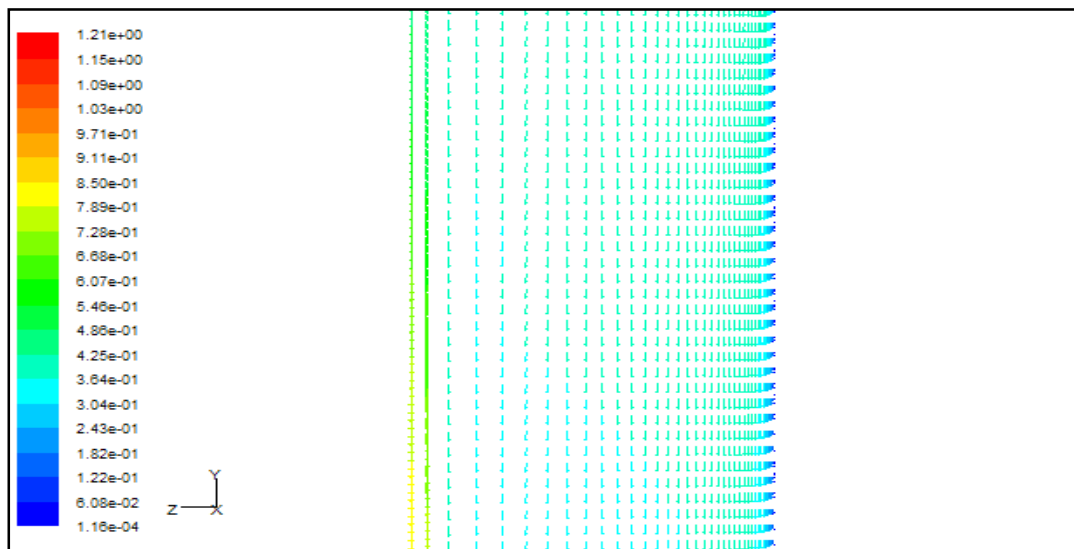
Figure 5.19 The velocity profile of pulsed flow with triangular wave form (mean

velocity inlet 1.02 m/s, amplitude 0.81 m/s, frequency 1.66 Hz) at

the plane x = 0.0012 m in the parallel plates, Time 1.6 s

As same as the cylindrical pipe, when the flow velocity immediately changes, there is the reverse flow occurs in the channel of parallel plates as in Figure 5.21. It causes higher wall shear stress in this region compares to the surrounding as shows in Figure 5.20. This phenomenon can be found when the flows are pulsating flows with rectangular and trapezoidal waveform pulsations.
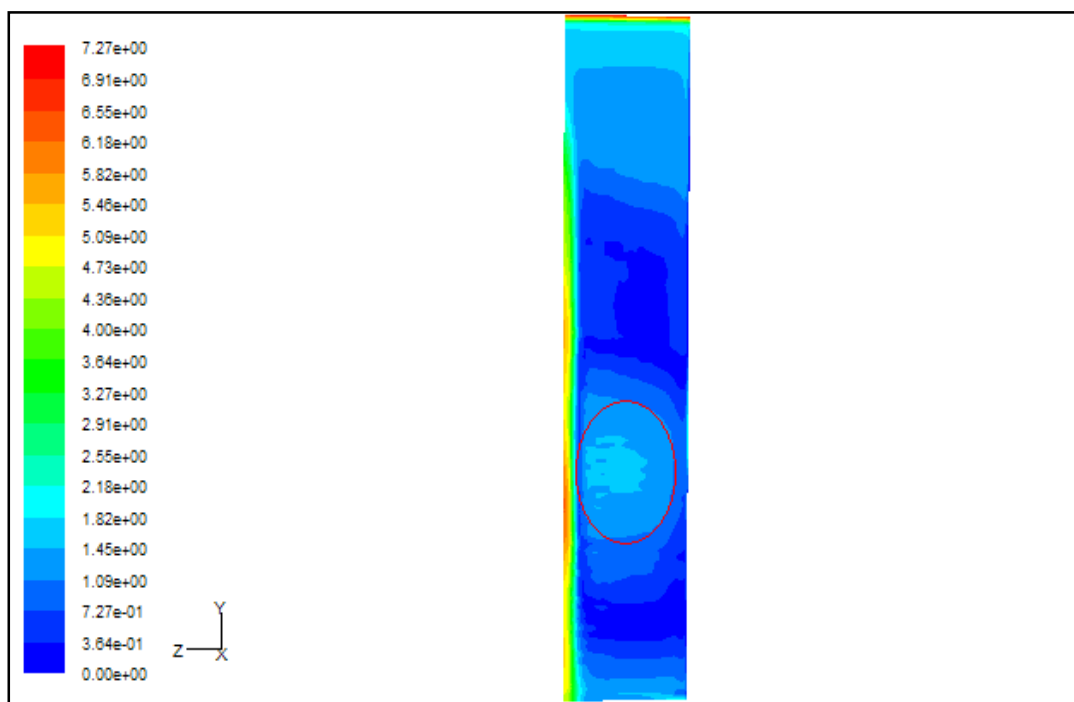
Figure 5.20 The wall shear stress distribution of pulsed flow with rectangular wave

form (mean velocity inlet 1.21 m/s, amplitude 0.73 m/s, frequency

2.5 Hz) in the parallel plates at 1.1 s

Figure 5.21 The reverse flow of pulsed flow with rectangular wave form (mean

velocity inlet 1.21 m/s, amplitude 0.73 m/s, frequency

2.5 Hz) in the parallel plates at 1.1 s

For wall shear stress distribution in corrugated channel of plat heat exchanger, there is no explicit difference between the general pulsed flows and the flows whose velocity suddenly change, because of the complexity of the flow channel geometry. Typically, wall shear stress is high at the furrow of the corrugated plates as in Figure 5.22 and Figure 5.23. The velocity is also high in this part of plates as in Figure 5.24. This is because this part of plate obstructs the flow in the serpentine channel, pressure is dropped and the velocity is increased as in Figure 5.25. At the same time, in the converging-diverging channel, this part of plate not only obstructs the flow but also reduces the cross-section area of the flow channel. This causes the raising of the velocity in this region as shows in Figure 5.26. Additionally, the vortices that occur in

both of those channels are another cause of the increase of wall shear stress in the
furrow region of the corrugated plates
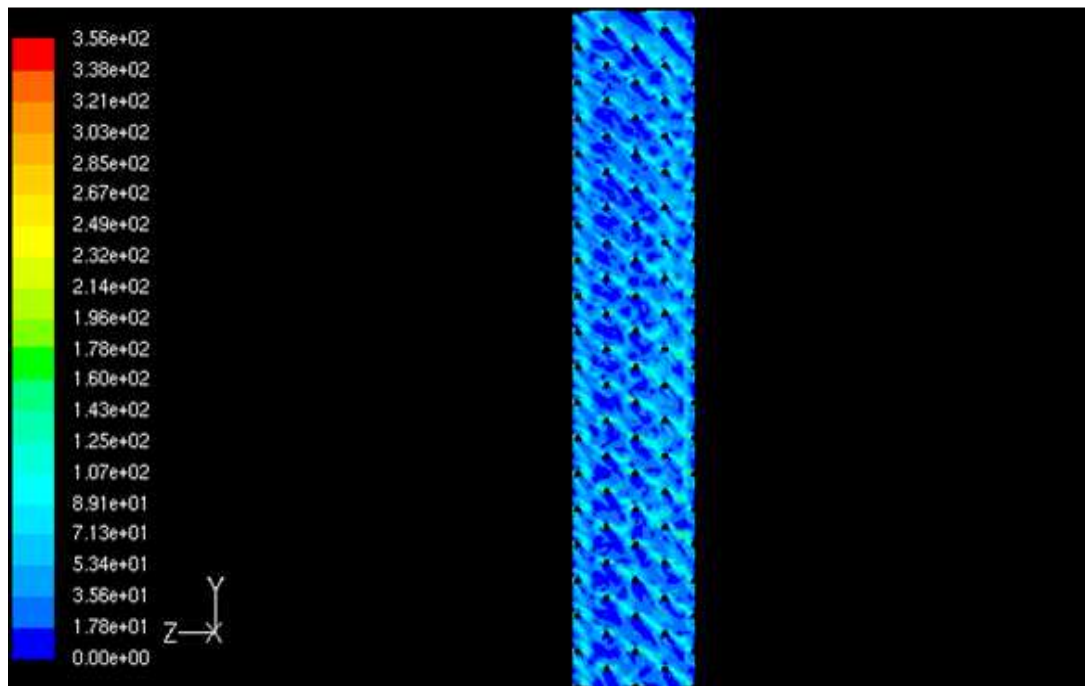
Figure 5.22 The wall shear stress distribution of pulsed flow with trapezoidal wave

form (mean velocity inlet 1.02 m/s, amplitude 0.81 m/s,

frequency 1.66 Hz) in the corrugated channel at 1.5 s
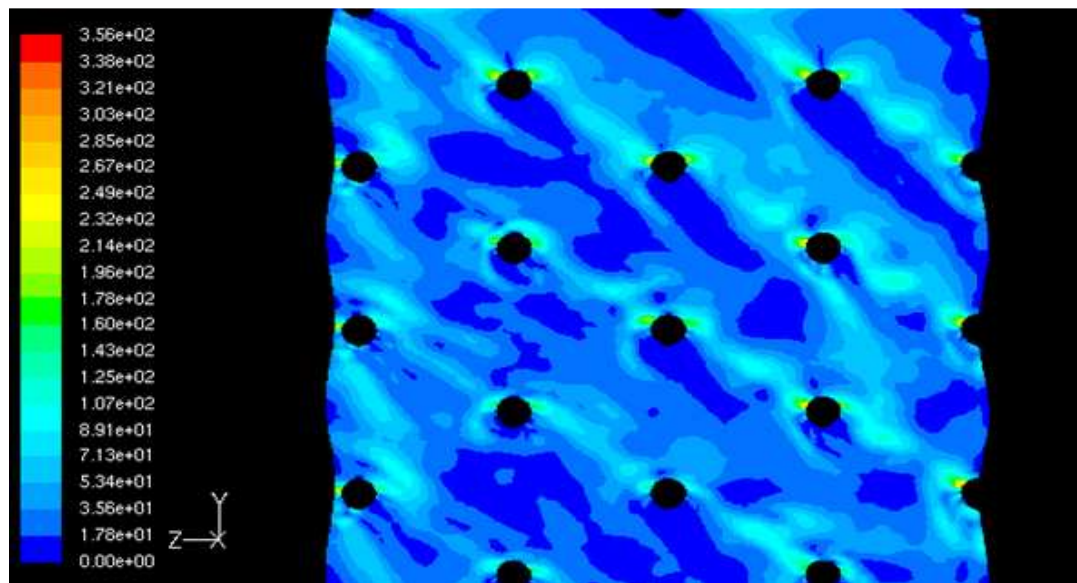
Figure 5.23 The wall shear stress distribution of pulsed flow with trapezoidal wave

form (mean velocity inlet 1.02 m/s, amplitude 0.81 m/s, frequency

1.66 Hz) in the corrugated channel at 1.5 s (large view)
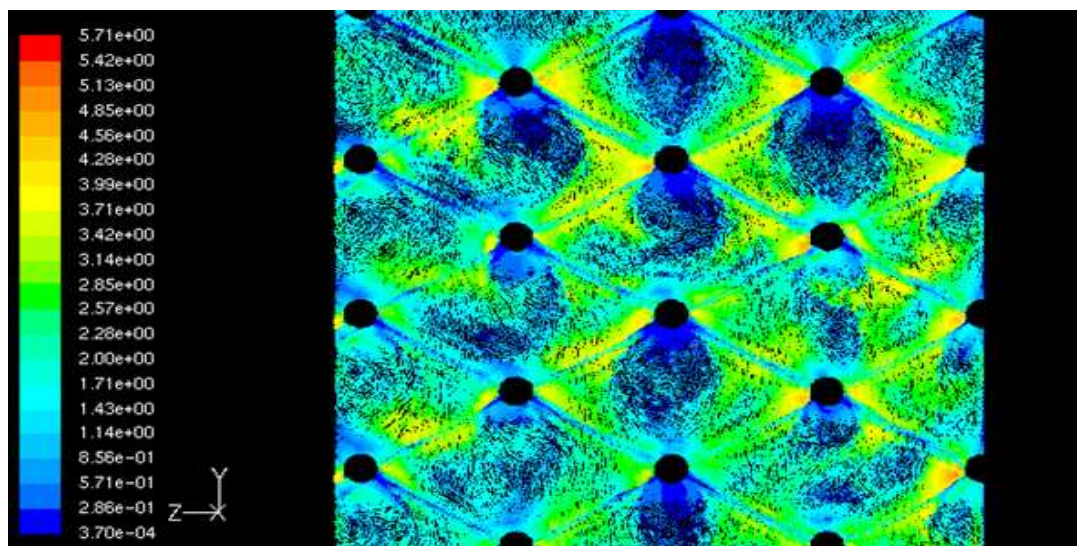
Figure 5.24 The velocity profile of pulsed flow with trapezoidal wave form (mean

velocity inlet 1.02 m/s, amplitude 0.81 m/s, frequency 1.66 Hz)

at the medium plane of corrugated channel, Time 1.5 s
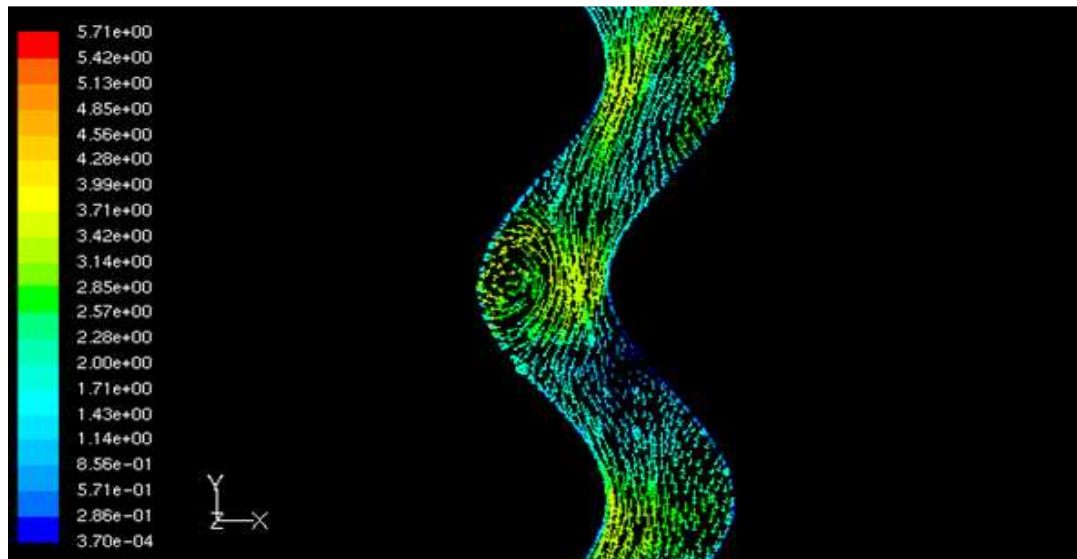
Figure 5.25 The velocity profile of pulsed flow with trapezoidal wave form (mean

velocity inlet 1.02 m/s, amplitude 0.81 m/s, frequency 1.66 Hz)

at the plane z = 0.00433 m of corrugated channel, Time 1.5 s
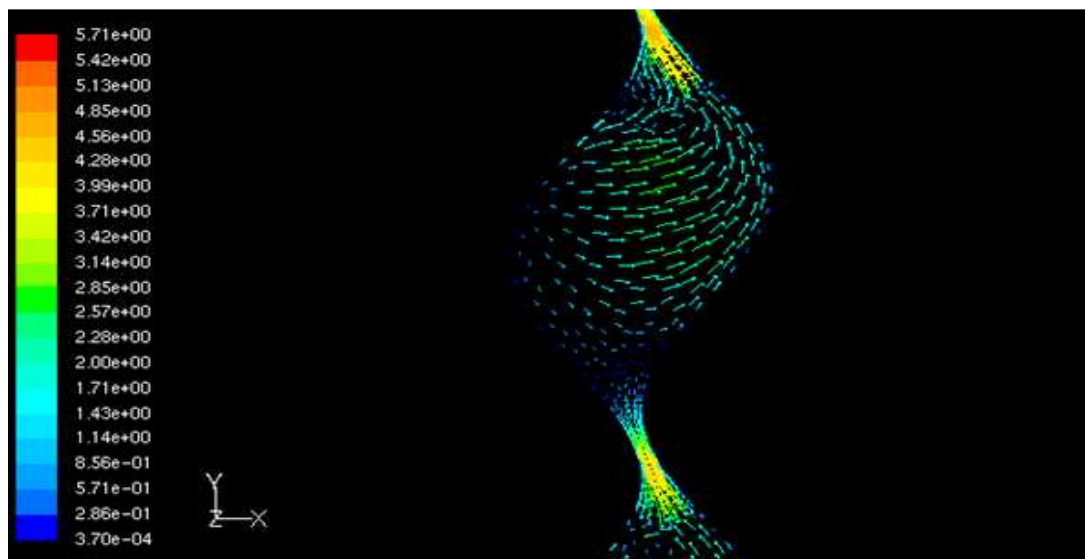
Figure 5.26 The velocity profile of pulsed flow with trapezoidal wave form (mean

velocity inlet 1.02 m/s, amplitude 0.81 m/s, frequency 1.66 Hz)

at the symmetry plane of corrugated channel, Time 1.5 s

Although there is no explicit difference of wall shear stress distribution between the general pulsed flow and the flows whose velocity suddenly change in the corrugated channel of plate heat exchanger, the differences can be observed in the cylindrical pipe and the parallel plates. The phenomena of wall shear stress distribution and the velocity profile of pulse flows show why mean wall shear stresses of pulsed flow with the rectangular and trapezoidal waveform pulsations are higher than the others.

5.3   The Effect of Amplitude of Pulsation on Wall Shear Stress

With the same mean velocity inlet and frequency of pulsation, wall shear stresses that generated by pulsed flows with different amplitude of pulsation as in Table 4.3 were analyzed under the same flow condition. This study was done in the cylindrical, corrugated channel of plate heat exchanger and parallel plates. The results show that the maximum wall shear stresses and mean wall shear stresses are proportional to the amplitude of pulsation. These relationships can be seen in all three domains as show in the Figure 5.27-5.29. Because the increase of amplitude raises the instantaneous velocity of the flow. This gives higher velocity gradient at the wall that relates to the wall shear stress in the channel.
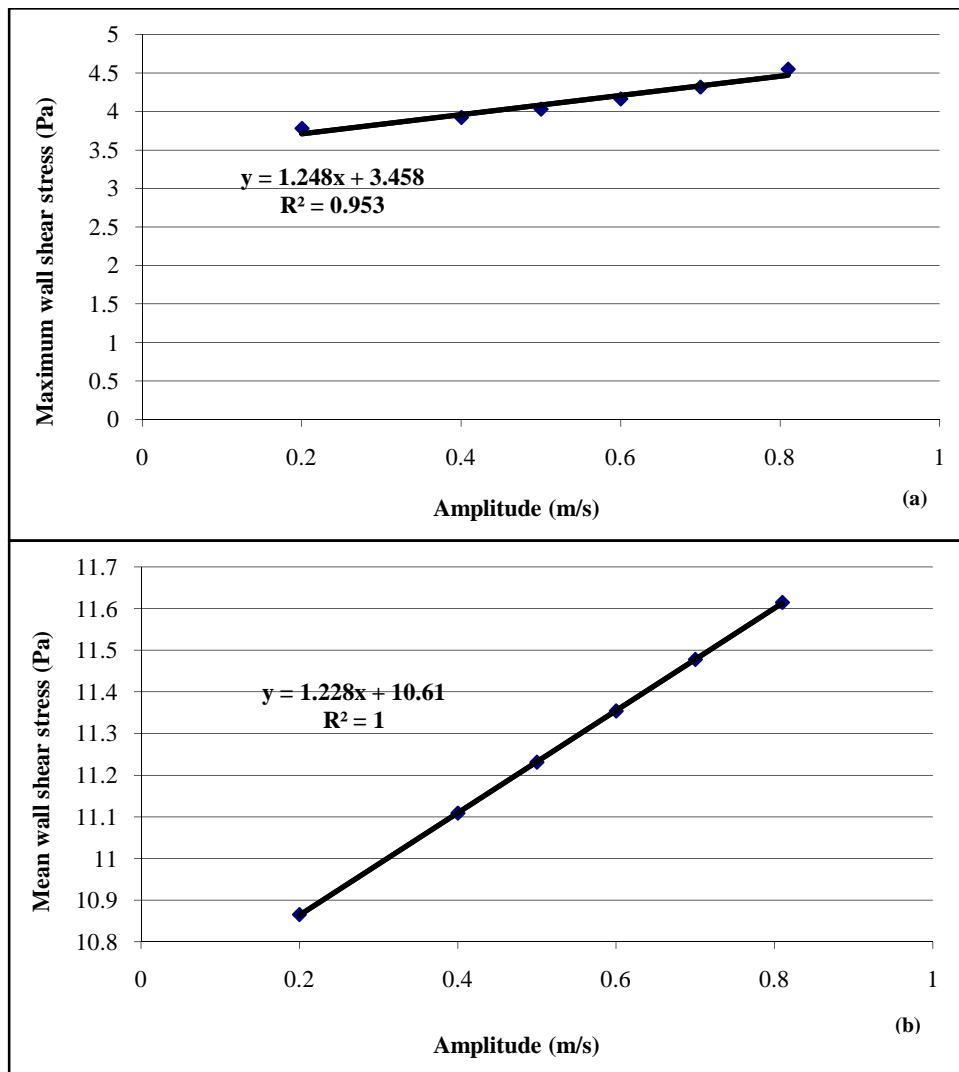
Figure 5.27 The relationship between maximum wall shear stress (a), mean wall

shear stress (b) and amplitude of pulsation in the cylindrical pipe
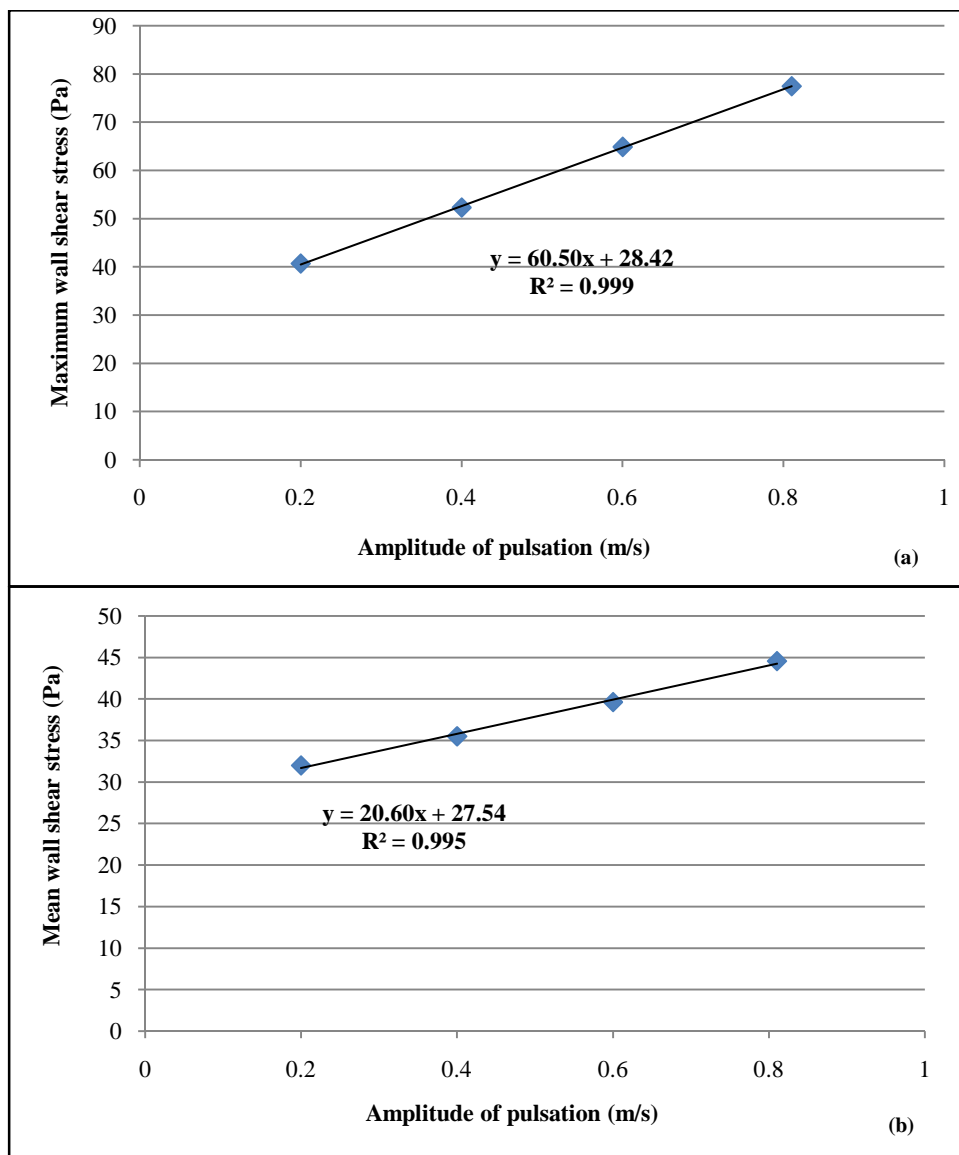
Figure 5.28 The relationship between maximum wall shear stress (a), mean wall

shear stress (b) and amplitude of pulsation in the corrugated channel
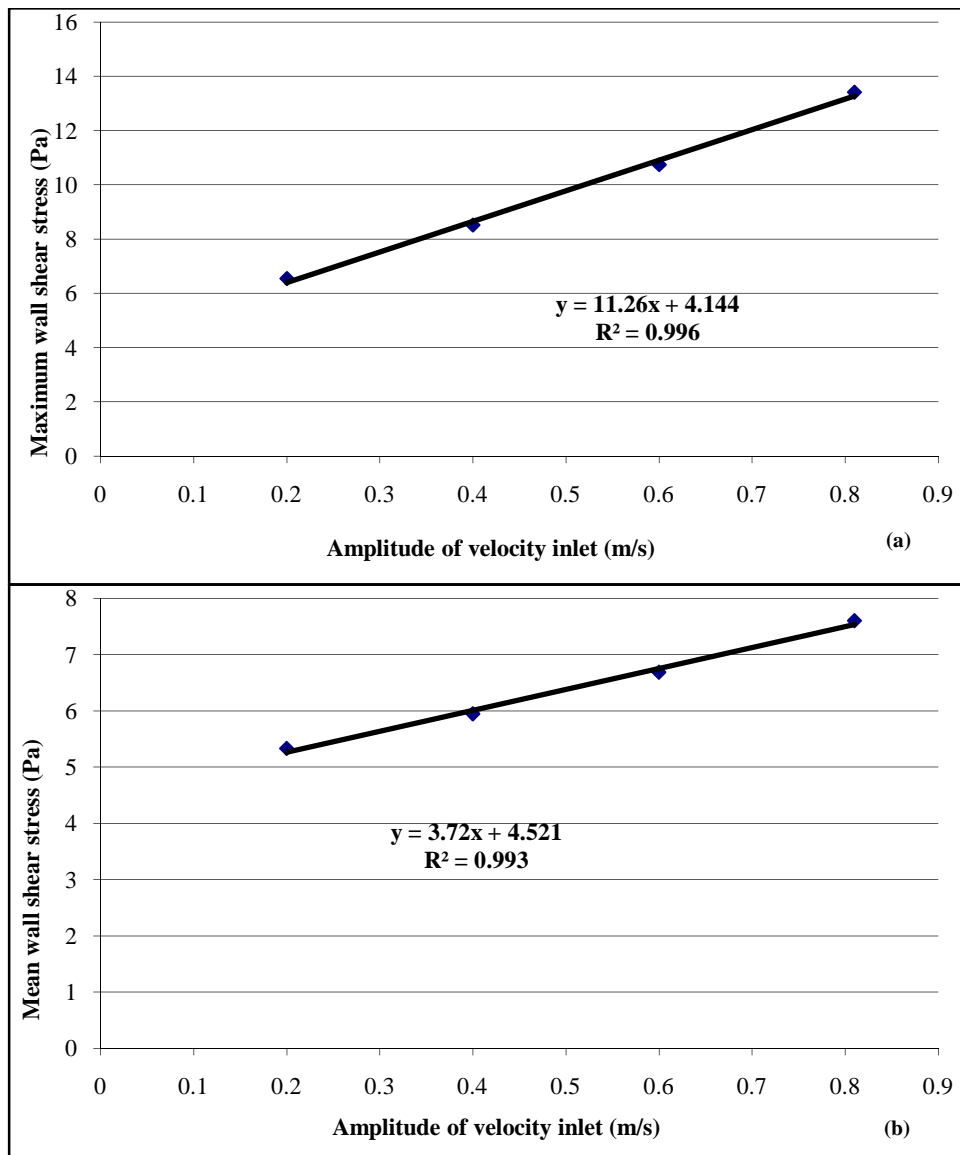
Figure 5.29 The relationship between maximum wall shear stress (a), mean wall shear stress (b) and amplitude of pulsation in the parallel plates

5.4   The Effect of Frequency of Pulsation on Wall Shear Stress

With the same mean velocity inlet and amplitude of pulsation, wall shear stresses that generated by pulsed flows with different frequency of pulsation as in Table 4.4 were analyzed under the same flow condition. The flows were simulated through all flow domain; cylindrical pipe, corrugated channel and parallel plates. The effect of frequency of pulsation on wall shear stress is presented in the form of the relationship between mean wall shear stress and frequency of pulsation. As the results of the study, in the cylindrical pipe, mean wall shear stress is proportional to the frequency of pulsation as shows in Figure 5.30.

$y = 0.237x + 4.232$
$R^2 = 0.906$
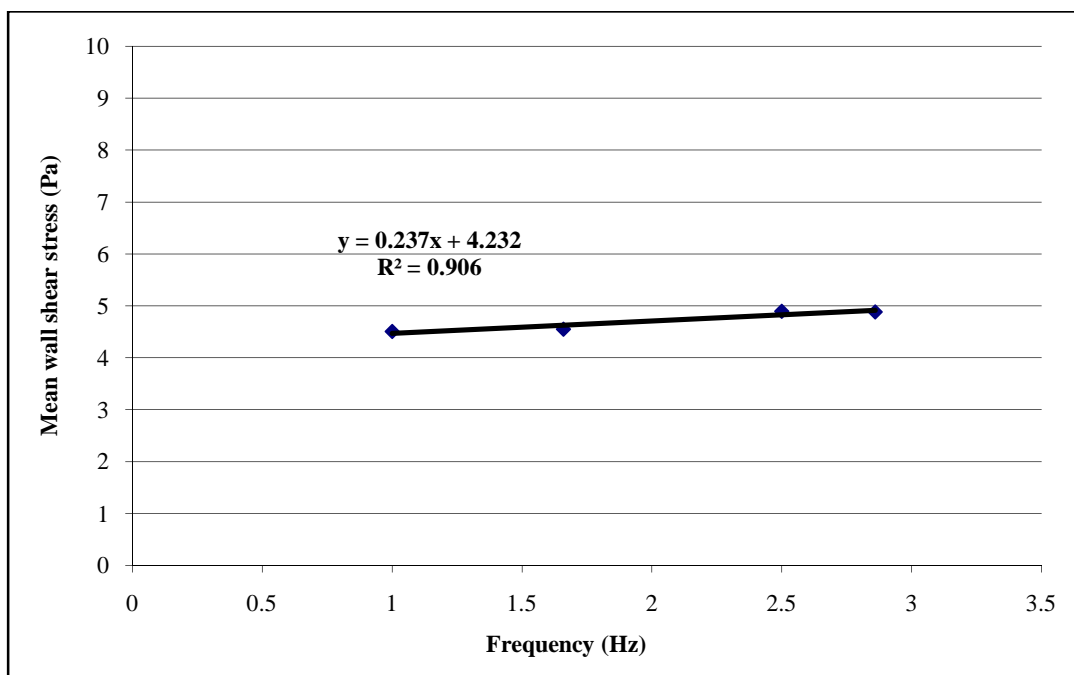
Figure 5.30 The relationship between mean wall shear stress and the frequency

of pulsation of pulsed flow in the cylindrical pipe

On the other hand, mean wall shear stress and the frequency of pulsation are inverse proportional in the parallel plates as shows in Figure 5.31.
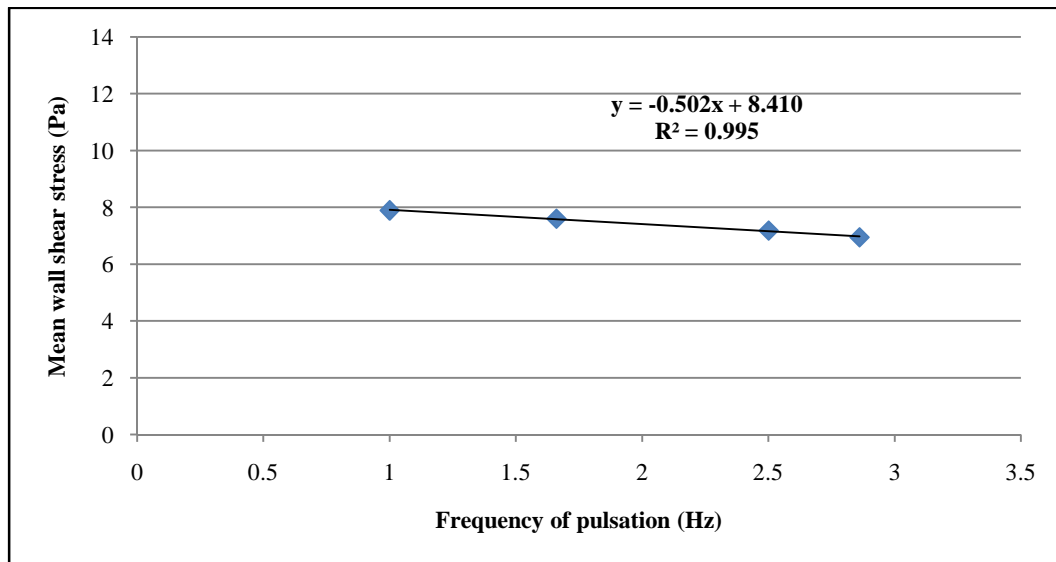
Figure 5.31 The relationship between mean wall shear stress and the frequency of pulsation of pulsed flow in the parallel plates

Although both of mean wall shear stresses in the cylindrical pipe and parallel plates vary with the frequency of pulsation, in the study range of frequency, the effects of frequency on mean wall shear stress in these flow domains are quite small. These results correspond to the study results of Mao and Hanratty (1986) who studied the wall shear stress in a turbulent pulsating pipe flow. One of their results showed that the frequency and the imposed oscillation had no effect on the time-mean velocity gradient at the wall and wall shear stress. Meanwhile, the study results of Blel et al. (2009) showed that the frequency of pulsation affected on mean wall shear stress; the frequency of pulsation was more effective in the increase of wall shear stress than the amplitude. The contrast between this study result and the study results

of Blel et al. (2009) causes by the difference of the methodology of wall shear stress measurement between the experiment and the simulation as described in the section 5.1.2.

However, the influence of frequency on mean wall shear stress is increased by changing the geometry of flow domain. When the flow domain is more complicated as in the corrugated channel of plate heat exchanger, the effect of frequency of pulsation on mean wall shear stress is obviously seen as in Figure 5.32.

The chart contains the equation $y = -2.958x + 49.19$ and $R^2 = 0.994$
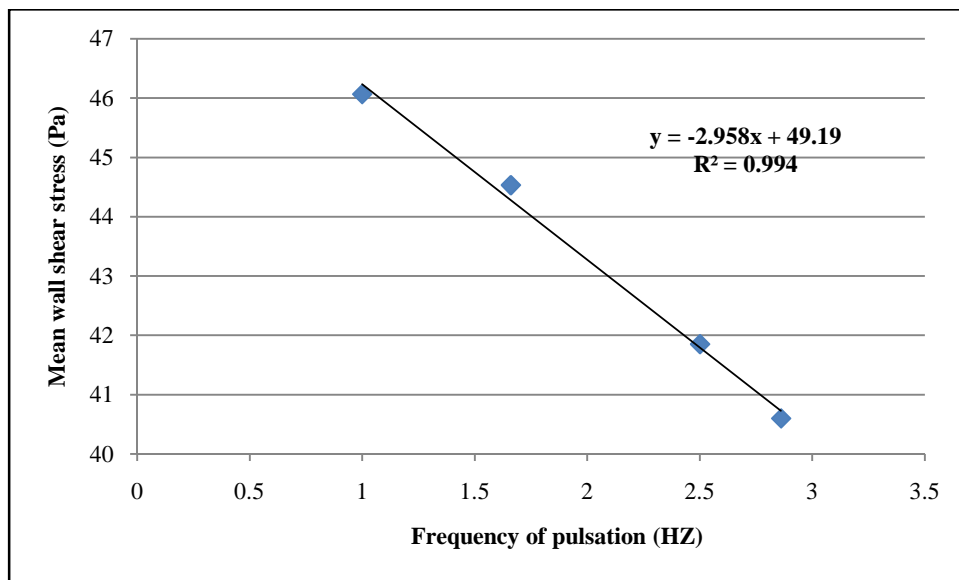
Figure 5.32 The relationship between mean wall shear stress and the frequency

of pulsation of pulsed flow in the corrugated channel

Figure 5.32 shows that mean wall shear stress inversely varies with the frequency of pulsation. This result corresponds to the results study of Nishimura and Matsune (1998) who studied vortices and wall shear stresses in the channel with sinusoidal wavy walls for pulsatile flow. Their results showed that the time-averaged vortex strength decreased when the frequency of pulsatile flow in the form of

Womersley number increased. This phenomenon can be observed in both asymmetric channel and symmetric channel. Figure 5.33 shows the effect of frequency on the growth of vortices which appears in the converging-diverging channel of plate heat exchanger.
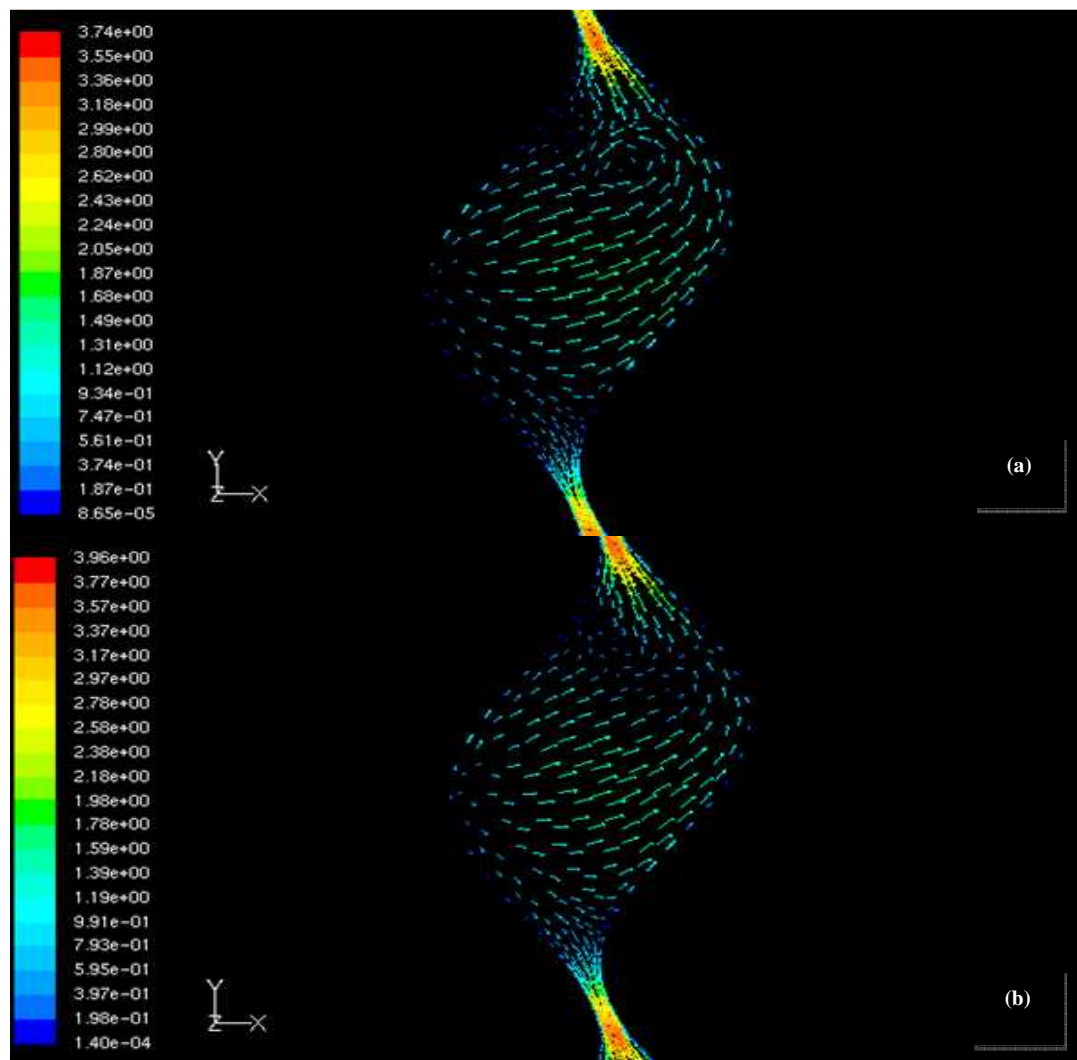
Figure 5.33 The velocity vector of sinusoidal pulsating flow with the similar

mean velocity but different frequency; 1.66 Hz (a) and

2.86 Hz (b), in the converging-diverging channel

The growth of vortices in the channel troughs increases the wall shear stress. When the time-averaged vortex strength decreases, wall shear stress also decreases. This is the reason why wall shear stress is inverse proportion to the frequency of pulsation in the corrugated channel of plate heat exchanger.

5.5 The Effect of Mean Velocity Inlet of Pulsation on Wall Shear Stress

To analyze the effect of mean velocity inlet on wall shear stress, pulsed flows with the pulsating condition as in Table 4.5 were simulated through all flow domain; cylindrical pipe, corrugated channel and parallel plates under the same flow condition. The effect of mean velocity inlet of pulsation on wall shear stress is presented in the form of the relationship between mean wall shear stress and mean velocity inlet. As the results of the study, in all three domains, mean wall shear stresses increase with mean velocity inlet of pulsation as shows in Figure 5.35, 5.36 and 5.37
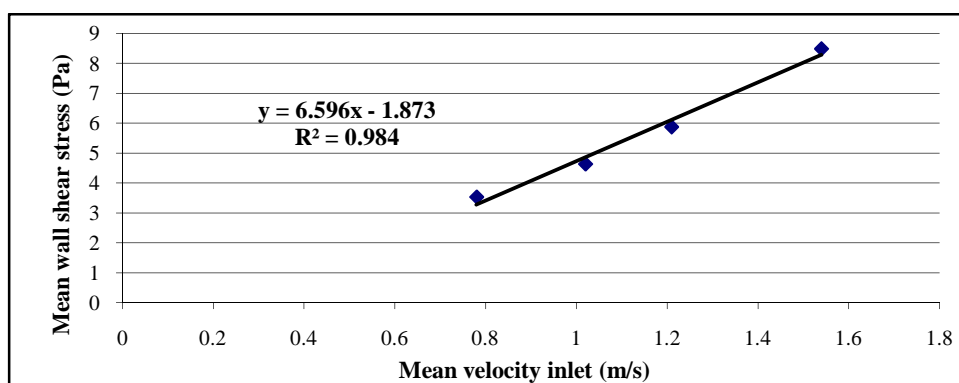
Figure 5.34 The relationship between mean wall shear stress and mean velocity inlet of pulsation of pulsed flow in the cylindrical pipe
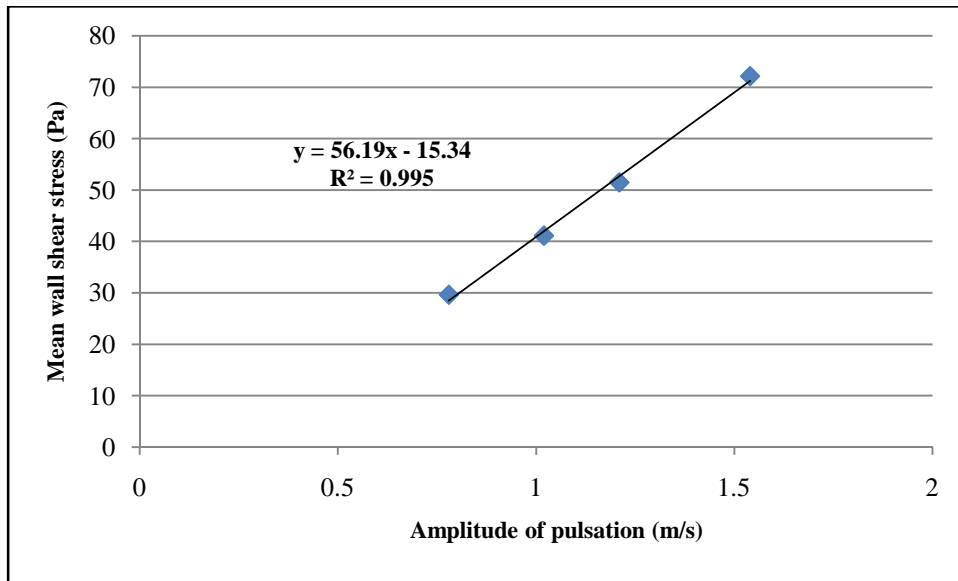
Figure 5.35 The relationship between mean wall shear stress and mean velocity

inlet of pulsation of pulsed flow in the corrugated channel
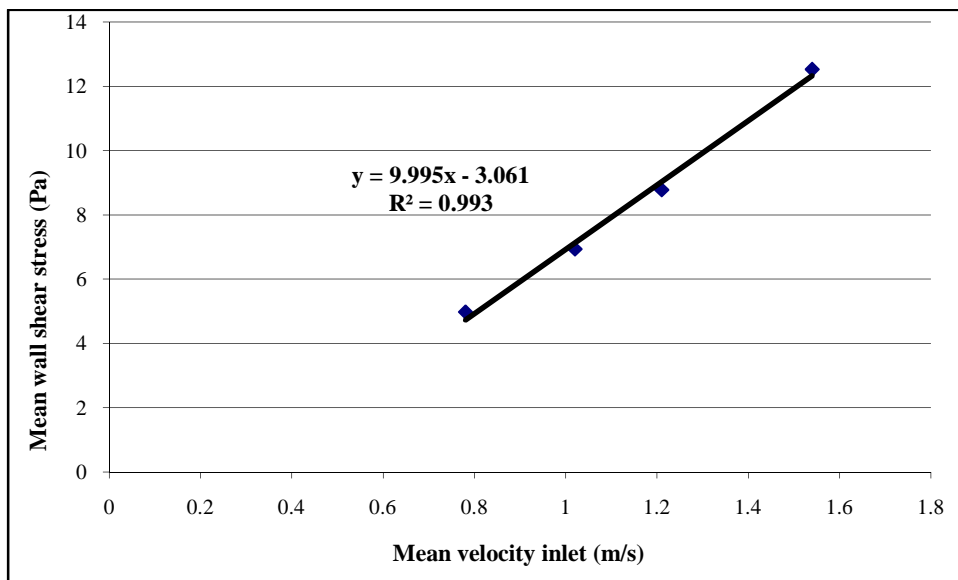
Figure 5.36 The relationship between mean wall shear stress and mean velocity

inlet of pulsation of pulsed flow in the parallel plates

The result of the cylindrical pipe corresponds to the study results of Blel et al. (2009) that mean wall shear stress increases with mean velocity inlet of pulsation. At the same time, the result of the corrugated channel corresponds to the study results of Metwally and Manglik (2004) who studied the response of the growth of vortices on Reynolds number of laminar flows in sinusoidal corrugated-plate channels. For their study results, when the Reynolds number of flow increased, the vortex strength also increased. This causes the raising of wall shear stress when mean velocity inlet of pulsed flow increases.

5.6 The Effect of the Geometry of Flow Channel on Wall Shear Stress

In this study, wall shear stresses generated by pulsed flows in the corrugated channel of plate heat exchanger and parallel plates were analyzed in order to study the effect of the geometry of flow channel on wall shear stress. Pulsating flows with the same pulsating condition were simulated through the both channels under the same flow conditions. The results of the study show that mean wall shear stresses generated by pulsed flows in the corrugated channel are greater than in the parallel plates as shows in Figure 5.38. This is because the complexity of the corrugated channel creates the vortices in the channel troughs as in Figure 5.39 and 5.40, whereas, they rarely appear in the parallel plates as in Figure 5.41. As the explanation in the previous section that the growth of vortices increases wall shear stress in the channel. This is the reason why wall shear stresses in the corrugated channel are higher than in the parallel plates.
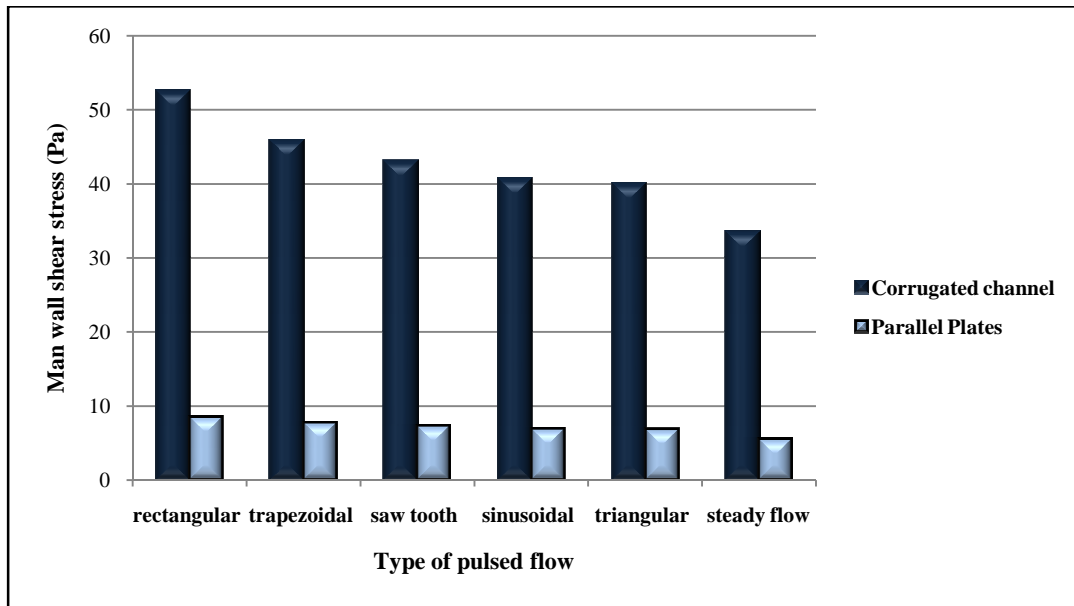
Figure 5.37 The comparison between mean wall shear stress in
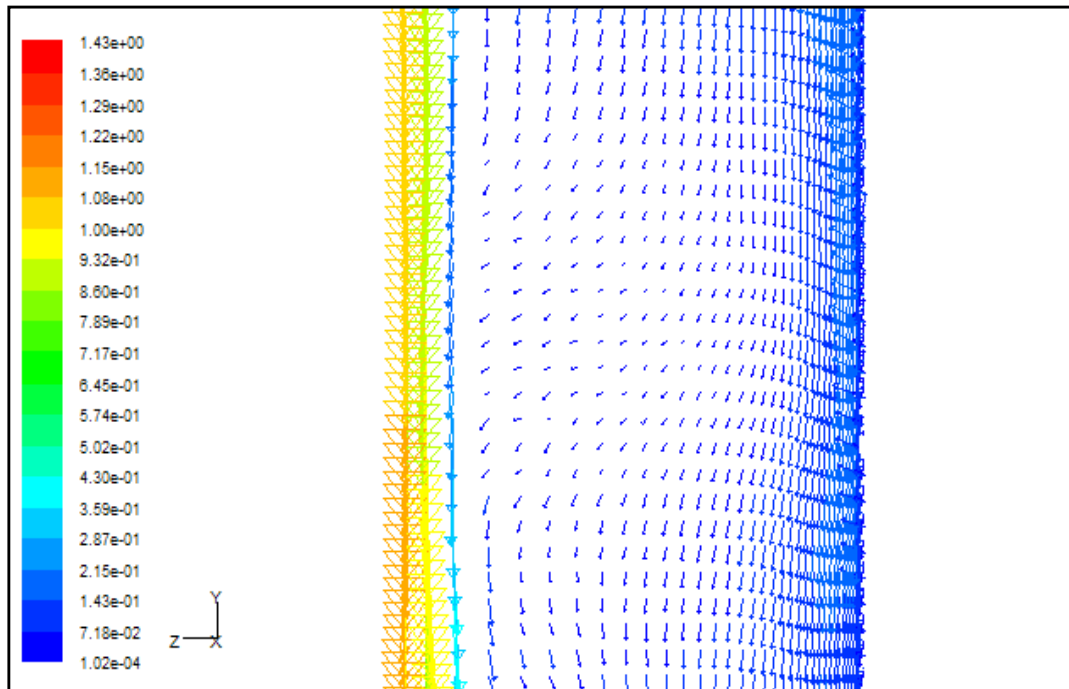
the corrugated channel and the parallel plates
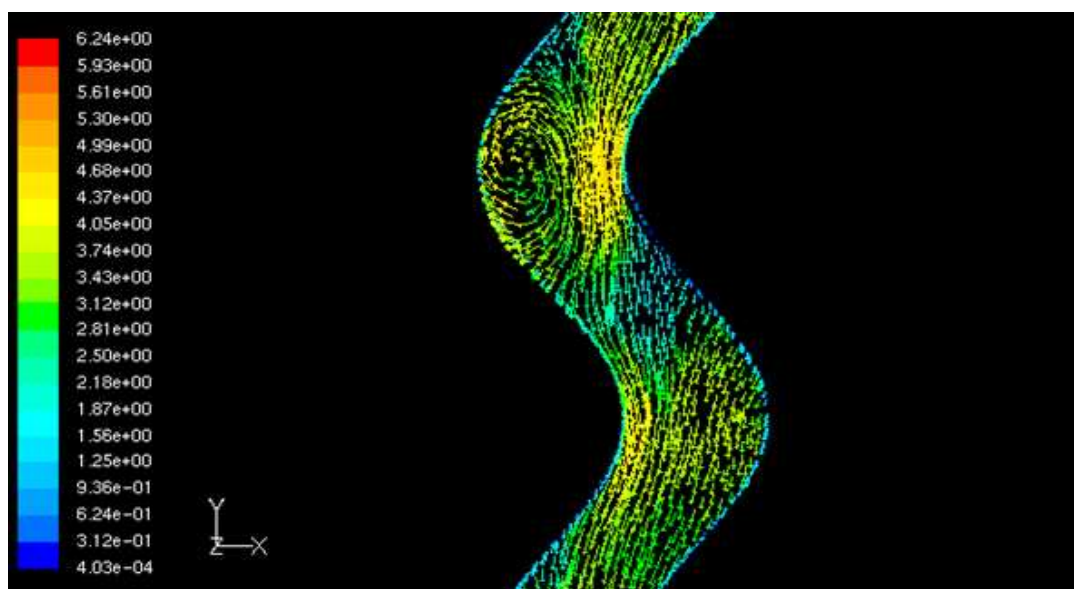
Figure 5.38 The velocity profile of pulsed flow with sawtooth wave form (mean

velocity inlet 1.02 m/s, amplitude 0.81 m/s, frequency 1.66 Hz) at

the plane z = 0.00433 m of corrugated channel, Time 1.4 s
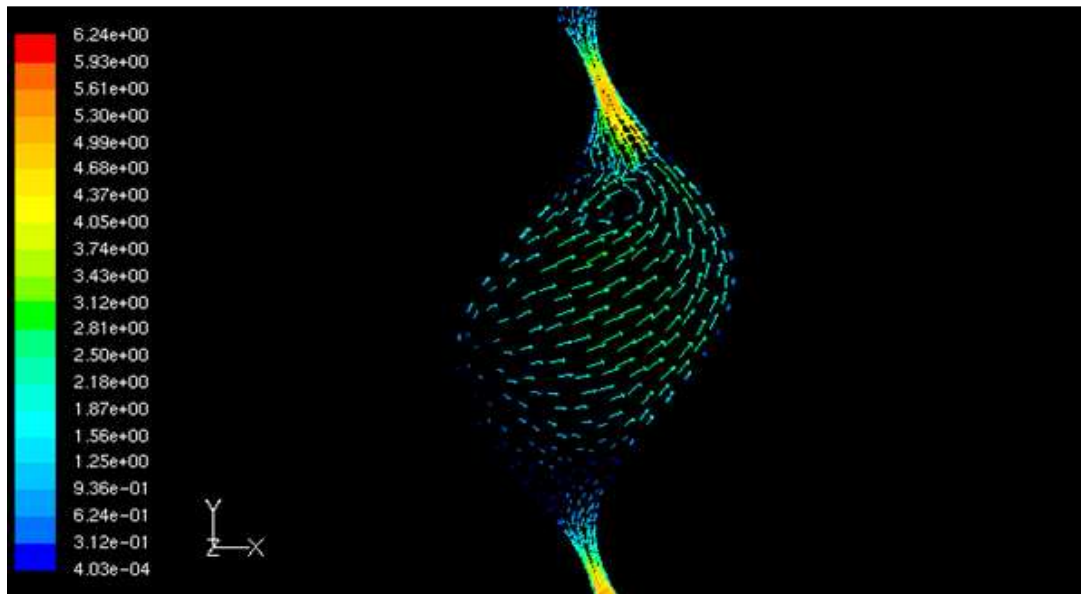
Figure 5.39 The velocity profile of pulsed flow with sawtooth wave form (mean

velocity inlet 1.02 m/s, amplitude 0.81 m/s, frequency 1.66 Hz) at

the symmetry plane of corrugated channel, Time 1.4 s
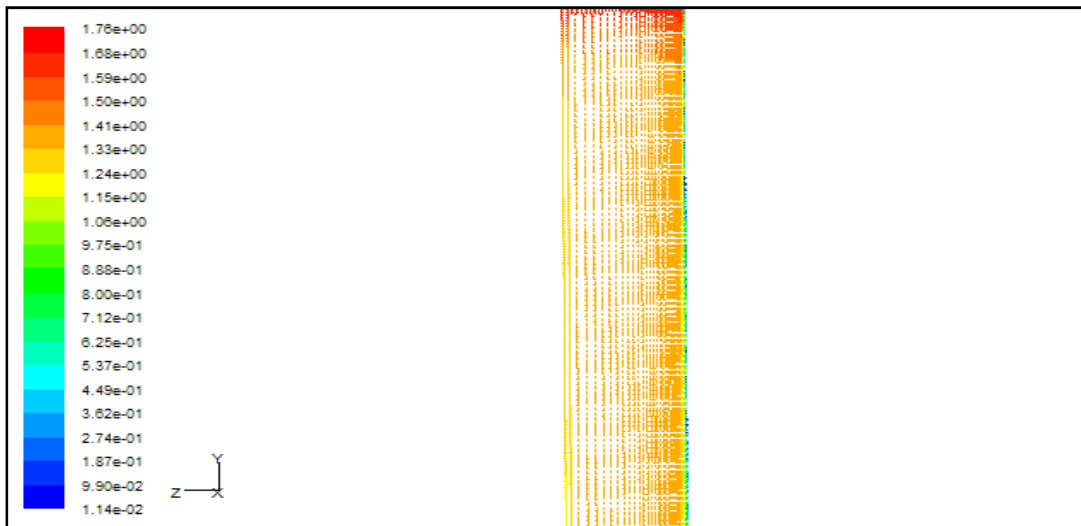
Figure 5.40 The velocity profile of pulsed flow with sawtooth wave form (mean

velocity inlet 1.02 m/s, amplitude 0.81 m/s, frequency 1.66 Hz) at

the plane x = 0.0012 m in the parallel plates, Time 1.4 s

5.7   Conclusion

In wall shear stress prediction, there are some differences between numerical simulation of FLUENT[®]6.3.26 and the experimental data.   However, the results of the numerical simulation give the trend for wall shear stress analysis. As the results of the study, type of pulsed flow affects to wall shear stress in the flow channels. Pulsating flow with the rectangular waveform of pulsation gives the greatest wall shear stress. Pulsed flows whose flow velocity suddenly change such as pulsed flow with the rectangular and trapezoidal waveform of pulsations can generate higher wall shear stresses than the pulsed flows whose flow velocity gradually change such as pulsed flow with the sinusoidal and triangular waveform pulsation. For the effects of pulsation parameters (amplitude, frequency and mean velocity inlet of pulsation) on wall shear stress, wall shear stress is proportion to the amplitude and mean velocity inlet of pulsation. Meanwhile, the effect of frequency in the cylindrical pipe and parallel plates is not obvious as in the corrugated channel where wall shear stress is inverse proportion to the frequency of pulsation. This is one effect of the geometry of the flow channels. The complicated channel of plate heat exchanger not only increases the wall shear stress but also affects the response of wall shear stress on the frequency of pulsations.

CHAPTER VI

CONCLUSIONS AND RECOMMENDATIONS

This study aims to serve the cleaning enhancement using pulsed flow. In this study, wall shear stress which is one key parameter of the cleaning enhancement was analyzed by using numerical simulation in order to implicitly indicate the efficiency of pulsed flows in the cleaning process. The conclusions of wall shear stress analysis are presented in the first part of this section. Then, the recommendation for the future work will be focused later.

6.1   Conclusions

6.1.1 There is a limit of using numerical simulation in wall shear stress prediction. In this study, wall shear stresses were analyzed by using the finite volume method which based on solving the Reynolds-averaged Navier-Stokes (RANS) equations only. This causes the difference between the numerical data and the experimental data. However, the numerical results can give the possible trends for wall shear stress analysis of pulsed flow.

6.1.2 The results of study of the effect of type of pulsed flow on wall shear stress show that pulsating flow with the rectangular waveform of pulsation gives the greatest wall shear stress. Pulsed flows whose flow velocity suddenly change such as pulsed flow with the rectangular and trapezoidal waveform of pulsations can generate higher wall shear stresses than the pulsed flows whose flow velocity gradually change such as pulsed flow with the sinusoidal and triangular waveform pulsation. This can

be inferred that pulsed flows whose flow velocity suddenly changes can enhance the cleaning efficiency better than pulsed flows whose flow velocity gradually changes. However, only wall shear stress analysis is not explicit enough to identify the cleaning efficiency of different type of pulsed flow.

6.1.3 The results of study of the effect of amplitude, frequency and mean velocity inlet of pulsation on wall shear stress show that wall shear stress increases with the amplitude and mean velocity inlet of pulsation. Meanwhile, the effect of frequency is obviously seen in the corrugated channel, wall shear stress is inverse proportion to the frequency of pulsation.

6.1.4 The effect of the geometry of the flow channel shows that the complicated channel of plate heat exchanger not only give higher wall shear stresses but also more effective response of wall shear stress on the frequency of pulsations than the simple geometry as the parallel plates.

6.2   Recommendations

6.2.1 Turbulence models such as the Reynolds stress equation models, large eddy simulation (LES) and direct numerical simulation (DNS) might be the alternative tools that give the accurate numerical results for wall shear stress prediction.

6.2.2 In wall shear stress analysis, mass transfer of chemical species in the flows should be additionally considered with the solving the Reynolds-averaged Navier-Stokes (RANS) equations.

6.2.3 From the study results, only wall shear stress analysis is not explicit enough to indicate the cleaning efficiency of different type of pulsed flow. The study

of force accumulation on the surface deposit, which is generated by different type of pulsed flow, might be another way to clarify the cleaning efficiency of different type of pulsed flow.

6.2.4 To clarify the cleaning efficiency of different type of pulsed flow using numerical simulation, the chemical reaction and the mechanism of the deposit removal should be considered in the simulation in order to obtain the realistic results.

REFERENCES

Barnes, J. W. (1994). **Statistical Analysis for Engineers and Scientists: a computer-Based Approach** (International ed.). Singapore: McGraw-Hill.

Blel, W., Legentilhomme, P., Bénézech, T., Legrand, J., and Le Gentil-Lelièvre C. (2009). Application of turbulent pulsating flows to the bacterial removal during a cleaning in place procedure. Part 1: Experimental analysis of wall shear stress in a cylindrical pipe. **Journal of Food Engineering** 90: 422-432.

Blel, W., Legentilhomme, P., Bénézech, T., Legrand, J., and Le Gentil-Lelièvre C. (2009). Application of turbulent pulsating flows to the bacterial removal during a cleaning in place procedure. Part 2: Effects on cleaning efficiency. **Journal of Food Engineering** 90: 433-440.

Bonis, M. V. D. and Ruocco, G. (2006). Fouling of heat exchangers in the dairy industry by coupling and kinetics modeling. **COMSOL Users Conference**.

Boysan, F. (1993). **Short Course: Advanced Turbulence Modelling** (Fluent Europe Ltd, Sheffield, UK).

Britz, T. J. and Robinson, R. K. (2008). **Advanced Dairy Science and Technology**. Singapore: Utopia Press.

Burton, H. (1988). **Ultra-High-Temperature Processing of Milk and Milk Products.** London: Elsevier Applied Science.

Christian, G. K. and Fryer, P. J. (2006). The effect of pulsing cleaning chemicals on the clean of whey protein deposits. **Food and Bioproducts Processing** 84: 320-328.

Fernandes, C. S., Dias, R., Nobrega, J. M., Afonso, I. M., Melo, L. F., and Maia, J. M. (2005). Simulation of stirred yoghurt processing in plate heat exchanger. **Journal of Food Engineering** 69: 281-290.

Fryer, P. J. and Bird, M. R. (1994). Factors which affect the kinetics of cleaning dairy soils. **Food Science and Technology Today** 8: 36-42.

Fryer, P. J., Christian, G. K., and Liu, W. (2006). How hygiene happens: physics and chemistry of cleaning. **International Journal of Dairy Technology** 59 (2): 76-84.

Gallot-Lavallee, Th. (1982). **Contribution á l' étude de la cinétique du nettoyage des pasteurisateurs de lait.** France: Diss. ENSIA.

Gallot-Lavallee, Th., Lalande, M., and Corrieu, G. (1984). Cleaning kinetics modeling of holding tubes fouled during milk pasteurization. **Journal of Food Process Engineering** 7: 123.

Gillham, C. R., Fryer, P. J., Hasting, A. P. M., and Wilson, D. I. (1999). Cleaning-in-place of whey protein fouling deposits: Mechanisms Controlling Cleaning. **Trans IChemE** 77: 127-136.

Gillham, C. R., Fryer, P. J., Hasting, A. P. M., and Wilson, D. I. (2000). Enhanced cleaning of whey protein soils using pulsed flows. **Journal of Food Engineering** 46: 199-209.

Graßhoff, A. (1983). Die örtliche Flüssigkeitsbewegung und deren Einfluss auf den Renigungsprozess in zylindrischen Toträumen. **Kiel. Milchwirtsch. Forschungsber** 35: 471.

Green, A. S. (2004). Modelling of peak-flow wall shear stress in major airways of the lung. **Journal of Biomechanics** 37: 661-667.

Grijspeerdt, K., Hazarika, B., and Vucinic D. (2003). Application of computational fluid dynamics to model the hydrodynamics of plate heat exchangers for milk processing. **Journal of Food Engineering** 57: 237-242.

He, S. and Jackson, J. D. (2009). An experimental study of pulsating turbulent flow in a pipe. **European Journal of Mechanics B/Fluids** 28: 309-320.

Heldman, D. R. and Lund, D. B. (ed.). (2007). **Handbook of Food Engineering** (2nd ed.). Boca Raton: CRC Press.

Hinton, A. R., Trinh, K.T., Brooks, J.D., and Manderson, G.J. (2002). Thermophile survival in milk fouling and on stainless steel during cleaning. **Trans IChemE** 80: 299-304.

Hoffmann, W. and Reuter, H. (1984). Zirgilationsreinigen (CIP) von geraden Rohren in Abhängigkeit physikalischen Einflussfaktoren. **Milchwissenschaft** 39: 594.

Ishii, Y. (1990). Numerical simulation of pulsatile flows passing through a pipe with sudden expansion. **Japan Aerospace Exploration Agency**: 45-52.

Jennings, W. G. (1959). Circulation cleaning. III. The kinetics of a simple detergent system. **Journal of Dairy Science** 42: 1763.

Jennings, W. G. (1963). A kinetic approach to detergent synergism. **Journal of the American Oil Chemist's Society** 40: 17.

Jennings, W. G. (1965). Theory and practice of hard surface cleaning. **Advanced Food Research** 14: 325.

Jensen, B. B. B., Bénézech, Th., Legentilhomme, P., and Lelièvre, C. (2005). Local wall shear stress variations predicted by computational fluid dynamics for hygienic design. **Trans IChemE** 83 (C1): 53-60.

Jun, S. and Puri, V. M. (2005). 3D milk-fouling model of plate heat exchangers using computational fluid dynamics. **International Journal of Dairy Technology** 58(4): 214-224.

Kakaç, S. and Liu, H. (2002). **Heat Exchangers: selection, rating, and thermal design** (2nd ed.). Florida: CRC Press.

Karagöz, İ. (2002). Similarity solution of the oscillatory pressure driven fully developed flow in a channel. **Uludağ Üniversitesi Mühendislik-Mimarlik Fakültesi Dergisi** 7: 161-169.

Lalande, M., Tissier, J.P., and Corrieu, G. (1985). Fouling of heat transfer surfaces related to β-lactoglobulin denaturation during heat processing of milk. **Biotechnology Progress** (1): 131-139.

Liu, W., Christian, G. K., Zhang, Z., and Fryer, P. J. (2006). Direct measurement of the force required to disrupt and remove fouling deposits of whey protein concentrate. **International Dairy Journal** 16: 164-172.

Mao, Z. and Hanratty, T. J. (1986). Studies of the wall shear stress in a tubular pulsating pipe flow. **Journal of Fluid Mechanics** 170: 545-564.

Metwally, H. M. and Manglik, R. M. (2004). Enhanced heat transfer due to curvature-induced lateral vortices in laminar flows in sinusoidal corrugated-plate channels. **International Journal of Heat and Mass Transfer** 47: 2283-2292.

Misra, J. C., Pal, A., Pal, B., and Gupta, A. S. (2001). Oscillatory entry flow in a plane channel with pulsating walls. **International Journal of Non-Linear Mechanics** 36: 731-741.

Nauman, E. A., Risic, K. J., Keaveny, T. M., and Satcher, R. L. (1999). Quantitative assessment of steady and pulsatile flow fields in a parallel plate flow chamber. **Annals of Biomedical Engineering** 27: 194-199.

Nishimura, T. and Matsune, S. (1998). Vortices and wall shear stresses in asymmetric and symmetric channels with sinusoidal wavy walls for pulsatile flow at low Reynolds. **International Journal of Heat and Fluid Flow** 19: 583-593.

Ooi, A., Blackburn, H. M., Zhu, S., Lui, E., and Tae, W. (2007). Numerical study of the behavior of wall shear stress in pulsatile stenotic flows. **Australian Fluid Mechanics Conference.**

Peacock, J., Jones. T., Tock, C., and Lutz, R. (1998). The onset of turbulence in physiological pulsatile flow in a straight tube. **Experiments in Fluids** 24: 1-9.

Pritchard, A.M. (1988). The economics of fouling. In Melo, L.F., Bott, T.R. and C. Bernardo (eds). **Fouling Science and Technology: NATO ASI Series**. (pp 31-45). The Netherlands: Kluwer.

Qi, X. G., Scott, D. M., and Wilson, D. I. (2008). Modelling laminar pulsed flow in rectangular microchannels. **Chemical Engineering Science** 63: 2682-2689.

Rosmaninho, R., Rizzo, G., Müller-Steinhagen, H., and Melo, L. F. (2008). Deposition from a milk mineral solution on noval heat transfer surfaces under turbulent flow conditions. **Journal of Food Engineering** 85: 29-41.

Schlüssler, H. J. (1970). Zur Reinigung fester Oberflächen, in der Lebensmittelindustrie. **Milchwissenschaft** 25: 133.

Shah, R. K., Heikal, M. R., Thonon, B., and Tochon, P. (2001). **Advances in Heat Transfer: Progress in the Numerical Analysis of Compact Heat Exchanger Surfaces** (Vol.34). n.p.: Academic Press.

Timperley, D. (1981). **Fundamentals and Applications of Surface Phenomena Associated with Fouling and Cleaning in Food Processing: The effect of Reynolds-number and mean velocity of flow on the cleaning in place of pipelines.** Lund, Sweden: Lund University Reprocentralen.

Ünsal, B., Ray, S., Durst, F., and Ertunç, Ö. (2005). Pulsating laminar pipe flows with sinusoidal mass flux variations. **Fluid Dynamics Research** 37: 317-333.

Versteeg, H. K. and Malalasekera, W. (2007). **An Introduction to Computational Fluid Dynamics: The Finite Volume Method** (2nd ed.). London: Pearson Education Limited.

Xin, H., Chen, X. D., and Zkan, N. O. (2002). Cleaning rate in the uniform cleaning stage for whey protein gel deposits. **Trans IChemE** 80: 240-246.

Yakhot, A., Arad, M., and Ben-Dor, G. (1999). Numerical investigation of a laminar pulsating flow in a rectangular duct. **International Journal for Numerical Methods in Fluids** 29: 935-950.

APPENDIX A

SUMMARY OF THE STUDIES THAT RELATE TO

PULSED FLOW AND WALL SHEAR STRESS

Table A.1 Summary of the previous studies that relate to pulsed flow and wall shear stress

Theme of Research	Year	Researcher	Research Procedure	Detail of research	Results
Pulsed Flow	1990	Ishii	CFD	Studied the velocity distribution of pulsatile flow in circular pipe with sudden expansion.	- Velocity profile became plug flow when the Reynolds and Womersley number increase. - The reverse flow near the wall increased with Womersley number. - The reattachment length increased with the Reynolds number.
	1998	Peacock et al.	Experiment	Studied the onset of turbulence of pulsatile flow in a straight tube.	The onset of turbulence was shown in the form of the critical peak Reynolds number which correlated with the Strouhal number.
	1999	Misra et al.	CFD	Studied the oscillating entry flow in a plane channel with pulsating walls.	- Velocity profile of oscillating flow tended to be parabolic shape in downstream region. - At high frequency of pulsating wall, there were reverse flows near the wall.
	2000	Gillham et al.	Experiment	Studied the whey protein cleaning enhancement using pulsed flow.	- The pulsating flow could enhance the cleaning rate. The cleaning rates in the uniform and decay stage were raised. The overall cleaning time was reduced. - The enhancement was controlled by the combination effect of amplitude and frequency of pulsation

Table A.1 Summary of the previous studies that relate to pulsed flow and wall shear stress (continued)

Theme of Research	Year	Researcher	Research Procedure	Detail of research	Results
Pulsed Flow	2002	Karagöz	CFD and Analytical	Studied the behavior of the laminar oscillating flow in a 2D channel.	- Velocity profile seemed to be quasi steady solution when the frequency of oscillation was low. - Velocity profile resembled the plug flow when the frequency parameter increased. - There was a phase lag between the induced velocity and pressure oscillation. - There was a phase shift between the skin friction coefficient and the imposed pressure gradient.
	2005	Ünsal et al.	Experiment and Analytical	Studied the behavior of laminar pulsating flows in a pipe.	- At very low frequency, the velocity profile resembled the parabolic profile of the steady laminar flow. - The velocity amplitudes in the center region of pipe decreased and the accelerating profiles tended to be flatter with the increase of frequency. - The velocity amplitudes near the wall increased and the decelerating profiles appeared to be more inflections near the pipe wall with the increase of frequency.
	2009	He and Jackson	Experiment	Studied the behavior of turbulent pulsating flow in a pipe.	- In the lowest frequency case, the velocity profile was similar to quasi-steady shape. - In the high frequency cases, the amplitude of velocity was constant in the center part of the pipe.

Table A.1 Summary of the previous studies that relate to pulsed flow and wall shear stress (continued)

Theme of Research	Year	Researcher	Research Procedure	Detail of research	Results
Pulsed Flow	2009	Blel et al.	Experiment	Studied the effect of turbulent pulsating flow on the bacterial removal during a cleaning in place procedure	- Pulsating flow was more effective than the steady flow in the cleaning procedure. - The bacterial removal enhancement was controlled by the combination effect of amplitude and frequency.
The combination of pulsed flow and wall shear stress	1986	Mao and Hanratty	Experiment	Studied the time variation of wall shear stress imposed by turbulent pulsating flows in a pipe.	- The imposed oscillation of pressure gradient had no effect on the time-mean velocity gradient at the wall. - Both of phase averaged velocity gradient and the intensity of velocity gradient at the wall were shifted from the phase averaged pressure gradient.
	1998	Nishimura and Matsune	CFD	Studied the behavior of vortices generated by pulsed flow in asymmetric and symmetric channel.	- There was rotating vortex in furrow of channel. - The frequency of pulsed flow affected on the vortex strength. An increase of frequency led to promote vortex strength which caused higher wall shear stress.
	1999	Yakhot et al.	CFD	Studied laminar pulsating flow in a rectangular duct and parallel plates.	- The frequency of pulsating flow affected phase lag or shift of the induced velocity and wall shear stress with respect to the imposed pressure gradient. - In parallel plates, at high frequency, mean velocity and the wall shear stress had phase lags relative to the imposed pressure gradient.

Table A.1 Summary of the previous studies that relate to pulsed flow and wall shear stress (continued)

Theme of Research	Year	Researcher	Research Procedure	Detail of research	Results
The combination of pulsed flow and wall shear stress	1999	Yakhot et al. (continued)	CFD	Studied laminar pulsating flow in a rectangular duct and parallel plates. (continued)	- Flow in rectangular duct had velocity profiles at the center plate similar to the velocity profile of 1D flow between parallel plates. The amplitude of the induced velocity and the wall shear stress decreased when approaching the side wall.
	2008	Qi et al.	Analytical	Modeled the laminar pulsating flow of an incompressible Newtonian fluid through rectangular duct using Green functions.	- There was the appearance of bulk flow reversal at sometime over a cycle. - The maximum wall shear stress of pulsating flow was greater than the steady flow.
	2009	Blel et al.	Experiment	Studied the effect of turbulent pulsating flow on mean wall shear stress and the fluctuation energy of the shear rate.	- Pulsating flow generated greater mean wall shear stress and the fluctuation energy of the shear rate than steady flow. - Wall shear stress increased with mean velocity, amplitude and frequency of pulsation. - Frequency of pulsation was more effective on the shear stress the amplitude of pulsation

Table A.1 Summary of the previous studies that relate to pulsed flow and wall shear stress (continued)

Theme of Research	Year	Researcher	Research Procedure	Detail of research	Results
Wall shear stress	2004	Metwally and Manglik	CFD	Studied the effect of corrugated-plate channel geometry and Reynolds number on the flow field and wall shear stress of the steady laminar flow.	- Swirl flows were generated in the corrugation troughs when the furrow of the channel was deeper. - The peak of wall shear stress increased with the corrugated aspect ratio and Reynolds number.
Wall shear stress	2005	Jensen et al.	CFD	Studied the local wall shear stress variations of the steady turbulent flow through the pipe with various diameter changes.	- The variation of mean wall shear stress and wall shear stress fluctuation could be seen explicitly at the expansion and contraction part of the pipe.

APPENDIX B

STATISTICAL TABLE

Table B.1 t-Distribution table

df	α = 0.1	0.05	0.025	0.01	0.005	.001	0.0005
∞	t_α=1.282	1.645	1.960	2.326	2.576	3.091	3.291
1	3.078	6.314	12.706	31.821	63.656	318.289	636.578
2	1.866	2.920	4.303	6.965	9.925	22.328	31.600
3	1.638	2.353	3.182	4.541	5.841	10.214	12.924
4	1.533	2.132	2.776	3.747	4.604	7.173	8.610
5	1.476	2.015	2.571	3.365	4.032	5.894	6.869
6	1.440	1.943	2.447	3.143	3.707	5.208	5.959
7	1.415	1.895	2.365	2.998	3.499	4.785	5.408
8	1.397	1.860	2.306	2.896	3.355	4.501	5.041
9	1.383	1.833	2.262	2.821	3.250	4.297	4.781
10	1.372	1.812	2.228	2.764	3.169	4.144	4.587
11	1.363	1.796	2.201	2.718	3.106	4.025	4.437
12	1.356	1.782	2.179	2.681	3.055	3.930	4.318
13	1.350	1.771	2.160	2.650	3.012	3.852	4.221
14	1.345	1.761	2.145	2.624	2.977	3.787	4.140
15	1.341	1.753	2.131	2.602	2.947	3.733	4.073
16	1.337	1.746	2.120	2.583	2.921	3.686	4.015
17	1.333	1.740	2.110	2.567	2.898	3.646	3.965
18	1.330	1.734	2.101	2.552	2.878	3.610	3.922
19	1.328	1.729	2.093	2.539	2.861	3.579	3.883
20	1.325	1.725	2.086	2.528	2.845	3.552	3.850
21	1.323	1.721	2.080	2.518	2.831	3.527	3.819
22	1.321	1.717	2.074	2.508	2.819	3.505	3.792
23	1.319	1.714	2.069	2.500	2.807	3.485	3.768
24	1.318	1.711	2.064	2.492	2.797	3.467	3.745
25	1.316	1.708	2.060	2.485	2.787	3.450	3.725
26	1.315	1.706	2.056	2.479	2.779	3.435	3.707
27	1.314	1.703	2.052	2.473	2.771	3.421	3.689
28	1.313	1.701	2.048	2.467	2.763	3.408	3.674
29	1.311	1.699	2.045	2.462	2.756	3.396	3.660
30	1.310	1.697	2.042	2.457	2.750	3.385	3.646
60	1.296	1.671	2.000	2.390	2.660	3.232	3.460
120	1.289	1.658	1.980	2.358	2.617	3.160	3.373
∞	1.282	1.645	1.960	2.326	2.576	3.091	3.291

Table B.2 F-Distribution table, α = 0.05

df2/df1	1	2	3	4	5	6	7	8	9	10	12	15
1	161.4476	199.5	215.7073	224.5832	230.1619	233.986	236.7684	238.8827	240.5433	241.8817	243.906	245.9499
2	18.5128	19	19.1643	19.2468	19.2964	19.3295	19.3532	19.371	19.3848	19.3959	19.4125	19.4291
3	10.128	9.5521	9.2766	9.1172	9.0135	8.9406	8.8867	8.8452	8.8123	8.7855	8.7446	8.7029
4	7.7086	6.9443	6.5914	6.3882	6.2561	6.1631	6.0942	6.041	5.9988	5.9644	5.9117	5.8578
5	6.6079	5.7861	5.4095	5.1922	5.0503	4.9503	4.8759	4.8183	4.7725	4.7351	4.6777	4.6188
6	5.9874	5.1433	4.7571	4.5337	4.3874	4.2839	4.2067	4.1468	4.099	4.06	3.9999	3.9381
7	5.5914	4.7374	4.3468	4.1203	3.9715	3.866	3.787	3.7257	3.6767	3.6365	3.5747	3.5107
8	5.3177	4.459	4.0662	3.8379	3.6875	3.5806	3.5005	3.4381	3.3881	3.3472	3.2839	3.2184
9	5.1174	4.2565	3.8625	3.6331	3.4817	3.3738	3.2927	3.2296	3.1789	3.1373	3.0729	3.0061
10	4.9646	4.1028	3.7083	3.478	3.3258	3.2172	3.1355	3.0717	3.0204	2.9782	2.913	2.845
11	4.8443	3.9823	3.5874	3.3567	3.2039	3.0946	3.0123	2.948	2.8962	2.8536	2.7876	2.7186
12	4.7472	3.8853	3.4903	3.2592	3.1059	2.9961	2.9134	2.8486	2.7964	2.7534	2.6866	2.6169
13	4.6672	3.8056	3.4105	3.1791	3.0254	2.9153	2.8321	2.7669	2.7144	2.671	2.6037	2.5331
14	4.6001	3.7389	3.3439	3.1122	2.9582	2.8477	2.7642	2.6987	2.6458	2.6022	2.5342	2.463
15	4.5431	3.6823	3.2874	3.0556	2.9013	2.7905	2.7066	2.6408	2.5876	2.5437	2.4753	2.4034
16	4.494	3.6337	3.2389	3.0069	2.8524	2.7413	2.6572	2.5911	2.5377	2.4935	2.4247	2.3522
17	4.4513	3.5915	3.1968	2.9647	2.81	2.6987	2.6143	2.548	2.4943	2.4499	2.3807	2.3077
18	4.4139	3.5546	3.1599	2.9277	2.7729	2.6613	2.5767	2.5102	2.4563	2.4117	2.3421	2.2686
19	4.3807	3.5219	3.1274	2.8951	2.7401	2.6283	2.5435	2.4768	2.4227	2.3779	2.308	2.2341
20	4.3512	3.4928	3.0984	2.8661	2.7109	2.599	2.514	2.4471	2.3928	2.3479	2.2776	2.2033
21	4.3248	3.4668	3.0725	2.8401	2.6848	2.5727	2.4876	2.4205	2.366	2.321	2.2504	2.1757
22	4.3009	3.4434	3.0491	2.8167	2.6613	2.5491	2.4638	2.3965	2.3419	2.2967	2.2258	2.1508
23	4.2793	3.4221	3.028	2.7955	2.64	2.5277	2.4422	2.3748	2.3201	2.2747	2.2036	2.1282
24	4.2597	3.4028	3.0088	2.7763	2.6207	2.5082	2.4226	2.3551	2.3002	2.2547	2.1834	2.1077
25	4.2417	3.3852	2.9912	2.7587	2.603	2.4904	2.4047	2.3371	2.2821	2.2365	2.1649	2.0889
26	4.2252	3.369	2.9752	2.7426	2.5868	2.4741	2.3883	2.3205	2.2655	2.2197	2.1479	2.0716
27	4.21	3.3541	2.9604	2.7278	2.5719	2.4591	2.3732	2.3053	2.2501	2.2043	2.1323	2.0558
28	4.196	3.3404	2.9467	2.7141	2.5581	2.4453	2.3593	2.2913	2.236	2.19	2.1179	2.0411
29	4.183	3.3277	2.934	2.7014	2.5454	2.4324	2.3463	2.2783	2.2229	2.1768	2.1045	2.0275
30	4.1709	3.3158	2.9223	2.6896	2.5336	2.4205	2.3343	2.2662	2.2107	2.1646	2.0921	2.0148

Table B.2 F-Distribution table, α = 0.05 (Continued)

df2/df1	1	2	3	4	5	6	7	8	9	10	12	15
40	4.0847	3.2317	2.8387	2.606	2.4495	2.3359	2.249	2.1802	2.124	2.0772	2.0035	1.9245
60	4.0012	3.1504	2.7581	2.5252	2.3683	2.2541	2.1665	2.097	2.0401	1.9926	1.9174	1.8364
120	3.9201	3.0718	2.6802	2.4472	2.2899	2.175	2.0868	2.0164	1.9588	1.9105	1.8337	1.7505
inf	3.8415	2.9957	2.6049	2.3719	2.2141	2.0986	2.0096	1.9384	1.8799	1.8307	1.7522	1.6664

Table B.2 F-Distribution table, α = 0.05 (Continued)

df2/df1	20	24	30	40	60	120	INF
1	161.4476	199.5	215.7073	224.5832	230.1619	233.986	236.7684
2	18.5128	19	19.1643	19.2468	19.2964	19.3295	19.3532
3	10.128	9.5521	9.2766	9.1172	9.0135	8.9406	8.8867
4	7.7086	6.9443	6.5914	6.3882	6.2561	6.1631	6.0942
5	6.6079	5.7861	5.4095	5.1922	5.0503	4.9503	4.8759
6	5.9874	5.1433	4.7571	4.5337	4.3874	4.2839	4.2067
7	5.5914	4.7374	4.3468	4.1203	3.9715	3.866	3.787
8	5.3177	4.459	4.0662	3.8379	3.6875	3.5806	3.5005
9	5.1174	4.2565	3.8625	3.6331	3.4817	3.3738	3.2927
10	4.9646	4.1028	3.7083	3.478	3.3258	3.2172	3.1355
11	4.8443	3.9823	3.5874	3.3567	3.2039	3.0946	3.0123
12	4.7472	3.8853	3.4903	3.2592	3.1059	2.9961	2.9134
13	4.6672	3.8056	3.4105	3.1791	3.0254	2.9153	2.8321
14	4.6001	3.7389	3.3439	3.1122	2.9582	2.8477	2.7642
15	4.5431	3.6823	3.2874	3.0556	2.9013	2.7905	2.7066
16	4.494	3.6337	3.2389	3.0069	2.8524	2.7413	2.6572
17	4.4513	3.5915	3.1968	2.9647	2.81	2.6987	2.6143
18	4.4139	3.5546	3.1599	2.9277	2.7729	2.6613	2.5767
19	4.3807	3.5219	3.1274	2.8951	2.7401	2.6283	2.5435
20	4.3512	3.4928	3.0984	2.8661	2.7109	2.599	2.514

Table B.2 F-Distribution table, α = 0.05 (Continued)

df2/df1	20	24	30	40	60	120	INF
21	4.3248	3.4668	3.0725	2.8401	2.6848	2.5727	2.4876
22	4.3009	3.4434	3.0491	2.8167	2.6613	2.5491	2.4638
23	4.2793	3.4221	3.028	2.7955	2.64	2.5277	2.4422
24	4.2597	3.4028	3.0088	2.7763	2.6207	2.5082	2.4226
25	4.2417	3.3852	2.9912	2.7587	2.603	2.4904	2.4047
26	4.2252	3.369	2.9752	2.7426	2.5868	2.4741	2.3883
27	4.21	3.3541	2.9604	2.7278	2.5719	2.4591	2.3732
28	4.196	3.3404	2.9467	2.7141	2.5581	2.4453	2.3593
29	4.183	3.3277	2.934	2.7014	2.5454	2.4324	2.3463
30	4.1709	3.3158	2.9223	2.6896	2.5336	2.4205	2.3343
40	4.0847	3.2317	2.8387	2.606	2.4495	2.3359	2.249
60	4.0012	3.1504	2.7581	2.5252	2.3683	2.2541	2.1665
120	3.9201	3.0718	2.6802	2.4472	2.2899	2.175	2.0868
inf	3.8415	2.9957	2.6049	2.3719	2.2141	2.0986	2.0096

Table B.3 The Studentized range upper quantiles q (k, df; 0.05)

df	Number of treatments																		
	2	3	4	5	6	7	8	9	10	11	12	13	14	15	16	17	18	19	20
1	18	27	32.8	37.2	40.5	43.1	45.4	47.3	49.1	50.6	51.9	53.2	54.3	55.4	56.3	57.2	58	58.8	59.6
2	6.09	8.33	9.8	10.89	11.73	12.43	13.03	13.54	13.99	14.39	14.75	15.08	15.38	15.65	15.91	16.14	16.36	16.57	16.77
3	4.5	5.91	6.83	7.51	8.04	8.47	8.85	9.18	9.46	9.72	9.95	10.16	10.35	10.52	10.69	10.84	10.98	11.12	12.24
4	3.93	5.04	5.76	6.29	6.71	7.06	7.35	7.6	7.83	8.03	8.21	8.37	8.52	8.67	8.8	8.92	9.03	9.14	9.24
5	3.64	4.6	5.22	5.67	6.03	6.33	6.58	6.8	6.99	7.17	7.32	7.47	7.60	7.72	7.83	7.93	8.03	8.12	8.21
6	3.46	4.34	4.9	5.31	5.63	5.89	6.12	6.32	6.49	6.65	6.79	6.92	7.04	7.14	7.24	7.34	7.43	7.51	7.59
7	3.34	4.16	4.68	5.06	5.35	5.59	5.80	5.99	6.15	6.29	6.42	6.54	6.65	6.75	6.84	6.93	7.01	7.08	7.16
8	3.26	4.04	4.53	4.89	5.17	5.4	5.6	5.77	5.92	6.05	6.18	6.29	6.39	6.48	6.57	6.65	6.73	6.8	6.87
9	3.2	3.95	4.42	4.76	5.02	5.24	5.43	5.6	5.74	5.87	5.98	6.09	6.19	6.28	6.36	6.44	6.51	6.58	6.65
10	3.15	3.88	4.33	4.66	4.91	5.12	5.3	5.46	5.6	5.72	5.83	5.93	6.03	6.12	6.2	6.27	6.34	6.41	6.47
11	3.11	3.82	4.26	5.58	4.82	5.03	5.2	5.35	5.49	5.61	5.71	5.81	5.9	5.98	6.06	6.14	6.2	6.27	6.33
12	3.08	3.77	4.2	4.51	4.75	4.95	5.12	5.27	5.4	5.51	5.61	5.71	5.8	5.88	5.95	6.02	6.09	6.15	6.21
13	3.06	3.73	4.15	4.46	4.69	4.88	5.05	5.19	5.32	5.43	5.53	5.63	5.71	5.79	5.86	5.93	6.00	6.06	6.11
14	3.03	3.7	4.11	4.41	4.64	4.83	4.99	5.13	5.25	5.36	5.46	5.56	5.64	5.72	5.79	5.86	5.92	5.98	6.03
15	3.01	3.67	4.08	4.37	4.59	4.78	4.94	5.08	5.2	5.31	5.4	5.49	5.57	5.65	5.72	5.79	5.85	5.91	5.96
16	3.00	3.65	4.05	4.34	4.56	4.74	4.9	5.03	5.15	5.26	5.35	5.44	5.52	5.59	5.66	5.73	5.79	5.84	5.9
17	2.98	3.62	4.02	4.31	4.52	4.7	4.86	4.99	5.11	5.21	5.31	5.39	5.47	5.55	5.61	5.68	5.74	5.79	5.84
18	2.97	3.61	4.00	4.28	4.49	4.67	4.83	4.96	5.07	5.17	5.27	5.35	5.43	5.5	5.57	5.63	5.69	5.74	5.79
19	2.96	3.59	3.98	4.26	4.47	4.64	4.79	4.92	5.04	5.14	5.23	5.32	5.39	5.46	5.53	5.59	5.65	5.70	5.75
20	2.95	3.58	3.96	4.24	4.45	4.62	4.77	4.9	5.01	5.11	5.2	5.28	5.36	5.43	5.5	5.56	5.61	5.66	5.71
30	2.89	3.48	3.84	4.11	4.3	4.46	4.6	4.72	4.83	4.92	5	5.08	5.15	5.21	5.27	5.33	5.38	3.43	5.48
40	2.86	3.44	3.79	4.04	4.23	4.39	4.52	4.63	4.74	4.82	4.9	4.98	5.05	5.11	5.17	5.22	5.27	5.32	5.36
120	2.8	3.6	3.69	3.92	4.1	4.24	4.36	4.47	4.56	4.64	4.71	4.78	4.84	4.9	4.95	5.00	5.04	5.09	5.13
INF	2.77	3.32	3.63	3.86	4.03	4.17	4.29	4.39	4.47	4.55	4.62	4.68	4.74	4.8	4.84	4.89	4.93	4.97	5.01

APPENDIX C

SOURCE CODE OF THE PERIODIC VELOCITY

INLET BOUNDARY CONDITIONS

C.1   The sample of source of the velocity inlet boundary condition:

Rectangular waveform pulsation.

```c
#include "udf.h"

DEFINE_PROFILE (unsteady_velocity,thread,position)

{     face_t f;

    real t = CURRENT_TIME;

    real k = 0.81;

    real L = 0.301204819277109;

    real Vave = 1.02;

    begin_f_loop (f,thread)

    {

    real i = 1.;

      real n = 50.;

       real bn,B,TB = 0;

      for (i = 1;i <= n;i++)

      {

            bn = (1.-(cos(i*3.14285714285714)))/i;

            B = bn*(sin((i*3.14285714285714*t)/L));

            TB = TB+B;

      }

      F_PROFILE (f,thread,position) = Vave+((2.*k)/3.14285714285714)*TB;

    }

    end_f_loop (f,thread)   }
```

C.2   The sample of source of the velocity inlet boundary condition: Sawtooth waveform pulsation.

```
#include "udf.h"

DEFINE_PROFILE (unsteady_velocity,thread,position)

{      face_t f;

    real t = CURRENT_TIME;

    real k = 0.81;

    real L = 0.301204819277109;

    real Vave = 1.02;

    begin_f_loop (f,thread)

    {

    real i = 1.;

      real n = 50.;

       real bn,B,TB = 0;

      for (i = 1;I <= n;i++)

      {

            bn = (cos(i*3.14285714285714))/i;

            B = bn*(sin((i*3.14285714285714*t)/L));

            TB = TB+B;

      }

      F_PROFILE (f,thread,position) = Vave+(-(2.*k)/3.14285714285714)*TB;

    }

    end_f_loop (f,thread) }
```

C.3　The sample of source of the velocity inlet boundary condition: Sinusoidal waveform pulsation.

```
#include "udf.h"

DEFINE_PROFILE (unsteady_velocity,thread,position)

{

    face_t f;

    real t = CURRENT_TIME;

    begin_f_loop (f,thread)

    {

    F_PROFILE (f,thread,position) = 1.02+(0.81*sin(3.14159265358979323846

                        *2.*1.66*t));

    }

    end_f_loop (f,thread)

}
```

C.4　The sample of source of the velocity inlet boundary condition: Trapezoidal waveform pulsation.

```
#include "udf.h"

DEFINE_PROFILE (unsteady_velocity,thread,position)

{

    face_t f;

    real t = CURRENT_TIME;

    real k = 0.81;

    real L = 0.301204819277109;
```

```
        real Vave = 1.02;

     begin_f_loop (f,thread)

      {

    real i = 1.;

       real n = 50.;

        real bn1,bn2,bn3,B,TB = 0;

       for (i = 1.;i <= n;i++)

       {

               bn1 = sin((i*3.14285714285714)/4.);

               bn2 = sin((3.*i*3.14285714285714)/4.);

               bn3 = (1/(i*i))*(bn1+bn2);

               B = bn3*(sin((i*3.14285714285714*t)/L));

               TB = TB+B;

         }

     F_PROFILE (f,thread,position) =Vave+(((8.*k)/(3.14285714285714

                                  *3.14285714285714))*TB);

     }

     end_f_loop (f,thread)

}
```

C.5 **The sample of source of the velocity inlet boundary condition: Triangular waveform pulsation.**

```c
#include "udf.h"

DEFINE_PROFILE (unsteady_velocity,thread,position)

{     face_t f;

    real t = CURRENT_TIME;

    real k = 0.81;

    real L = 0.301204819277109;

    real Vave = 1.02;

    begin_f_loop (f,thread)

    {      real i = 1.;

        real n = 50.;

        real bn,B,TB = 0;

      for (i = 1.;i <= n;i++)

      {

            bn = sin((i*3.14285714285714)/2.)/(i*i);

            B = bn*(sin((i*3.14285714285714*t)/L));

            TB = TB+B;

      }

    F_PROFILE (f,thread,position) = Vave+((8.*k)/(3.14285714285714

                                    *3.14285714285714))*TB;

    }

    end_f_loop (f,thread)

}
```

APPENDIX D

SUMMARY OF THE SIMULATION TIME

Table D.1 The summary of the simulation time for the cylindrical pipe

Sample	Size of Time Step (s)	Number of Time Step	Maximum Iteration per Time Step	Times (s)
A - Q	0.01	300	30	3.00

Table D.2 The summary of the simulation time for the corrugated channel and

parallel plates

Sample	Order of Calculation	Size of Time Step (s)	Number of Time Step	Maximum Iteration pre Time Step	Times (s)
B, O, P, Q	First	0.001	250	30	0.25
	Second	0.005	150	30	0.75
	Third	0.01	50	30	0.50
	Total		450	15000	1.50
D, G, H, J	First	0.001	350	30	0.35
	Second	0.005	210	30	1.05
	Third	0.01	70	30	0.70
	Total		630	20400	2.10
L	First	0.001	500	30	0.50
	Second	0.005	300	30	1.50
	Third	0.01	10	30	0.10
	Total		810	25800	2.10
M	First	0.001	200	30	0.20
	Second	0.005	280	30	1.40
	Third	0.01	50	30	0.50
	Total		530	17400	2.10
N	First	0.001	175	30	0.18
	Second	0.005	315	30	1.58
	Third	0.01	35	30	0.35
	Total		525	17250	2.10

APPENDIX E

STATISTICAL DATA OF MEAN WALL SHEAR

STRESS COMPARISON TEST

Table E.1 The analysis of variance of flows in the cylindrical pipe

Between-Subjects Factors			
			Number of data
Type of pulsed flow		Rectangular	769
		Sawtooth	769
		Sinusoidal	769
		Steady	769
		Trapezoidal	769
		Triangular	769
Sample		C	1344
		B	1572
		D	1698

Tests of Between-Subjects Effects					
Dependent Variable: wall shear stress					
Source	**Type III Sum of Squares**	**df**	**Mean Square**	**F**	**Sig.**
Corrected Model	2084.954[a]	17	122.644	13.090	.000
Intercept	76994.187	1	76994.187	8217.750	.000
Type of pulsed flow	639.451	5	127.890	13.650	.000
Sample	1433.766	2	716.883	76.514	.000
Type of pulsed flow * Sample	10.448	10	1.045	0.112	1.00
Error	43061.090	4596	9.369		
Total	124306.629	4614			
Corrected Total	45146.044	4613			

Remark: a. R Squared = 0.046 (Adjusted R Squared = 0.043)

Table E.2 The mean wall shear stress comparison test between different types of

pulsed flows in the cylindrical pipe

Type of pulsed flow	Number of data	Subset			
		1	2	3	4
Steady	769	3.5015			
Triangular	769		3.9432		
Sinusoidal	769		4.1431	4.1431	
Sawtooth	769		4.1804	4.1804	
Trapezoidal	769			4.3655	
Rectangular	769				4.7182
Sig.		1.000	0.153	0.180	1.000

Means for groups in homogeneous subsets are displayed. Based on observed means.
The error term is Mean Square (Error) = 9.369.

Alpha = 0.05.

Table E.3 The mean wall shear stress comparison test between different samples of

pulsed flows in the cylindrical pipe

Sample	Number of data	Subset	
		1	2
B	1572	3.6771	
C	1344	3.7647	
D	1698		4.8711
Sig.		0.430	1.000

Means for groups in homogeneous subsets are displayed. Based on observed means.
The error term is Mean Square (Error) = 9.369.
Alpha = 0.05.

Table E.4 The analysis of variance of flows in the corrugated channel of plate heat exchanger

Between-Subjects Factors			
			Number of data
Type of pulsed flow	Rectangular		397
	Sawtooth		397
	Sinusoidal		397
	Steady		397
	Trapezoidal		397
	Triangular		397
Sample	B		1380
	D		1002

Tests of Between-Subjects Effects					
Dependent Variable: wall shear stress					
Source	**Type III Sum of Squares**	**df**	**Mean Square**	**F**	**Sig.**
Corrected Model	117652.559[a]	11	10695.687	16.277	.000
Intercept	4338438.604	1	4338438.604	6602.332	.000
Type of pulsed flow	36632.655	1	36632.655	55.748	.000
Sample	76040.691	5	15208.138	23.144	.000
Type of pulsed flow * Sample	734.688	5	146.938	0.224	0.952
Error	1557343.558	2370	657.107		
Total	5996661.531	2382			
Corrected Total	1674996.118	2381			

Remark: a. R Squared = 0.070 (Adjusted R Squared = 0.066)

Table E.5 The mean wall shear stress comparison test between different types of

pulsed flows in the corrugated channel of plate heat exchanger

Type of pulsed flow	Number of data	Subset			
		1	**2**	**3**	**4**
Steady	397	33.4787			
Sawtooth	397		40.0359		
Triangular	397		40.6851		
Sinusoidal	397		43.0515	43.0515	
Trapezoidal	397			45.7989	
Rectangular	397				52.51739
Sig.		1.000	0.118	0.131	1.000

Means for groups in homogeneous subsets are displayed.

Based on observed means.

The error term is Mean Square (Error) = 657.107.

Table E.6 The mean wall shear stress comparison test between different samples of

pulsed flows in the corrugated channel of plate heat exchanger

Group Statistics					
	case	**N**	**Mean**	**Std. Deviation**	**Std. Error Mean**
Wall shear stress	B	1380	39.25299003	2.626300365E1	0.706976293
	D	1002	47.19685170	2.620149026E1	0.827736550

Table E.6 The mean wall shear stress comparison test between different samples of pulsed flows in the corrugated channel of plate heat

exchanger (continued)

		Levene's Test for Equality of Variances		t-test for Equality of Means					95% Confidence Interval of the Difference	
		F	Sig.	t	df	Sig. (2-tailed)	Mean Difference	Std. Error Difference	Lower	Upper
Wall_shear_stress	Equal variances assumed	.253	0.615	-7.295	2380	0.000	-7.943861675	1.088965506	-1.00792802E1	-5.80844251
	Equal variances not assumed			-7.298	2159.828	0.000	-7.943861675	1.088560184	-1.00785967E1	-5.80912663

Independent Samples Test

Table E.7 The analysis of variance of flows in the parallel plates

Between-Subjects Factors		
		Number of data
	Rectangular	369
	Sawtooth	369
	Sinusoidal	369
Type of pulsed flow	Steady	369
	Trapezoidal	369
	Triangular	369
Sample	B	936
	D	1278

Tests of Between-Subjects Effects					
Dependent Variable: wall shear stress					
Source	**Type III Sum of Squares**	**df**	**Mean Square**	**F**	**Sig.**
Corrected Model	2732.093[a]	11	248.372	12.172	.000
Intercept	112854.129	1	112854.129	5530.825	.000
Type of pulsed flow	1776.240	5	355.248	17.410	.000
Sample	829.021	1	829.021	40.629	.000
Type of pulsed flow * Sample	21.724	5	4.345	.213	.957
Error	44930.871	2202	20.405		
Total	160234.732	2214			
Corrected Total	47662.965	2213			

Remark: a. R Squared = 0.057 (Adjusted R Squared = 0.053)

Table E.8 The mean wall shear stress comparison test between different types of

pulsed flows in the parallel plates

Type of pulsed flow	Number of data	Subset			
		1	2	3	4
Steady	397	5.5130			
Sawtooth	397		6.8070		
Triangular	397		6.9135		
Sinusoidal	397		7.2893	7.2893	
Trapezoidal	397			7.7371	
Rectangular	397				8.5229
Sig.		1.000	0.172	0.178	1.000

Means for groups in homogeneous subsets are displayed. Based on observed means.
The error term is Mean Square (Error) = 20.405.

Table E.9 The mean wall shear stress comparison test between different samples of

pulsed flows in the parallel plates

Group Statistics					
	case	N	Mean	Std. Deviation	Std. Error Mean
Wall shear stress	B	936	7.84562290	4.686335973	0.153177683
	D	1278	6.60691721	4.538162616	0.126944716

Table E.9 The mean wall shear stress comparison test between different samples of pulsed flows in the parallel plates (continued)

| | | Levene's Test for Equality of Variances | | t-test for Equality of Means | | | | | 95% Confidence Interval of the Difference | |
		F	Sig.	t	df	Sig. (2-tailed)	Mean Difference	Std. Error Difference	Lower	Upper
Wall_shear_stress	Equal variances assumed	1.173	0.279	-6.257	2212	0.000	-1.238705690	0.197958094	-1.626908839	-.850502540
	Equal variances not assumed			-6.226	1977.426	0.000	-1.238705690	0.198943116	-1.628865843	-.848545536

Independent Samples Test

APPENDIX F

THE STRUCTURE OF FLUENT®6.3.26

F.1 **The structure of FLUENT®6.3.26**

The FLUENT®6.3.26 includes the following program:

F.1.1 GAMBIT – the pre-processor for the geometry modelling and mesh generation

F.1.2 TGrid – the pre-processor for the volume mesh generation. This program generates volume mesh from the existing boundary meshes.

F.1.3 FLUENT – the solver that includes the operations of setting boundary conditions, defining fluid properties, executing the solution, refining the mesh and viewing the post processing results.

F.1.4 Filters – the translators that used to import the surface and volume meshes from CAD/CAE packages.

The structure of Program is shown in Figure F.1
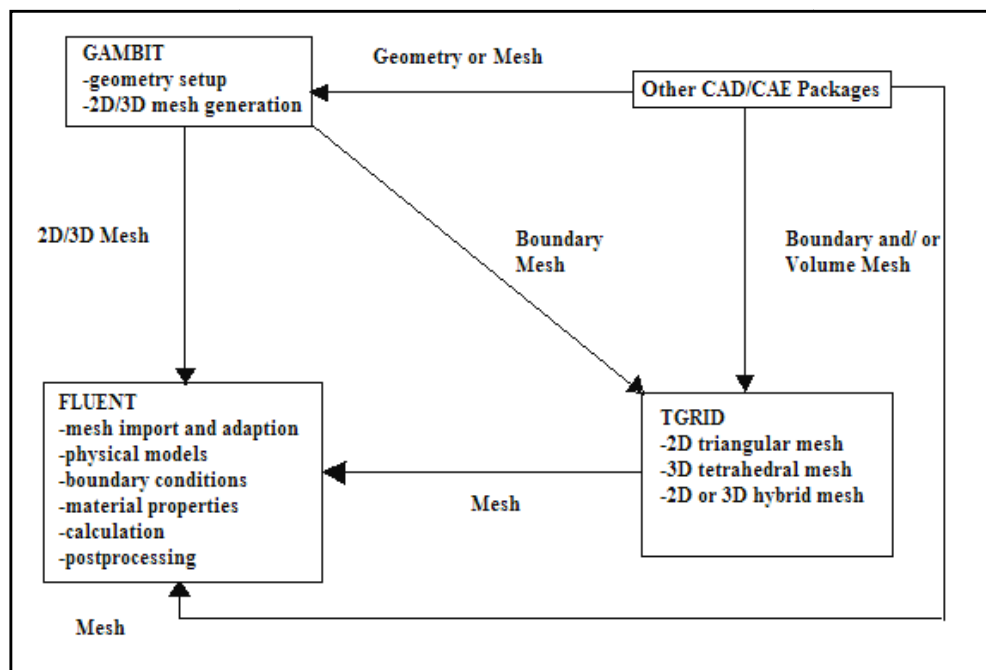
Figure F.1 Basic program structure

APPENDIX G

PUBLICATION

Numerical Simulation and Wall Shear Stress Analysis of Pulsed Flow in a Cylindrical Pipe for a Cleaning in Place Process

Pichitra Uangpairoj[1*] and Kontorn Chamniprasart [1]

[1] School of Mechanical Engineering, Institute of Engineering, Suranaree University of Technology, Nakhon Ratchasima, Thailand 30000

* Corresponding Author: E-mail: pichitrau@hotmail.com

Abstract

Pulsed flow has the effect of raising the maximum wall shear stress which is one parameter of cleaning enhancement in cleaning in place (CIP) system. Thus, types of pulsed flow are considered to improve the cleaning efficiency of CIP system. To indicate the cleaning efficiency of pulsed flows, wall shear stresses of various types of pulsed flow in cylindrical pipe were investigated by using finite volume method of the commercial computational fluid dynamics code (FLUENT®). As a result of the study, there are some differences of mean wall shear stresses between the numerical simulations and the experimental data. These wall shear stresses were generated by pulsed flows whose velocity varies with time as sine function. Additionally, the numerical simulations of various types of pulsed flow showed that wall shear stress corresponds to the velocity inlet function. Mean wall shear stress is proportional to mean velocity inlet, amplitude and frequency of pulsation. Maximum wall shear stress and frequency of wall shear stress are also proportional to amplitude and frequency, respectively. Meanwhile, type of pulsed flow also affects to mean wall shear stress. When pulsed flow behaves like rectangular wave, it generates the highest wall shear stress.

Keywords: Computational fluid dynamics (CFD), Pulsed flow, Wall shear stress

1. Introduction

During thermal treatment in dairy industry, there is an undesired build-up of deposits on the surfaces of pipes and equipments, especially heat exchangers. The undesired deposits, fouling, can be created when denatured protein in milk, especially β-lactoglobulin and some saturated and the decrease in cross section area of the flow channels [11]. For safety impact, fouling is the source of contamination in dairy product because of the accumulation of microorganisms. Fouling is used to protect microorganisms from cleaning, especially thermophile microorganisms [7]. These problems lead to an attempt of fouling mineral deposit on the heat transfer surface [3]. Build-up of fouling reduces heat transfer because an insulated property of the fouling increases the heat resistance at the heat transfer surface. This effect leads to energy losses in dairy thermal system. Fouling also increases the pressure drop due to the increase in surface roughness

water to remove loosely bound substances from the surface; 2. Cleaning – removal of the deposit from the surface by the chemicals. In this step, the deposit is swollen after react with the chemicals. Then, the swollen deposit is removed from the surface by shear forces and diffusion; 3. Interrinse – removal and rinsing away of the

Nomenclature

		Greek symbols	
$C_{1\varepsilon}, C_{2\varepsilon}, a, b$	constants		
f	frequency (Hz)	$\alpha_k, \alpha_\varepsilon$	the inverse effective Prandtl numbers for k and ε, respectively
k	the turbulent kinetic energy (J)		
r	the rate constant		
t	time (s)	ε	turbulent dissipation rate(W.kg^{-1})
S	the deformation tensor	η_0, β	the coefficients
S_{ij}	the mean strain rate (s^{-1})	δ	the kronecker delta
$u(t)$	instantaneous velocity (m/s)	ρ	density (kg/m^3)
$\bar{u}$	average velocity (m/s)	μ	dynamic viscosity (kg.m^{-1}.s^{-1})
u_p	amplitude velocity (m/s)	μ_t	turbulent viscosity (kg.m^{-1}.s^{-1})
u	velocity component (m/s)	τ_w	wall shear stress (Pa)
u'	fluctuating components (m/s)	Subscripts	
x	Cartesian coordinate	i, j, k	equal to 1, 2 and 3 which correspond to x, y, z in Cartesian coordinate

reduction. The deposits can be reduced by modifying the geometry of heat exchangers (especially in plate heat exchangers) [10] and surface properties of heat exchanger [13].

Cleaning in place (CIP) is one part of cleaning systems which is used in large-scale production. In the CIP system, chemicals in the solution tanks are circulated through the equipments by a supply pump. The flow circuit is regulated by the pneumatic valves. At the same time, pressure and temperature are recorded in order to check the progress of cleaning. Typically, there are five basic steps in the cleaning procedure: 1. Prerinse – rising with shear stress. There is another study that related to Gillham's study. Blel et al. [2] studied the effect of turbulent pulsating flow to the bacteria removal in straight pipe. Pulsed flow can reduce the number of bacteria more than steady flow. The bacteria removal is affected by the

chemicals from the surface; 4. Sanitizing – rinsing with the sanitizer to inactivate microorganisms; 5. Postrinse – removal of sanitizer with water from the system.

The cleaning efficiency is affected by chemical concentration, temperature and fluid flow [4]. Therefore, one way to enhance the cleaning is fluid flow adjustment. Gillham et al. [5] studied the effect of pulsed flow on cleaning enhancement of whey protein soil in tube. The results of this study show that pulsing both increases the rate of cleaning and changes cleaning rate behavior. Because reverse flow, generated by pulsed flow, can increase wall

2. Material and Method

2.1 Flow domain and computational mesh

To investigate wall shear stress of pulsed flow by using commercial CFD code, fluid was flowed in a cylindrical pipe (23 mm inner diameter and 1630 mm length) made of

combination of amplitude and frequency of pulsating flow. Moreover, the recirculation of pulsating flow induces high fluctuating shear rate at the wall. This effect can enhance deposit removal as same as Gillham's study

Wall shear stress affects on the cleaning rate as show in Table. 1. Thus, wall shear stress could be considered as one parameter which is used to indicate the cleaning efficiency of flows.

Table 1 Models Expressing the effect of wall shear stress on cleaning rates.

Relation	Wall shear stress range (Pa)	
$r = a + b\tau_w$	1-14	[14]
$\ln r = a + b\tau_w$	0.19-7.5	[6]
$\ln r = a - b\ln \tau_w$	0.8-1.3	[9]
$\ln r = a - b\tau_w$	1-50	[8]

In this study, a commercial computational fluid dynamics (CFD) code (FLUENT®) was employed to predict the shear stresses, generated by pulsed flow at the wall of pipe, compare with the experimental data which was measured by Blel et al [1]. The effects of amplitude, frequency and type of pulsed flow on wall shear stress were investigated as well. The expected results might be useful for the cleaning in place enhancement in pipe and tubular heat exchanger which is normally used in dairy process.

At the inlet of cylindrical pipe, fluid flowed with velocity as show in Table. 2. The turbulence inlet conditions were set as turbulence intensity and a hydraulic diameter. The turbulence intensity varied with the mean velocity of pulsed flow. The outlet was set as outflow boundary and no-slip conditions were applied to the wall. In the comparison between the numerical data and the experimental data,

stainless steel (average absolute roughness 0.3±0.05μm). The cylindrical pipe was separated into 3 zones (zone1 690 mm lengths, zone2 250 mm lengths and zone3 690 mm lengths) as in Fig.1. Wall shear stresses were investigated in zone2 in order to eliminate the entrance and exit effects as same as the experiment [1]. The entire flow domain was created from blocks of hexahedral and wedge mesh elements in GAMBIT™. The total number of mesh elements is 228,852 elements. Non-uniform mesh in the radial direction was performed to satisfy the y^+ value limits ($y^+<5$) valid for the enhance-wall treatment which was used for wall shear stress analysis as in Fig.2.
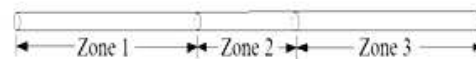
Fig.1 Flow domain (the cylindrical pipe with 23 mm inner diameter and 1630 mm length).
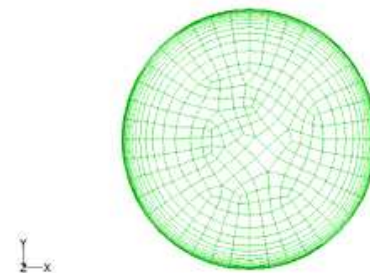
Fig.2 Example of hexahedral and wedge mesh elements in the radial direction of flow domain.

2.2 Computational Methods

The finite volume method of CFD code (FLUENT®) was employed to investigate wall shear stress of pulsating flow in cylindrical pipe. Steady and unsteady conditions were assumed for turbulent steady flow and turbulent pulsating flow, respectively. The velocity inlet could set as a constant and periodic function as in Eq. (1)-(4) for steady flow and pulsating flow, respectively.

fluid material was assigned to be electrolytic solution. The density of the solution is 1028 kg/m³ and its dynamics viscosity is 0.985 x 10⁻³ Pa.s. Meanwhile, water was adopted for the analysis of wall shear stresses that are generated by various type of pulsed flow.

Table 2 Hydrodynamic parameters for each pulsation condition

No.	Mean velocity (m/s)	Amplitude of the pulsations (m/s)	Frequency of the pulsations (Hz)
A	1.47	0.40	2.50
B	1.21	0.73	2.50
C	1.03	0.60	2.86
D	1.02	0.81	1.66
E	0.78	0.73	2.50
F	1.02	0.20	1.66
G	1.02	0.40	1.66
H	1.02	0.50	1.66
I	1.02	0.60	1.66
J	1.02	0.70	1.66
K	1.02	0.81	2.86
L	1.02	0.81	2.50
M	1.02	0.81	1.00
N	1.47	0.00	0.00
O	1.02	0.73	2.50
P	1.54	0.73	2.50

The Reynolds stress, $-\rho\overline{u_i'u_j'}$ can be related to the mean velocity gradients by using Boussinesq hypothesis as in Eq. (7).

$$-\rho\overline{u_i'u_j'} = \mu_t\left(\frac{\partial u_i}{\partial x_j} + \frac{\partial u_j}{\partial x_i}\right) - \frac{2}{3}\left(\rho k + \mu_t \frac{\partial u_k}{\partial x_k}\right)\delta_{ij} \quad (7)$$

Sine wave: $u(t) = \overline{u} + u_p \sin(2\pi f t)$ (1)

Square wave:

$$u(t) = \overline{u} + \frac{2u_p}{\pi}\sum_{n=1}^{\infty}\left(\frac{1-\cos n\pi}{n}\right)\sin(2n\pi f) \quad (2)$$

Triangular wave:

$$u(t) = \overline{u} + \frac{8u_p}{\pi^2}\sum_{n=1}^{\infty}\left(\frac{1}{n^2}\sin\left(\frac{n\pi}{2}\right)\right)\sin(2n\pi f) \quad (3)$$

Saw tooth wave:

$$u(t) = \overline{u} + \frac{2u_p}{\pi}\sum_{n=1}^{\infty}\left(\frac{\cos n\pi}{n}\right)\sin(2n\pi f) \quad (4)$$

In this study, fluid was assumed to be constant object property and incompressible. Pipe was laid on horizon level; the effect of gravitation could be ignored. Flow was performed under isothermal condition.

The numerical model was based on solving the conservation of mass, momentum of turbulent flow which can be written in the Cartesian form of Reynolds-averaged Navier-Stokes equations as in Eq. (5)-(6).

$$\frac{\partial \rho}{\partial t} + \frac{\partial}{\partial x_i}\left(\rho u_i\right) = 0 \quad (5)$$

$$\frac{\partial}{\partial t}\left(\rho u_i\right) + \frac{\partial}{\partial x_j}\left(\rho u_i u_j\right) =$$

$$-\frac{\partial p}{\partial x_i} + \frac{\partial}{\partial x_j}\left[\mu\left(\frac{\partial u_i}{\partial x_j} + \frac{\partial u_j}{\partial x_i} - \frac{2}{3}\delta_{ij}\frac{\partial u_i}{\partial x_i}\right)\right] \quad (6)$$

$$+\frac{\partial}{\partial x_j}\left(-\rho\overline{u_i'u_j'}\right)$$

rate in each control volume. The SIMPLE algorithm was applied for the iteration procedure.

3. Results and Discussion

3.1 Mean Wall Shear Stress Predictions

Fig. 3 shows the comparison of mean wall shear stress between the numerical data

The turbulent viscosity, μ_t, in Eq. (7) can be determined from turbulent kinetic energy, k, and turbulent dissipation rate, ε. Both of k and ε are obtained from RNG k-ε model in Eq. (8)-(9) which was more accurate and reliable for a wider class of flows than the standard k-ε model, especially for prediction of the wall shear stress [7]. Due to the k-ε models are not valid in the near wall region. Thus, enhance wall treatment was added to captured flow behavior in viscous sub-layer.

$$\rho \frac{Dk}{Dt} = \frac{\partial}{\partial x_j}\left(\alpha_k \mu_{eff}\frac{\partial k}{\partial x_j}\right) + \mu_t S^2 - \rho\varepsilon_k \quad (8)$$

$$\rho \frac{D\varepsilon}{Dt} = \frac{\partial}{\partial x_j}\left(\alpha_\varepsilon \mu_{eff}\frac{\partial \varepsilon}{\partial x_j}\right)$$
$$+ \frac{\varepsilon}{k}\left(C_{1\varepsilon}\mu_t S^2 - \rho C_{2\varepsilon}^*\varepsilon\right) \quad (9)$$

Where $\mu_{eff} = \mu + \mu_t$ (10)

$$S = \sqrt{2S_{ij}S_{ij}} \quad (11)$$

$$S_{ij} = \frac{\partial u_j}{\partial x_i} + \frac{\partial u_i}{\partial x_j} \quad (12)$$

$$C_{2\varepsilon}^* = C_{2\varepsilon} + \frac{C_\mu \rho \eta^3 \left(1 - \frac{\eta}{\eta_0}\right)}{1 + \beta\eta^3} \quad (13)$$

$$\eta = S\frac{k}{\varepsilon} \quad (14)$$

The second order upwind difference scheme was chosen to predict momentum, turbulent kinetic energy and turbulent dissipation same mean velocity of flow, the amplitude of pulsations is more effective on mean wall shear stress than the frequency when analyzed by numerical simulation as in Fig. 4-5.

and the experimental data. Both of the numerical data and the experimental data show that mean wall shear stress increases with mean velocity of flow. However, there are some differences between the numerical data and the experimental data.
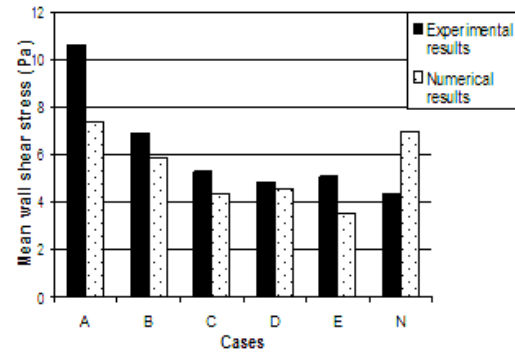
Fig.3 The comparison of mean wall shear stress between the numerical data and the experimental data.

The comparison of mean wall shear stress between pulsed flow (case A) and steady flow (case N) is seen that there is no difference between them when they are analyzed by numerical simulation [12]. Whereas, mean wall shear stress of pulsed flow is higher than mean wall shear stress of steady flow in the experiment. Additionally, for the experimental results, the frequency of pulsations is more effective on mean wall shear stress than the amplitude when the mean velocity is the same (Case C and D). On the other hand, for the

3.2 Wall Shear Stress Distribution of pulsed flow

Because of the entrance effect, wall shear stress is highest at the inlet of pipe. Then

Fig.4 The effect of amplitude of pulsations on mean wall shear stress by numerical simulation.
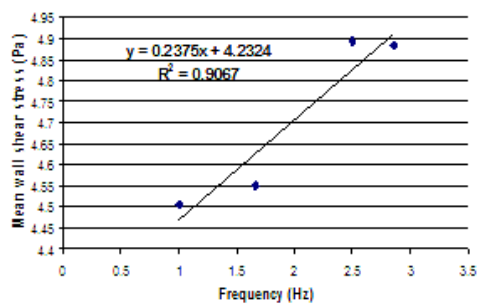
Fig.5 The effect of frequency of pulsations on mean wall shear stress by numerical simulation.

These differences are caused by the difference of the methodology of wall shear stress measurement between the experiment and the simulation. Electrochemical technique [1], which considers mass transfer of the chemical in the flow in form of Sherwood number and transform it into wall shear stress, were used to measure wall shear stress in the experiment. Meanwhile, for the numerical simulation, wall shear stress was obtained by solving the Reynolds-averaged Navier-Stokes equations which does not consider mass transfer of the chemical in the flow.

3.3 The Effect of Type of Pulsed Flow on Wall Shear Stress by Numerical Simulation

Wall shear stress corresponds to the velocity inlet function as shown in Fig. 8. When the velocity inlet is sine or square function, the variation of wall shear stress with time is sine or square function as well.

wall shear stress is decreased to the finite value when flow is fully developed as show in Fig. 6. This phenomenon can be seen in every kind of flows, including pulsed flows, except the flow whose velocity is changed immediately such as pulsed flow with square function of velocity inlet. When velocity inlet is change suddenly, there is reverse flow near the wall of pipe. This flow causes the increasing of wall shear stress as in Fig. 7.

Fig.6 Wall shear stress distribution of general pulsed flow in pipe.

Fig.7 Wall shear stress distribution of pulsed flow with square function of velocity inlet at the time that velocity inlet changes suddenly.

Fig.8 The variation of velocity inlet (a) and wall shear stress (b) with time for sine wave.

Mean wall shear stress increases with mean velocity inlet, amplitude and frequency of pulsation. Mean velocity inlet is the most effective on the mean wall shear stress as in Fig. 4, 5 and 9. Maximum wall shear stress and frequency of wall shear stress are also proportional to mean velocity inlet, amplitude and frequency of velocity inlet, respectively.

Mean wall shear stress is also affected by type of pulsed flow as Fig. 10. When pulsed flow behaves like rectangular wave, it generates the highest wall shear stress. Meanwhile, mean wall shear stresses, which are generated by saw tooth, sinusoidal and triangular wave, are not statistically different. Therefore, only wall shear stress analysis is not enough to clarify the cleaning efficiency of different type of pulsed flow. Consequently, the force accumulation on the surface deposit, which is generated by different type of pulsed flow, should be investigated for future work.

5. References

[1] Blel, W., Le Gentil-Lelievre, C., Benezech, T., Legrand, J. and Legentilhomme, P. (2009). Application of turbulent pulsating flows to the bacterial removal during a cleaning in place procedure. Part 1: Experimental analysis of wall shear stress in a cylindrical pipe, *Journal of Food Engineering*, vol.90, pp.422-432.
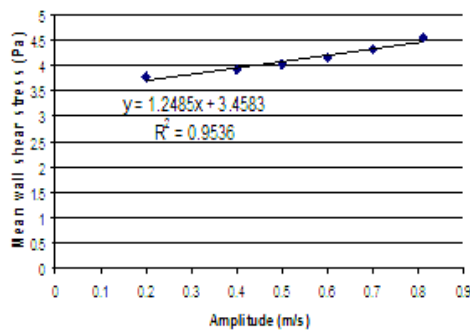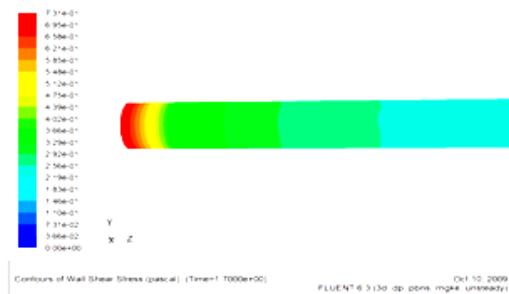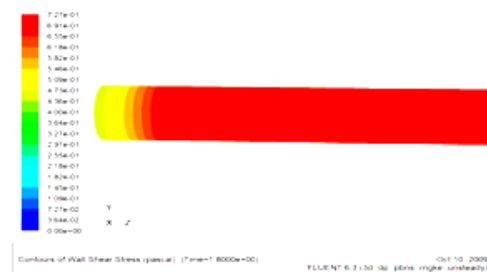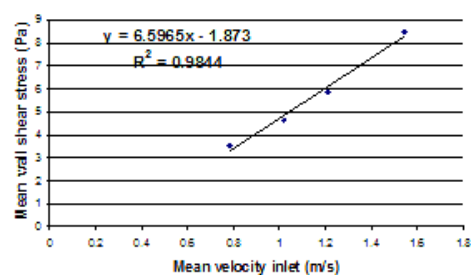
Fig.9 The effect of mean velocity of pulsations on mean wall shear stress by numerical simulation.

Fig.10 The effect of type of pulsed flow on mean wall shear stress.

4. Conclusion

Wall shear stress of turbulent flow can be calculated by using numerical simulation. But the numerical results are still different from the experimental data because of the difference of the methodology of wall shear stress measurement between the experiment and the simulation. Meanwhile, the numerical simulations of various types of pulsed flow showed that wall shear stress corresponds to the velocity inlet function. Mean wall shear stress is proportional to mean velocity inlet, amplitude and frequency of pulsation. Maximum wall shear stress and frequency of wall shear stress are also proportional to amplitude and frequency of velocity inlet, respectively.

[8] Hoffmann, W. and Reuter, H. (1984). Zirkulationsreinigen (CIP) von geraden Rohren in Abhängigkeit on physikalischen Einflußfaktoren. Milchwissenschaft, vol.39, pp.594.

[9] Jackson, A.T. and Low, M.W. (1982). Circulation cleaning of the plate heat exchanger fouled by tomato juice. III. The effect of fluid flow rate on cleaning efficiency, *Journal of Food*

[2] Blel, W., Le Gentil-Lelievre, C., Benezech, T., Legrand, J. and Legentilhomme, P. (2009). Application of turbulent pulsating flows to the bacterial removal during a cleaning in place procedure. Part 2: Effects on cleaning efficiency, *Journal of Food Engineering*, vol.90, pp.433-440.

[3] Changani, S.D., Belmar-Beiny, M.T. and Fryer, P.J. (1997). Engineering and chemical factors associated with fouling and cleaning in milk processing, *Experimental Thermal and Fluid Science*, vol.14, pp.392-406.

[4] Fryer, P.J., Christian, G.K. and Liu, W. (2006). How hygiene happens: physics and chemistry of cleaning, *International Journal of Dairy Technology*, vol.59 (2), May 2006, pp.76-84.

[5] Gillham, C.R., Fryer, P.J., Hasting, A.P.M. and Wilson, D.I. (2000). Enhanced cleaning of whey protein soils using pulsed flows, *Journal of Food Engineering*, vol.46, pp.199-209.

[6] Graßhoff, A. (1983). Die örtliche Flüssigkeitsbewegung und deren Einfluss auf den Renigungsprozess in zylindrischen Toträumen. *Kiel Milchwirtsch. Forxchungsber*, vol.35,pp.471.

[7] Hinton, A.R., Trinh, K.T., Brooks, J.D. and Manderson, G.J. (2002). Thermophile survival in milk fouling and on stainless steel during cleaning, *Trans IChemE*, vol.80, December 2002, pp.299-304.

Technology, vol. 17,pp.745.

[10] Jun, S. and Puri, V.M. (2005). 3D milk-fouling model of plate heat exchangers using computational fluid dynamics, *International Journal of Dairy Technology*, vol.58(4), November 2005, pp.214-224.

[11] Kakac, S. and Liu, H. (2002). Heat exchangers selection, rating and thermal design, CRc Press, Florida.

[12] Mao, Z. and Hanratty, T. (1986). Studies of the wall shear stress in a turbulent pulsating pipe flow, *Journal of Fluid Mechanic*, vol.170, pp.545-564.

[13] Rosmaninho, R., Rizzo, G., Muller-Steinhagen, H. and Melo, L.F. (2008). Deposition from a milk mineral solution on novel heat transfer surfaces under turbulent flow conditions, *Journal of Food Engineering*, vol.85, pp.29-41.

[14] Timperley, D. (1981). The effect of Reynolds-number and mean velocity of flow on the cleaning in place of pipelines. *In Fundamentals and Applications of Surface Phenomena Associated with Fouling and Cleaning in Food Processing*, Lund University, Lund, Sweden, pp.402.

BIOGRAPHY

Miss. Pichitra Uangpairoj was born on 12 September, 1985 in Nakhon Ratchasima, Thailand. She went to primary and secondary school at St. Mary College. She graduated with a Bachelor of Science in Food Technology in 2007 from Suranaree University of Technology (SUT) Nakhon Ratchasima, Thailand. She has received scholarships for students with outstanding academic performance from SUT to study for the master degree in mechanical engineering since 2007. During she was studying her master degree, she also worked as teacher and laboratory assistant of School of Mechanical Engineering. In November 2009, she published her paper about Numerical Simulation and Wall Shear Stress Analysis of Pulsed Flow in Cylindrical Pipe for a Cleaning in Place System in the 23rd Conference of the Mechanical Engineering Network of Thailand.